2015

Numerical modelling and control of an oscillating water column wave energy converter

Freeman, Kate

Numerical modelling and control of an oscillating water column wave energy converter

by

Kate Freeman

A thesis submitted to Plymouth University

in partial fulfilment of the degree of

Doctor of Philosophy

Marine Science and Engineering Doctoral Training Centre

March 2014

Abstract

An oscillating water column (OWC) wave energy converter (WEC) is a device designed to extract energy from waves at sea by using the water to move trapped air and thus drive an air turbine. Because the incident waves and the force caused by the power take-off (PTO) interact, control of the power take off (PTO) system can increase the total energy converted.

A numerical model was developed to study the interaction of an OWC with the water and other structures around it. ANSYS™ AQWA® is used here to find the effects on the water surface in and around the central column of a five-column, breakwater-mounted OWC. For open OWC structures, coupled modes were seen which lead to sensitivity to incident wave period and direction.

The frequency-domain displacements of the internal water surface of the central column were turned into a force-displacement, time-domain model in MATLAB® Simulink® using a state space approximation. The model of the hydrodynamics was then combined with the thermodynamic and turbine equations for a Wells turbine. A baseline situation was tested for fixed turbine speed operation using a wave climate for a region off the north coast of Devon.

A linear feedforward controller and a controller based on maximising turbine efficiency were tested for the system. The linear controller was optimised to find the combination of turbine speed offset and proportional constant that gave maximum energy in the most energy abundant sea state. This increased the converted energy by 31% in comparison to the fixed speed case. For the turbine efficiency control method, the increase was 36%. Energy conversion increases are therefore clearly possible using simple controllers. If increased converted energy is the only criterion for controller choice, then the turbine efficiency control is the best method, however the control action involves using very slow turbine speeds which may not be physically desirable.

Acknowledgements

This research was funded by Plymouth University, and my thanks go to my supervisors Ming Dai, Robert Sutton and Alison Raby for their guidance.

I would also like to thank everyone at Plymouth University who has helped me during this project, as well as my parents, for supporting me and providing advice and perspective.

Author's declaration

At no time during the registration for the degree of Doctor of Philosophy has the author been registered for any other University award without prior agreement of the Graduate Committee.

Work submitted for this research degree at Plymouth University has not formed part of any other degree either at Plymouth University or at another establishment. This study was financed by Plymouth University.

Relevant scientific seminars and conferences were regularly attended at which work was often presented and papers were prepared for publication.

Publications:

Freeman K, Dai M and Sutton R. Control Strategies for Oscillating Water Column Wave Energy Converters. *Underwater Technology*, Vol 32, No 1, 2014, pp3-13.

Major Conferences Attended:

European Wave and Tidal Energy Conference, 2011, Southampton

International Conference on Ocean Energy, 2012, Dublin

European Wave and Tidal Energy Conference, 2013, Aalborg

Word count of main body of thesis: 44,933

Name:

Date:

Nomenclature

A_w	horizontal area of water within the OWC [m^2]
$A_E(\omega)$	amplitude of wave [m]
$A(\omega)$	added mass [kg]
$B(\omega)$	damping [$kg\,s^{-1}$
C	capture width [m]
d	ocean depth [m]
E	total energy [$kg\ m^2\ s^{-1}$]
$F(\omega)$	force acting on the WEC from the undisturbed incident wave described in the time domain [N]
$f_e(t)$	excitation force [$kg\,m\,s^{-2}$]
$f_\mu(t)$	damping force [$kg\,m\,s^{-2}$]
$\underline{f}$	external force on a fluid element per unit volume [$kg\,m^{-2}\,s^{-2}$]
g	acceleration due to gravity [ms^{-2}]
$G(\omega)$	a transfer function which takes wave force as its input and produces mean vertical motion of the OWC free water surface as its output [$m\,N^{-1}$]
$G(s)$	a transfer function (in the s-plane) which takes wave force as its input and produces mean vertical motion of the OWC free water surface as its output [$m\,N^{-1}$]
$g(t)$	a state space model in the time domain which takes wave force as its input and produces mean vertical motion of the OWC free water surface as its output [$m\,N^{-1}$]
h	draft of the water column [m]
H_s	significant wave height [m]
k	wave number [m^{-1}]
K_l	constant of proportionality for linear controller [$rad\,s^{-1}\,Pa^{-1}$]
k_s	spring constant [$kg\,s^{-2}$]
l_OWC	horizontal length of OWC (width of wave front) [m]
m	mass of air in the chamber [kg]
m_c	mass of the water column [kg]
n	a vector normal to a surface [m]

N_f	fixed turbine speed [rpm]
N_l	turbine speed offset for the linear controller [rpm]
N_r	turbine speed [rad s^{-1}]
N_t	turbine speed [rpm]
p	absolute air pressure [Pa]
p_{atm}	atmospheric air pressure at standard temperature and pressure [Pa]
Δp	relative chamber pressure [Pa] ($p - p_{atm}$)
p_{tot}	total pressure within a fluid [Pa]
P	power [W]
P_m	mechanical power [W]
P_p	pneumatic power [W]
P_{abs}	power absorbed by a WEC [W]
$\tilde{P}_{inc}$	power incident on a WEC per metre of wave front [W/m]
r	reference input to a controller
S_1, S_2	the regions of water surface inside and outside an OWC
S_s	the free water surface
S_b	the sea bed
S_∞	a surface connecting the free water surface and the sea bed
S_t	the internal surface of the OWC
S_w	the wetted surface of the structure
$S(\omega)$	spectral shape [$m^2\ s^{-1}$]
T	wave period [s]
T_1	modal peak wave period for a spectrum [s]
$\boldsymbol{u}$	velocity of a fluid [$m\ s^{-1}$]
$U_{WEC}(\omega)$	velocity of a WEC [$m\ s^{-1}$]
u	input to a system
$\underline{v}$	vector velocity of a fluid element [$m\ s^{-1}$]
$X(\omega)$	displacement of the water surface as a function of frequency [m]
$\hat{X}$	magnitude of the displacement of the water surface [m]
$x(t)$	displacement of the water surface as a function of time [m]
y	output from a controller
z	the vertical co-ordinate [m]

$Z_{PTO}(\omega)$	impedance of the PTO of a WEC [$\mathrm{kg\,s^{-1}}$]
$Z^{ideal}_{PTO}(\omega)$	ideal impedance of the PTO of a WEC [$\mathrm{kg\,s^{-1}}$]
$Z_{WEC}(\omega)$	impedance of a WEC [$\mathrm{kg\,s^{-1}}$]
α	the scale factor [-]
η	efficiency of a turbine [-]
ϵ	error input to a controller
ϕ	velocity potential [$\mathrm{m^2 s^{-1}}$]
μ	damping coefficient [$\mathrm{kg\,s^{-1}}$]
μ_r	radiative damping coefficient [$\mathrm{kg\,s^{-1}}$]
μ_t	turbulent damping coefficient [$\mathrm{kg\,s^{-1}}$]
μ_{PTO}	coefficient of damping due to WEC PTO [$\mathrm{kg\,s^{-1}}$]
ν	kinematic viscosity coefficient [$\mathrm{m^2 s^{-1}}$]
θ	wave direction [rad]
ρ	density of air [$\mathrm{kg\,m^{-1}}$]
ρ_w	density of water [$\mathrm{kg\,m^{-1}}$]
σ	phase shift with respect to incident wave [rad]
ω	frequency [rad s−1]
ω_0	modal frequency for a spectrum [rad s−1]
$\Delta\omega$	width of frequency bins for discrete spectra [rad s−1]
Ψ	non-dimensional pressure for the turbine [-]
Ψ_{max}	is the non-dimensional pressure for the turbine at which maximum efficiency occurs [-]

Subscripts

iso	for a single isolated OWC
cen	for the central column of a five column OWC system
PTO	associated with the PTO
WEC	associated with a WEC

Superscripts

D	diffracted wave
I	incident wave
R	radiated wave
*	complex conjugate

Acronyms

MPC	model predictive control
OWC	oscillating water column
PTO	power take-off
RAO	response amplitude operator
SHO	simple harmonic oscillator
WEC	wave energy converter

Contents

List of Figures

List of Tables

Chapter 1

Introduction

The motion of ocean waves can be used as a source of renewable energy. An oscillating water column (OWC) wave energy converter (WEC) can be used to convert this energy into electricity. Such a wave energy converter (WEC) could look like that shown in Figure 1.1. A structure is used which channels the water into a vertical column. As the waves oscillate up and down, the air above this column is then moved through an air turbine to produce electricity.

Because in designing and building renewable energy plants, the cost of the energy is the factor which determines their effectiveness, OWCs may often be positioned next to one another, formed into a line along a cliff, or as a breakwater. This decreases the unit cost of each one by sharing out the foundation and cabling costs. If a breakwater construction is used, this has the advantage that the WEC can be used to protect the area of sea behind it.

In order to increase the energy which is converted by such a device, the properties of the air turbine may be changed as the waves approach. Changing the power take-off (PTO) parameters can change the mass of air that flows through the turbine and the pressure in the air chamber. This in turn changes the converted power, and thus the energy converted by the WEC may be increased by adapting the PTO parameters.

In order to test such control of the power take-off (PTO) parameters, a numerical model should be developed. This model should be as wave-to-wire as possible in that the system is modelled from the incident wave, through the water column motion and the pressure of the air in the chamber, to the behaviour of the turbine and the power available on the electricity grid. A large OWC motion does not necessarily leas to large energy conversion: the coupled system of the column and the PTO works jointly to convert energy. The effect

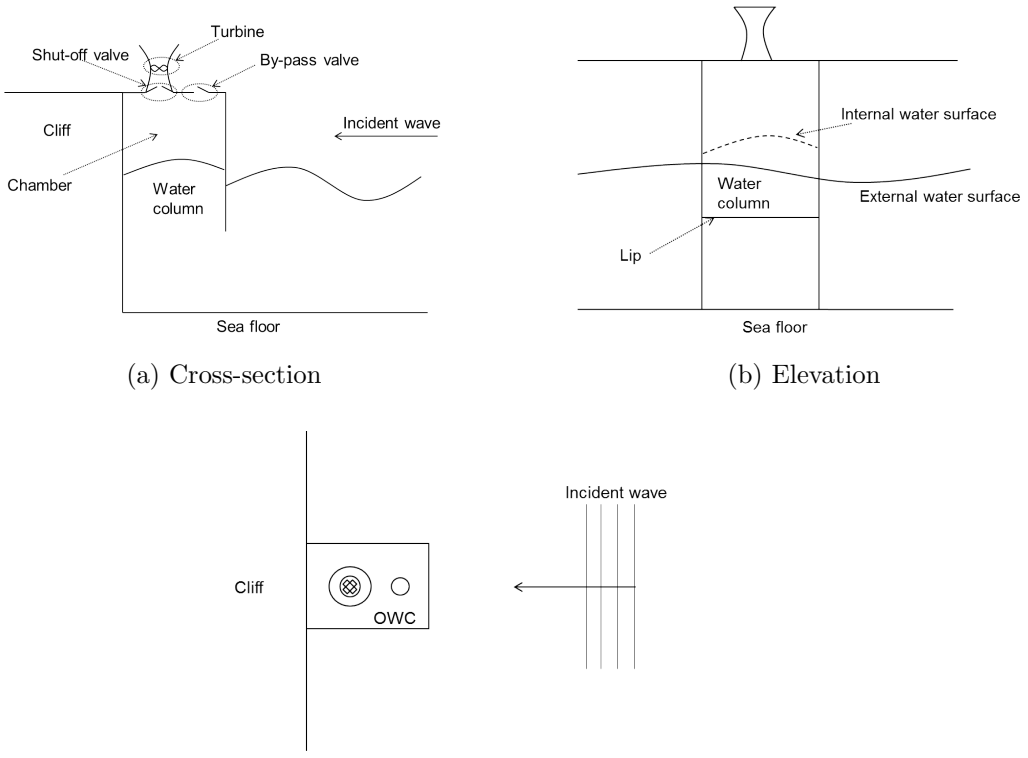

(a) Cross-section

(b) Elevation

(c) Plan

Figure 1.1: Schematic diagram of an oscillating water column (OWC) wave energy converter (WEC)

of the PTO parameters on the chamber pressure should thus be included in this model so that the force of the chamber pressure on the water surface within the chamber can be fed back into the system dynamics.

Because the motion of the water in neighbouring OWCs affects the performance of any individual OWC through coupled modes of motion, these neighbours should be included from the start so that the sensitivity of the OWC to incident wave period can be included.

1.1 OWC fundamentals

In this section the basic operating principle and types of OWCs will be described. First the basic operation will be explored, then in Section 1.1.2 different configurations for OWC-WECs will be explored. In Section 1.1.3, the different power take-off (PTO) methods are explained.

1.1.1 A simple OWC

An OWC-WEC is structured as in Figure 1.1, with one or more chambers that are open to the sea at their bases. The motion of the water within the chamber drives the motion of the air above it and the air drives a turbine to produce electricity, with the turbine operating

such that electricity is produced as the air flows both in and out of the chamber.

In Figure 1.1a, the wave enters from the right of the figure and encounters the OWC structure positioned on a cliff. The water extends under the front lip of the structure, so that the wave motion causes the column of water to oscillate. This water oscillation drives the air in the chamber above through a turbine. The turbine is set up so that it converts the air motion to electricity both when the water column is moved up and when it moves down. This is done using a bi-directional turbine.

If the pressure difference between the chamber and the atmosphere is too large, a by-pass valve may be used to allow the air to move in and out of the chamber without going through the turbine. The air flow through the turbine may also be limited. A shut-off valve is indicated which restricts the flow of air through the turbine. This may enable the turbine to work in a more efficient regime, or may extend the range of operation to seas which would otherwise have pressure differences and air flows through the turbine which are too large.

In Figure 1.1b, the walls of the OWC are shown extending to the sea floor. The lip of the OWC does not extend to the sea floor and so the water of the open sea reaches under the lip to the water confined by the structure.

Figure 1.1c, shows the plan view of the OWC. The waves are shown incident to a cliff-mounted structure. This is not the only configuration available for OWCs. Further options will be described in Section 1.1.2. The incident wave is shown as a plane wave. In the ocean, waves would in fact come from all directions.

Forces acting on an OWC

It is not the case only that the wave changes the displacement of the water column and this drives changes in pressure: the pressure difference also affects the displacement of the water column. The system is coupled.

The forces which act on the water forming the column are: wave excitation, radiative damping, restoration due to buoyancy, turbulent damping and the chamber pressure force. The wave excitation force is that which comes from the incident wave. This force is clearly dependent on the frequency of the wave as well as the wave height. The radiation damping describes the force due to the production of waves by the oscillating column. When the water column moves, it produces waves which radiate away from the OWC. These waves depend on the frequency of the oscillation, therefore so does the radiative damping force.

Location	Shape	PTO
Cliff/shore	Cylinder	Rectification by valves
Bottom-mounted	Cuboid	Wells turbine
Fixed: open ocean	Other "prism"	Impulse turbine
Floating	Duct	Radial turbine

Table 1.1: OWC features

The buoyancy force is the restoring force caused when the water column moves away from the still water level: the water tends to move back to its equilibrium position under gravity. Turbulent action in the water damps the motion of the water column, as does the relative pressure in the chamber.

For different configurations of OWC-WEC, the different forces play a greater or lesser role. The different configurations are therefore described in Section 1.1.2.

1.1.2 Classification of OWCs by location and shape

OWCs may be classified by their location, shape and power take off (PTO) mechanism. Such location and shape classifications will be introduced in this section, with PTO classification described in Section 1.1.3. These classifications are necessary in order to discuss those different factors which are important for a specific OWC.

Within the broad distinctions which separate different types of OWCs (location, shape of water column and PTO), the sub-categories of classification are summarised in Table 1.1.

The different possible locations are shown in Figure 1.2, and the different possible shapes in Figure 1.3. These are explored next. A table in which categorisations of OWC type have been made for a number of studies is given in Table 1.2 at the end of this section. This table enables the groups of different geometries of OWC to become clear, with the studies are separated into numerical and physical versions. Those studies which deal with multiple water columns in arrays or in other packed formations are shown in bold.

Location of OWCs

For the cliff-mounted OWC (Figure 1.2a), the waves may only exist on the sea side of the OWC. The bottom-mounted OWC appears at first sight to be very similar (Figure 1.2b). However, the incident wave can pass around the structure and, although the back-board of the OWC forms a barrier that the water cannot pass through, when waves are radiated they may spread out into that region. The open-ocean fixed device (Figure 1.2c) does not

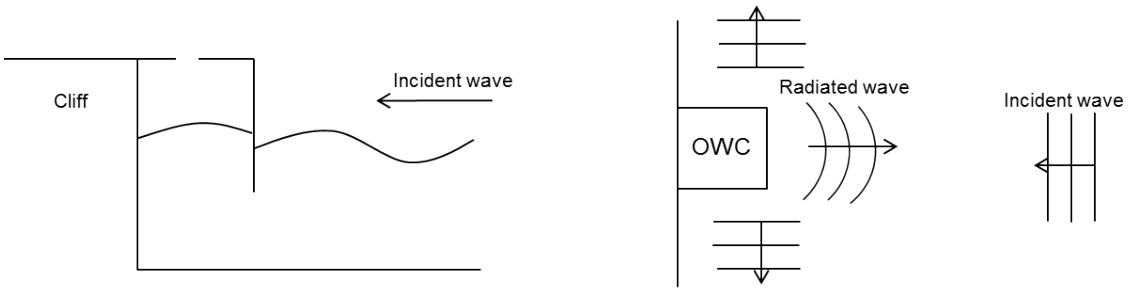

(a) Cliff

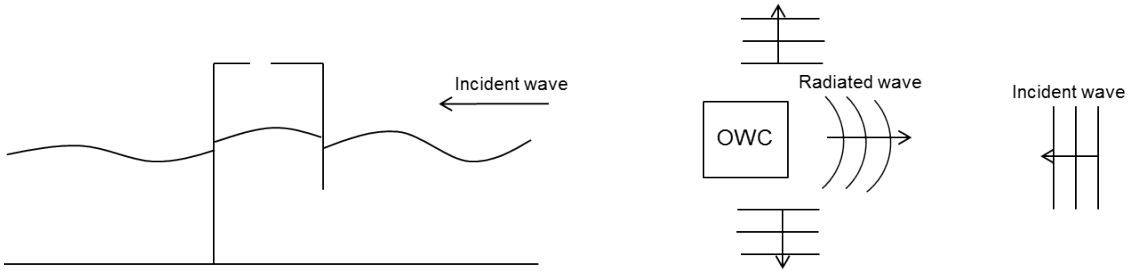

(b) Bottom-mounted

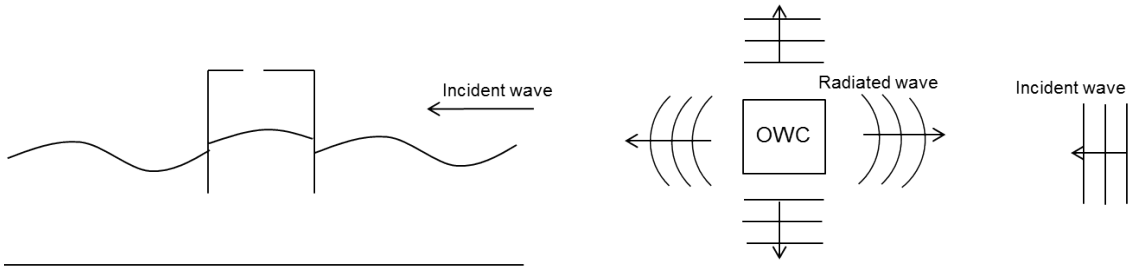

(c) Open ocean: fixed

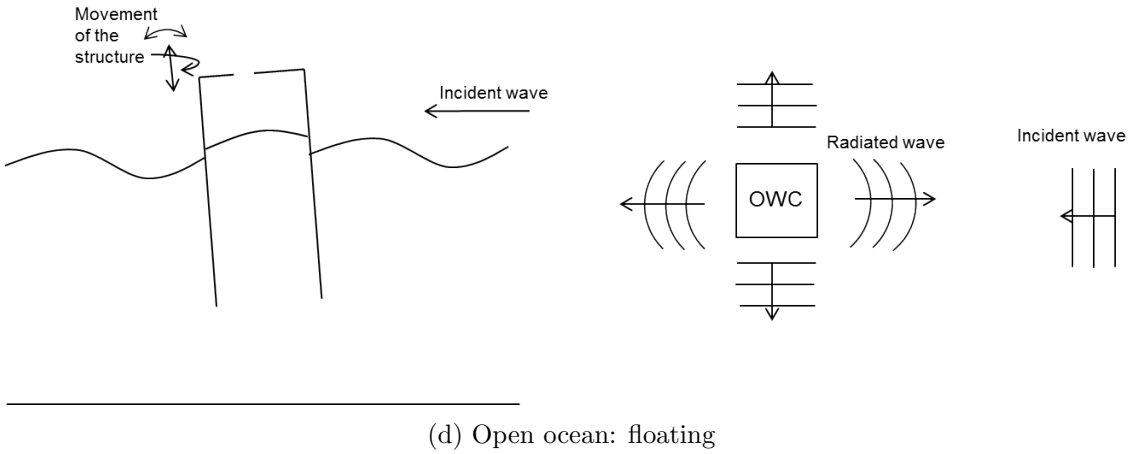

(d) Open ocean: floating

Figure 1.2: Possible locations for OWCs. On the left are shown cross-sections through the OWC, with the radiation patterns of the wave on the right.

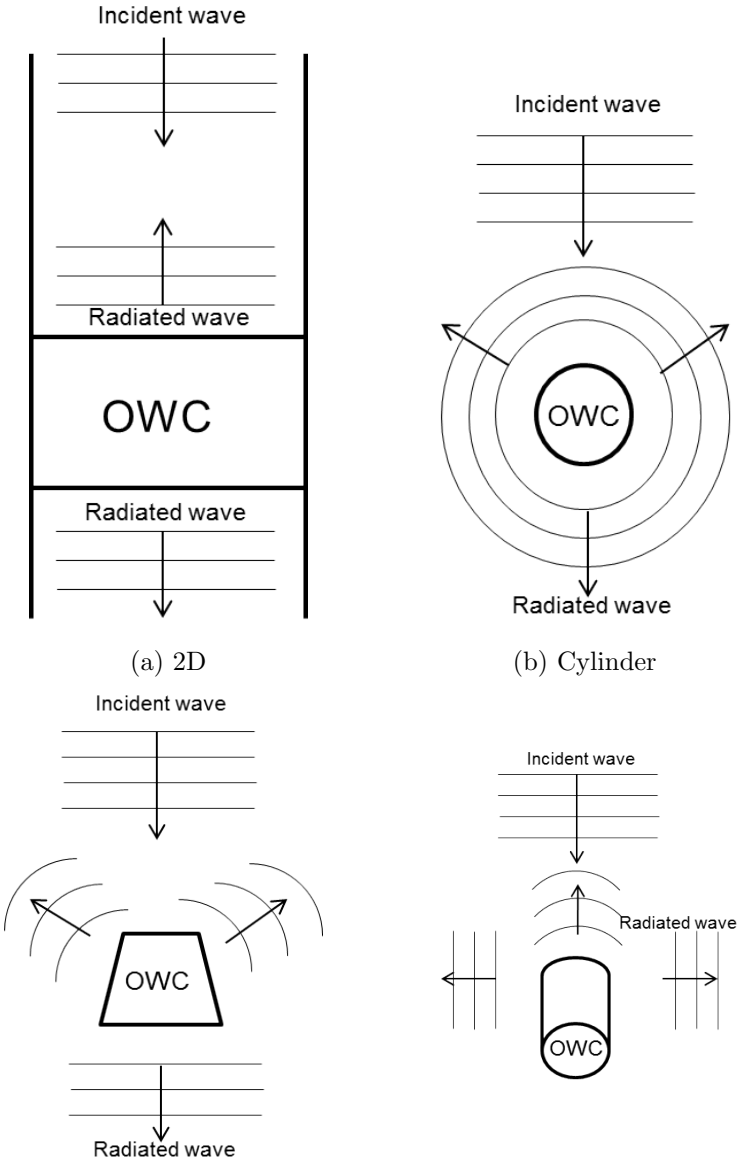

(a) 2D (b) Cylinder

(c) Prism (d) Duct

Figure 1.3: Possible shapes for OWCs in plan view, for open ocean configurations

have this restriction - the waves may pass under and around the structure. The floating device shown in Figure 1.2d has the same interaction options as the fixed open ocean device. Now, however, the whole structure can move, which complicates the scattering and radiation of waves. Note that for each of the locations, the incident waves are shown coming from a single direction. This would clearly not be true in the real sea, where waves are formed from many directional components.

Two dimensional (2D) OWCs

A 2D OWC is one in which the incident and diffracted wave may only move in a single direction, for example the numerical model of Evans & Porter (1995). The wave may only come from a head-on direction and radiation and scattering are confined to this same direction. An at-sea OWC would obviously radiate waves in all directions, and waves heading towards the OWC would come from a spread of directions. The 2D model of Figure 1.3a is therefore simpler than a 3D model, but is not realistic due to the directions from which waves may be incident, and the directions in which waves may be scattered and radiated.

Another way of looking at this directionality problem is that the 2D version does not include a whole structure: the *edges* of a structure are important for an OWC. Even for a series of OWCs along a cliff, the structure is not infinite and thus the 2D model cannot fully describe what happens at the end of the OWC.

The main advantage of 2D cliff- or shore-based models is that they are useful in comparison of numerical and physical models. Physical models in flumes and numerical models in numerical flumes are easily compared and the differences seen. Computationally, the solutions are less intensive than for 3D. This means that Navier-Stokes solvers (Section 1.2.2) may be used with a relatively short computational time (as in Zhang *et al.* (2012)).

The bottom-mounted OWCs differ from the cliff- and shore-based ones in that the water *does* extend behind the OWC. For a 2D structure this is not possible - if the OWC wall extends to the sea bed, the water cannot get around it without the third dimension. A 2D version of the bottom-mounted structure is invalid, but an open ocean version is not. Here the wave can pass under the structure. Of course, the directions of the waves are still restricted because of only having two dimensions. A floating 2D OWC could exist, but the six degrees of freedom motion crucial for the behaviour of the device may not be captured, so 2D floating OWCs are rarely investigated (Koo, 2009).

Cylindrical OWCs

Moving from the 2D OWC to a 3D OWC, a cylindrical housing in the open ocean is often envisaged, and is shown in Figure 1.3b, as this allows for a maximum amount of symmetry. Waves incident from any direction see the same shape, and waves are radiated equally in all directions. Of course, this is only true in the open ocean. If the OWC is cliff-, shore- or bottom-mounted, some (large) fraction of the wave field will be blocked by the presence of walls or the absence of water. That said, the research by Martins-rivas & Mei (2009) looked at a cylindrical OWC positioned as part of a cliff and found that the displacement of the internal water surface of the water column was not horizontal and that the cliff acted to increase the energy converted.

In the open ocean, a cylinder may be fixed with respect to the sea bed or may be a floating, moored system. For the fixed versions, the draft of the device is made quite small and it is the water column which moves. For the floating OWCs, the action is different: the draft is large, with the lip of the OWC below the level at which the wave induced motion of the water is great: in Figure 1.2d the water column is very deep. The water column is thus not forced by the motion in and out of the column. To prevent the OWC from sinking, a buoyant float is positioned at the top of the structure around the column. This float which supports the structure is at the water surface. This means that the wave motion forces the float. As such, the water column is used as the reference against which the float motion occurs. Of course, the dynamics are not really so simple, as it is coupled motion which causes the relative motion of the internal water surface providing the energy conversion.

OWCs with other uniform cross-sections

As well as cylindrical OWCs, other uniform shapes may be used in which the water column has the same horizontal area for its whole depth. See Figure 1.3c. These "prisms" include water columns with rectangular horizontal areas, the segments of Deng *et al.* (2013) and the packed rhombi of Gervelas *et al.* (2011). While uniform shapes are simple to model for bulk movement, assuming the mass of water in the water column moves as one solid block with no change of area at the waterline, unlike cylindrical OWCs they scatter and radiate waves differently depending on direction; both the direction of the incident wave and the direction in which scattering/radiation is considered.

Such simple shapes may also be packed together or aligned with neighbouring ones

to produce array structures which have interactions with one another as well as with the wave. This is the case in Kelly *et al.* (2013b), in which two rows of cuboid OWCs are formed together in a floating 'V'-shape.

Non-uniform and duct-like OWCs

OWCs may be formed from non-uniform structures or ducts which do not have the same horizontal area for their whole draft, as in Figure 1.3d. For example, the real structures that form shoreline OWCs are likely to have walls which fit with the shape of the particular shore and thus are not uniform at the waterline, as in Brito-melo *et al.* (1999) - a numerical study of the Pico plant. Another class of non-uniform OWC are those with ducts. Here the water turns a corner, as in the case of thick tubes at the shoreline described by Magagna *et al.* (2011) and Patel *et al.* (2011), or in the floating square-sectioned ducts of the backward bent duct buoy (BBDB) of Imai *et al.* (2011) and the forward BDB of Fleming *et al.* (2012). In Deng *et al.* (2014), the wave is channelled towards the OWC using two plates.

Multiple column OWCs

When there is more than one water column in close proximity, the way that the waves interact with one will affect the amount of energy available to the other(s). This is true for all WECs, but with OWCs there is a standard configuration that takes one OWC and puts it very close to many others: the breakwater. Breakwater OWCs can be fixed or floating. A floating breakwater OWC acts more like a fixed breakwater OWC than it does like a floating isolated OWC, as the operation is such that the breakwater float does not move significantly, but the water columns do move. The dynamics of a floating device are unlikely to see such large motions as for a single floating OWC version, nonetheless, estimation of the internal water surface will be much more complicated.

Breakwater OWCs exist as in-situ or planned projects around the world (Amundarain *et al.*, 2011; Hotta *et al.*, 1996; Hong & Song, 2012; Joubert & Niekerk, 2013; Ruol *et al.*, 2011) so the design challenges are current. For such projects, a very specific design may be tested, but an understanding of the generic design principles is worthwhile for considerations of future projects.

Shape: / **Location**	**2D**		**Cylinder**		**Prism**		**Duct**	
	Numerical	Physical	Numerical	Physical	Numerical	Physical	Numerical	Physical
Cliff/shore	Alves & Sarmento (2005), Gkikas *et al.* (2006), Zhang *et al.* (2012)	Mendes & Monteiro (2007), Morris-Thomas *et al.* (2005)	Martins-rivas & Mei (2009)		Josset & Clement (2007)			**Magagna *et al.* (2011)**, Patel *et al.* (2011)
Bottom-mounted	-	-			Hong & Hong (2012), **Deng *et al.* (2013)**		**Deng *et al.* (2014)**	
Open ocean - fixed		Iturrioz *et al.* (2013)	Sykes *et al.* (2007), Lopes *et al.* (2007), **Nader *et al.* (2012)**	Sykes *et al.* (2007)	Gervelas *et al.* (2011)	**Gervelas *et al.* (2011)** **Ruol *et al.* (2011)**		
Open ocean - floating	-	-	Falcão (2002), Gomes *et al.* (2012)	Sykes *et al.* (2009), Stappenbelt *et al.* (2013), Weber (2007)		**Kelly *et al.* (2013b)**, **Johnson (2003)**	Bull & Johnson (2013)	Fleming *et al.* (2012), Imai *et al.* (2011)

Table 1.2: Classification of hydrodynamics studies of OWCs based on the location and shape of the OWC. Those studies shown in bold are for arrays of devices.

1.1.3 Power take-off for OWC-WECs

The previous sections talked about how a wave may interact with the OWC. In order to understand how an OWC will behave in real sea conditions, the PTO system should be included. A model should include PTO damping which is as close as possible to what would happen in the real sea. This means that the PTO should be modelled in the time domain.

Ideal damping may be used which can be described in the frequency domain or by a damping force proportional to velocity in the time domain. This is useful as a frequency domain approximation for the hydrodynamic section, but is not like the PTO experienced by a real OWC. This requires a time-domain model for the PTO.

For the velocity potential methods, only very simple differences to the pressure above the internal water surface of the OWC may be included. For example, pressure as a function of time would require a very large amount of extra effort and potentially a change of method. Simple PTO inclusion is often described by the term "lid", which implies an even damping over a certain surface area. This damping may be even in the sense of constant pressure or be in proportion to surface velocity. Clearly a suitable pressure approximation must be made so that the PTO's effect is well described. Of course, one of the reasons for making the hydrodynamical model is so as to find good parameters for the PTO. Thus the process of whole system design should be an iterative one.

In order to convert the internal water surface motion, OWC-WECs use the air in the chamber to drive turbines. For a turbine to be effective in an OWC, it needs to provide some kind of motion both when the air flows and of the chamber and when the air flows into the chamber. This can be done by using valves to rectify the air flow such that it always travels in the same direction.

Alternatively, turbines may be used in which in pressure difference across the turbine causes the turbine to turn in the same sense. There are many such turbines (for an overview, see Setoguchi & Takao (2006) for example), with the Wells turbine was designed for OWC use.

In order to protect the turbine from extreme events and/or to control the amount of flow through the turbine, valves may be used in series or parallel with the turbine. These were shown as shut-off and by-pass valves in Figure 1.1.

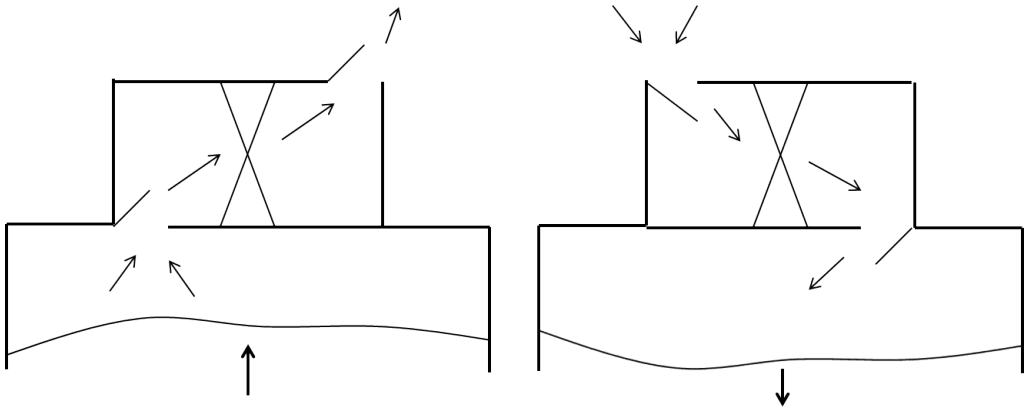

Figure 1.4: Rectification of air flow via valves

Rectifying air flow using valves

One way to rectify this alternating air flow is to use valves such that air is only let into and out of the turbine housing in one direction, as in Figure 1.4. The turbine is represented by the hour-glass shape. Note that the air flows through the turbine from left to right in both the in- and out-flow cases. This means that a standard, unidirectional turbine can then be used as is done in Jayashankar *et al.* (2009); Ruol *et al.* (2011); Kelly *et al.* (2013a,b).

The Wells turbine

Figure 1.5 shows a cross-section through one of the blades of a Wells turbine (Thakker, 2008). Each blade is like an aircraft wing attached to a central hub and the air flows in the same direction as the axis of this hub. If a rotational speed is given to the turbine, the blades move in the direction indicated in the figure. When there is a pressure difference across the blade (i.e. when the air pressure is different above the blade indicated in the figure in comparison to the air pressure below, or vice versa), a lift force is produced. Because the blades are already moving, the resultant direction of this force is forwards, and thus the blades are pulled into rotating faster. The turbine blades are symmetrical, so no matter what the sign of the pressure difference, the force is always forwards.

Impulse turbines

In an impulse turbine, guide vanes are used to align the air flow such that it forces the motion of the turbine. Such forcing is shown in Figure 1.6. The guide vanes are arranged so that the air motion forces the turbine to turn in the same direction for inflow and outflow. The turbine blades and guide vanes may be arranged so that the turbine is of

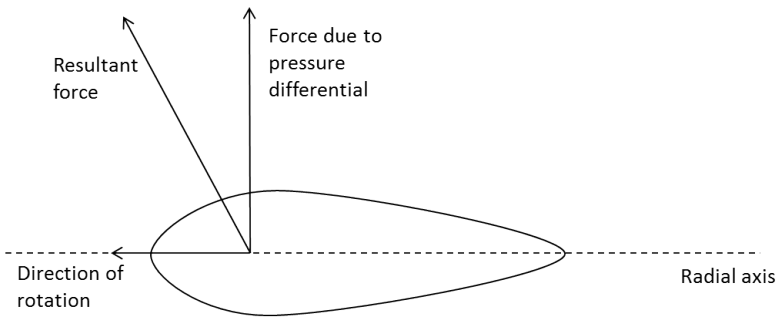

Figure 1.5: The forces on a Wells turbine

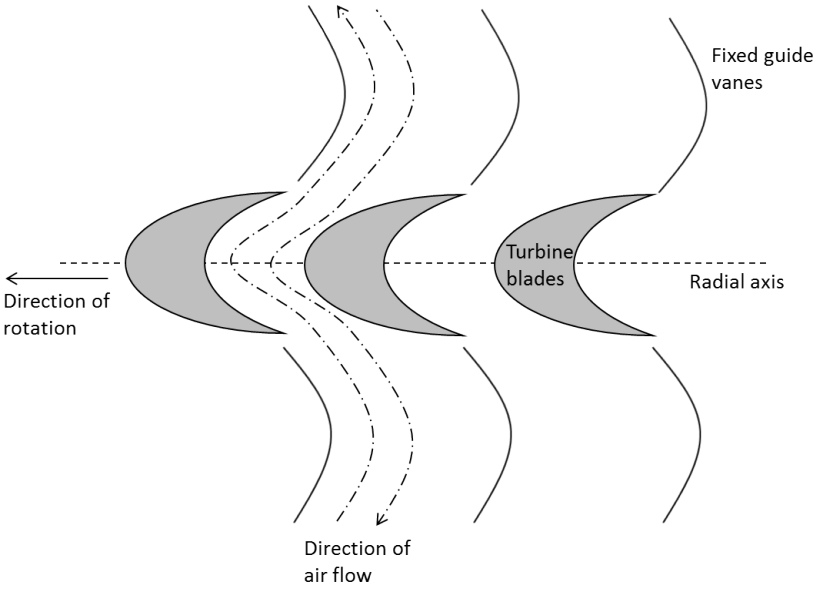

Figure 1.6: The function of an axial impulse turbine

the axial (Thakker, 2004) or radial (Pereiras *et al.*, 2011b) type.

In order to design such a turbine, a full model which includes the specific air flow around the turbine should be used. This requires a high-powered CFD approach (Taha & Sawada, 2010; Natanzi *et al.*, 2011; Moisel & Carolus, 2013) and is beyond the scope of this thesis. A simplified model of an existing turbine may be used to take the volume changes of the chamber and turn this into converted energy via chamber pressure and mass flow.

1.2 Wave to wire modelling of OWC-WECs

The aspects which require modelling in the case of an OWC-WEC are the waves and how they interact with the structure, how that system interacts with the air in the chamber, the way the air flows through the turbine and the turbine interaction with the generator and the grid. If a model describes all of these aspects, it is a "wave to wire" model. In

this section, the different parts of wave to wire modelling will be described.

1.2.1 Modelling waves

In order to represent a single frequency wave, the frequency (period) and height of the wave are needed. In the equation below, $x(t)$ represents the displacement of the water surface at a point, A_E is the amplitude of the wave, ω is the frequency of the wave, t is time and σ is a phase shift.

$$x(t) = A_E \sin(\omega t + \sigma) \tag{1.1}$$

A wave field is made by summing over many waves with different ω, A_E and σ. Different spectral representations describe how the quantity of energy is shared amongst the frequencies. For example, the energy may be concentrated into a very narrow band of frequencies, or may have a long tail. This is covered in more detail in Chapter 4. The other variable that should be used is a variable to represent the spread of incident wave directions.

Directionality

Directional spreading should be included, but is often ignored as a first approximation, particularly in cases where the WEC (and its mooring configuration) is insensitive to direction, or where plane waves may be assumed.

One way of representing the directional spreading of the waves is to assume a distribution

$$f(\theta) = \frac{2}{\pi} \cos^2(\theta) \tag{1.2}$$

for $-\pi/2 \leq \theta \leq \pi/2$ around the mean direction.

1.2.2 Modelling wave-structure interaction

Physical models

Physical models of the system may be made and is generally done at scale due to cost and risk. For a floating device scale modelling can enable capture of the interacting motion in different degrees of freedom. For the cliff- or shore-based device, however, there are very many things that must be converted to the scale model - not least the bathymetry of the system.

For OWCs scale modelling can be particular challenge. While the geometry is scaled down as the scale factor, α, the waves and air pressure scale differently. is that the water scales with Reynolds number (turbulence), but the waves scale with Froude number, and the air above will also be Reynolds (but this will be a case of changing the volumes involved, because changing the pressures would be extremely computationally costly).

In order to include more complicated damping, for turbulent behaviour for example, a computational fluid dynamics CFD model should be used.

Navier-Stokes approaches

The Navier-Stokes equations may be solved for all elements within the fluid. Falnes (2002a) gives the Navier-Stokes equation as

$$\frac{\partial \underline{v}}{\partial t} + (\underline{v}.\nabla)\underline{v} = -\frac{1}{\rho_w}\nabla p_{tot} + \nu\nabla^2\underline{v} + \frac{1}{\rho_w}\underline{f} \tag{1.3}$$

where $\underline{v}$ is the velocity of the water element, ρ_w is the density of the water, p_{tot} is the pressure of the water, ν is the kinematic viscosity coefficient and $\underline{f}$ is the external force per unit volume.

Various assumptions and approximations may be made to simplify these equations: incompressible fluids or irrotational flow, for example. Solution of these equations enables good capture of the water motion and the forces on the structure. However, such detailed calculation is very computationally intensive. Thus these and other computational fluid dynamics (CFD) approaches are only used where particularly nonlinear conditions are important, such as for extreme loading.

For OWCs, Alves & Sarmento (2005), Zhang *et al.* (2012) and Iturrioz *et al.* (2013) used CFD to investigate 2D structures. Koo (2009) looked at a similar design, but for a moon pool structure (i.e. one with no PTO): a floating 2D breakwater with one chamber was used to decrease wave motion behind the structure.

A Navier-Stokes CFD approach is too involved for estimation of energy conversion or optimisation of control strategies so is not investigated in this thesis.

Velocity potential methods

In order to investigate the interaction between the water and the structure, a velocity potential method may be used.

Velocity potential solutions mean that $\nabla\phi = \underline{v}$ where $\underline{v}$ is the velocity of the fluid

and ϕ is the velocity potential that is being solved for. Because of certain simplifications and mathematical parallels, it can be simpler to solve for velocity potential than to solve for velocity directly. The particular simplification is that the water is assumed to be incompressible. Thus, the velocity must follow $\nabla.\underline{v} = 0$ and so, the potential must satisfy

$$\nabla^2\phi = 0 \tag{1.4}$$

which is the Laplace equation. It is an equation of interest in many areas of mathematics and physical science, thus there are many approaches to find solutions to it. When solving for specific (simple) OWC geometries, analytical methods may be used in which the simplifications to the boundary conditions are done manually to match the geometry, e.g. Deng *et al.* (2013); Evans & Porter (1995). The potential may then be solved for analytically or by numerical calculation. For more complicated geometries, a panel or boundary element method is often used, e.g. Sykes *et al.* (2009); Gomes *et al.* (2012), in which the boundaries are separated into small areas and numerical solutions are calcualated which enable the matching of the velocity potential on all of these boundaries. This results in a solution of the velocity potential for all regions within the fluid.

As an alternative to a boundary element method, a finite element method may be used to find the velocity potential throughout a fluid. The whole region of the fluid is subdivided into three-dimensional elements and the velocity potential changes are calculated for all of them (Nader *et al.*, 2012). In the finite element method, the velocity potential is solved at all points in the fluid region, not just on the surface of the OWC wall.

Velocity potentials are only able to solve for linear conditions, however, approximations to second order waves exist.

Simple harmonic oscillator models

Perhaps the simplest way of modelling an OWC-WEC is to treat it as a simple harmonic oscillator (SHO). This is particularly useful for investigating resonance phenomena.

For a spring mass damper system like the one in Figure 1.7, Netwon's Second Law gives

$$m_c\ddot{x}_m = f_e(t) - \mu\dot{x}_m + k_s x_m \tag{1.5}$$

where x_m is the position of the mass, m_c is the water column mass, k_s is the spring coefficient, μ is the damping coefficient and $f_e(t)$ is the time-varying excitation force.

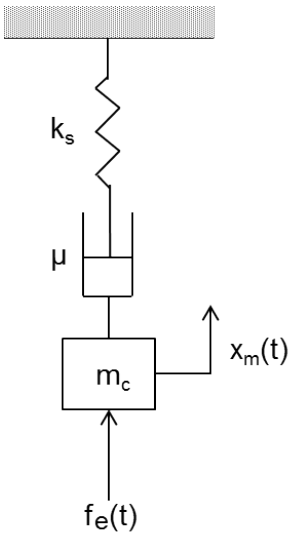

Figure 1.7: Simple harmonic oscillator (SHO)

For an OWC, if a constant internal water area is chosen then this becomes

$$(\rho_w A_w l)\ddot{x} + \mu\dot{x} + (\rho_w A_w g)x = f_e(t) \tag{1.6}$$

where $(\rho_w A_w l)$ is the mass of the water column and $(\rho_w A_w g)$ is the buoyancy spring caused by the displacement of the water column from its equilibrium position. ρ_w is the density of the water, A_w is the horizontal area of the water column, l is the draft of the water column and g is the gravitational acceleration.

Note that the damping coefficient, μ, has not been substituted for. This damping is the part which is difficult to model. The major causes of damping in an OWC are radiation of waves caused by the motion of the water column and turbulent losses within the water. Both of these effects are highly dependent on the frequency of oscillation. For more on radiation models for OWCs, see Alves *et al.* (2011). Another way of assessing this damping value is to determine it through physical modelling.

For the case with no damping and assuming a sinusoidal displacement of the internal water surface, the undamped natural frequency can be calculated. The displacement x, is taken to vary with frequency ω and magnitude $\widehat{X}$, as $\widehat{X}e^{i\omega t}$. As μ and $f_e(t)$ are zero,

$$(\rho_w A_w l)(-\omega^2\widehat{X}) = -(\rho_w A_w g)\widehat{X} \tag{1.7}$$

Thus the undamped natural frequency for the oscillator is

$$\omega_{nat} = \sqrt{\frac{g}{l}} \tag{1.8}$$

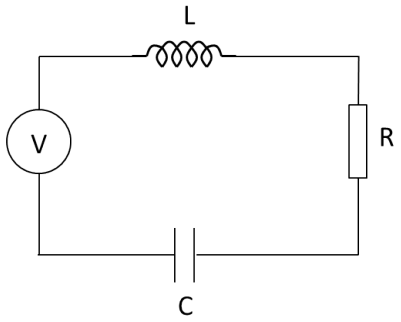

Figure 1.8: A standard LRC circuit, where V is voltage, L is inductance, R is resistance, C is capacitance and a current, i flows through the circuit

For the undamped natural frequency therefore, the only design parameter that is important is l, the draft of the OWC. For a draft of 2.5 m (used in Chapter 2), the corresponding period of resonance is 3.1 s. This is quite a short period to see in the oceans.

However, ω_{nat} is the *undamped* natural frequency. There will always be some damping due to viscosity and turbulence, and, if the OWC is to extract energy rather than simply oscillate, there must be a PTO damping.

An alternative SHO approach used in OWC-WEC modelling is based on an electrical (rather than mechanical) SHO.

In the case of a standard LRC circuit (Figure 1.8), the current, i, and driving voltage, V, are related by

$$V(t) = L\frac{di}{dt} + iR + \frac{1}{C}\int i dt \tag{1.9}$$

where L is inductance, R is resistance and C is capacitance. This may be converted into the frequency domain as

$$V(\omega) = \left(j\omega L + R + \frac{1}{j\omega C}\right) I(\omega) \tag{1.10}$$

If this relationship is written as

$$V(\omega) = Z(\omega)I(\omega) \tag{1.11}$$

and Z is the complex impedance, there then exists a simple shorthand for the voltage-current relationship in the frequency domain.

For a WEC this then becomes

$$U_{WEC}(\omega) = Z_{WEC}(\omega)X(\omega) \tag{1.12}$$

where $U_{WEC}(\omega)$ is the velocity of the WEC and $Z_{WEC}(\omega)$ is the impedance of the WEC.

More complicated systems can be analysed by additional terms in Equation (1.5), such as the air spring damping in Folley & Whittaker (2005). This is also the same basis which underpins the impedance models for a WEC (see Chapter 3) or the models which define each of the coefficients as functions of frequency, for example Alves *et al.* (2011) in which the added mass and radiation damping are calculated as frequency dependent functions.

Clearly the number of parameters that may be included is limited in this simple harmonic oscillator set-up. For a fixed mass floating buoy WEC with up to six degrees of freedom, this is no difficulty. For an OWC, however, where the internal water surface may take on many shapes, this limitation is important.

This issue goes hand in hand with the difficulty of definition of the m_c, μ and k_s terms. Experiments (either physical or numerical) must be performed which take into account a fuller picture of the water interaction.

Definitions for wave forces which include nonlinearities are also ignored. This SHO set-up is designed for linear forces and responses. The m_c, μ and k_s definitions may approximate such changes, but they cannot fully capture them. Nonlinear power take-off damping may be included as further simultaneous equations, again using bulk properties, for example, average pressure. The general approach of bulk property definitions can be very useful; few parameters are required and thus computation is relatively fast.

1.2.3 The interaction of the air with the wave-structure system

The displacement of the water surface causes thermodynamic changes to the air in the chamber. These are generally modelled as bulk properties, such that the pressure is assumed to be uniform throughout the chamber. The air does not remain in the chamber, however. The air may flow out or in through a turbine or a by-pass valve as in Figure 1.1 (Falcão & Justino, 1999).

Assuming that there is no by-pass valve, the air within the chamber volume may be thought of as being acted upon purely by the changing chamber volume, V. This volume is given by

$$V(t) = (l - h - x(t))A_w \tag{1.13}$$

where l is the full chamber height, h is chamber depth below the still water level, x is the displacement of the internal water surface with respect to the still water level and A_w is the horizontal area of the water column.

Bulk thermodynamics

This discussion follows that of Gervelas *et al.* (2011). The ideal gas law says that the pressure of a given gas is related to its volume, mass and temperature by

$$p_c V = mR^* T \tag{1.14}$$

where p_c is the pressure, V is the volume, m is the mass R^* is the molar gas constant divided by the molar mass: $R^* = \overline{R}/M_{gas}$ and T is the temperature.

Differentiating equation (1.14) with respect to time gives

$$p_c \frac{dV}{dt} + V\frac{dp_c}{dt} = R^* T \frac{dm}{dt} + mR^* \frac{dT}{dt} \tag{1.15}$$

$$\Rightarrow \frac{p_c}{V}\frac{dV}{dt} + \frac{dp_c}{dt} = \frac{R^* T}{V}\frac{dm}{dt} + \frac{p_c}{T}\frac{dT}{dt} \tag{1.16}$$

Now, if the changes are adiabatic, such that no energy is lost from the system and the process is approximately reversible (Falcão & Justino, 1999), then the product $p_c V^\gamma$ is a constant. This means that

$$p_c \left(\frac{T}{p_c}\right)^\gamma = constant \tag{1.17}$$

$$\Rightarrow p_c^{(1-\gamma)} T^\gamma = constant \tag{1.18}$$

Differentiating with respect to time gives

$$\gamma T^{(\gamma-1)} p_c^{(1-\gamma)} \frac{dT}{dt} + (1-\gamma) p_c^{-\gamma} T^\gamma \frac{dp_c}{dt} = 0 \tag{1.19}$$

$$\Rightarrow \frac{p_c}{T}\frac{dT}{dt} = \frac{\gamma - 1}{\gamma}\frac{dp_c}{dt} \tag{1.20}$$

Substituting equation (1.20) into equation (1.16) gives

$$\frac{p_c}{V}\frac{dV}{dt} + \frac{dp_c}{dt} = \frac{R^* T}{V}\frac{dm}{dt} + \frac{\gamma - 1}{\gamma}\frac{dp_c}{dt} \tag{1.21}$$

$$\Rightarrow \frac{dp_c}{dt} = \frac{\gamma R^* T}{V}\frac{dm}{dt} - \frac{\gamma p_c}{V}\frac{dV}{dt} \tag{1.22}$$

Substituting for $\gamma R^* T$, which is the square of the speed of sound in the medium, c_s gives

$$\frac{dp_c}{dt} = \frac{c_s^2}{V}\frac{dm}{dt} - \frac{\gamma p_c}{V}\frac{dV}{dt} \tag{1.23}$$

Note that in equation (1.23), the derivative of pressure is a function of the pressure. If the density, ρ of the medium is included explicitly, the fraction $\frac{p_c}{V}$ may be given as $\frac{p_c \rho}{m}$.

Thus, as $c_s^2 = \gamma p_c / \rho$, substitution into Equation (1.23) leads to

$$\frac{dp_c}{dt} = \frac{c_s^2}{V}\left(\frac{dm}{dt} - \frac{\rho}{V}\frac{dV}{dt}\right) \tag{1.24}$$

The density must be accounted for separately. The speed of sound in the fluid has already been given as $c^2 = \gamma p_c / \rho$. Differentiating with respect to time gives,

$$\frac{d\rho}{dt} = \frac{\gamma}{c^2}\frac{dp_c}{dt} \tag{1.25}$$

Thus equations have been derived to calculate the pressure difference and density for the air within the OWC chamber, but these are based on the mass flow in and out of the chamber. In order to define this, a turbine model must be chosen.

1.2.4 Modelling the turbine

In this section, two models for the mass flow through a turbine are described. First, a simple orifice model. Second, a Wells turbine model. Both of these models calculate the mass flow through the turbine on the basis of the chamber pressure difference.

Orifice models

For small scale models, an orifice is sometimes used to represent the PTO. Blocking the top of the chamber all but for a small hole of defined diameter enables the build up of pressure differences and the dissipation of energy at the edges of the orifice.

In an orifice model, the mass flow through the orifice is given by

$$\frac{dm}{dt} = -A_{ori} c_{ori} \sqrt{2\rho|\Delta p|}, \ \forall \Delta p > 0 \tag{1.26}$$

$$= A_{ori} c_{ori} \sqrt{2\rho_{atm}|\Delta p|}, \ \forall \Delta p < 0 \tag{1.27}$$

where m is the mass of air in the chamber, A_{ori} is the area of the orifice, c_{ori} is a constant the depends upon the sharpness of the transition from chamber to orifice, ρ is the air density within the chamber, ρ_{atm} is the atmospheric air density and Δp is the pressure difference between chamber and atmosphere, defined as $\Delta p = p_{cham} - p_{atm}$.

A Wells turbine model

For a Wells turbine, the mass flow is calculated using

$$\frac{dm}{dt} = \frac{-K_t D \Delta p}{N_r} \tag{1.28}$$

where K_t is some constant associated with the specific turbine design, D is the diameter of the turbine, N_r is the rotational speed and Δp is the pressure difference (Falcão & Rodrigues, 2002). For a given turbine operating at a constant speed, the mass flow is linearly dependent on the pressure difference.

This approximation is used for Gervelas *et al.* (2011) and Nunes *et al.* (2011) as well as for Falcão & Rodrigues (2002).

1.2.5 From pneumatic power to mechanical power

In using Equation 1.13 to drive Equations 1.28, 1.24 and 1.25, the mass flow and pressure may be estimated such that the energy converted may be estimated as the integral with respect to time of the pneumatic power,

$$P_{pneum} = \frac{dm}{dt} \frac{\Delta p}{\rho_{atm}} \tag{1.29}$$

Wells turbines in particular, but all turbines to some extent, do not run at the same efficiency in all conditions. That is, the efficiency of the turbine at turning the pressure drop into mechanical motion is not uniform. Crucially, there is generally a point at which stall occurs. (See Section 3.2.2.) As this is usually close to the point of maximum efficiency, anything which can alter the way the pressure head is built up can prevent the inevitable loss of power associated with a stalled turbine.

It is possible to use an efficiency model curve, as in Falcão & Rodrigues (2002), in order to have an estimate of actual converted power. Alternatively, the torque may be investigated, with losses set at fixed percentages, as for Le Crom *et al.* (2007). A model that describes the conditions under which such stall, or changes of efficiency, occur is thus vital for the development of a good estimate of energy conversion.

1.2.6 The turbine-generator interaction

An OWC-WEC is generally designed to use the fast rotational speeds generated by the air turbine for driving a generator at the fast rotational speeds needed for electricity

conversion. The efficiency of this process is around 70-80% according to Hodgins *et al.* (2008).

For more detailed design considerations, the generator settings are matched to the turbine torque as in Amundarain *et al.* (2011); Pereiras *et al.* (2011a). Such modelling is beyond the scope of this thesis.

1.3 Modelling of performance

In order to look at the performance that may be expected for a device deployed at sea, the measures of performance should be as close to wave-to-wire as possible.

The idea behind the OWC-WEC is that the energy from the waves is converted into useful energy in the form of electricity. Thus, the guiding factor is that the maximum possible energy be converted.

The amount of energy converted is very dependent on the energy that hits the WEC in the form of the wave motion. In designing the WEC only one structure may be built, but many sea states will be experienced. Therefore, the WEC should be able to change its operation with the incident sea.

As well as maximising the amount of energy converted, the WEC may have to operate with certain limits; for example, limits for turbine speed or maximum chamber pressure.

1.3.1 Annual energy conversion

Annual energy conversion can be a very useful measure of WEC performance as it averages over the various seasons within a year while also providing a physical value which can be understood.

The method of calculating annual energy conversion usually uses a numerical model in which the wave is described by a spectrum. The frequency of occurrence of such spectra are then given for different locations and the energy converted by the WEC in such conditions is multiplied by the frequency of occurrence. Of course, for a system in the real sea, the total energy converted over the year may be quoted.

Although having specific measurements for given locations is important for estimating energy conversion, and thus for deciding on the feasibility of different projects, the frequency of occurrence for spectra disguises the range of spectral shapes which are included within any frequency of occurrence measure. It is also the case that the difference between the frequency of occurrence from one year to the next can be very large (Guanche *et al.*,

2013; Neill & Hashemi, 2013).

Annual energy conversion may also suffer as a performance measure from uncertainty in energy conversion rates in large seas. Here numerical models are not at their most reliable, while the amount of energy converted is large. This difference can be made clear for the case of a WEC operating in a survival mode. For the sea state slightly below this survival mode, the energy conversion is likely to be large, while for the sea state just in the survival mode, the energy converted is zero.

1.3.2 Energy conversion in different sea states

The energy converted should therefore be presented for different sea states. This is often done as a power table (Tietje *et al.*, 2011). This enables the WEC to be relocated for an annual energy conversion assessment. Alternatively, the difference in seasonal energy conversion may be investigated if this data is available. It also enables performance to be assessed with more confidence for those sea states where a model is deemed to act well, while allowing for uncertainty in large sea state operation.

1.3.3 Efficiency and capture width

One performance parameter which is often used in engineering application is efficiency. In the case of a WEC, this is not in fact of great importance. As the waves are free, "wasting" energy does not particularly affect the cost of the converted energy. Clearly anyone owning a WEC would like that WEC to convert more energy (and thus bring in more money), but having a very efficient WEC which does not convert a lot of energy is not useful.

Capture width, C, is one way of describing efficiency for WECs. Capture width is the width that a WEC capturing all of the wave power incident per metre would be to convert as much power as the WEC in question, and is given by

$$C = \frac{P_{abs}}{\tilde{P}_{inc}} \tag{1.30}$$

where P_{abs} is the power absorbed by the WEC and $\tilde{P}_{inc}$ is the incident power per metre of wave-front (Price *et al.*, 2009). For example, if a WEC has a capture width of 4 m, this is equivalent to a perfectly efficiency WEC which is 4 m in width. If the WEC in question has a width of 4 m, the efficiency would therefore be 100%. If it had a width of 20 m, the efficiency would therefore be 20%. Capture width may be given as a function of

device size. The variables, C, P_{abs} and $\tilde{P}_{inc}$ may be taken for single frequency waves, for individual irregular sea states or for average values in a given wave climate.

If capture width is used as a way of scaling between devices of different sizes, or for identifying performance areas which could be made more efficient it can be of use. However, the values for energy conversion (average power) should be given for each sea state in order to asses performance, and thus the use of capture width is additional in energy conversion performance assessment, rather than fundamental.

In this thesis the total energy converted in a sea state will be used as the ultimate measure, but the average mechanical power converted for each sea state will also be given so that the effectiveness of such an OWC in other conditions may be estimated. Thus the conversion of energy from the incident wave to the estimated mechanical power output may be traced.

1.4 Control for OWC-WECs

As discussed in section 1.3, good performance of a WEC is deemed to have occurred if a maximal amount of energy is converted subject to constraints.

One way of increasing the amount of energy converted is to control the PTO settings to allow different amounts of air to pass in and out of the chamber through the turbine (or through a by-pass valve). There are two obvious effects of such changes. First, the air pressure within the chamber will change, which could allow power to be stored or dissipated at different rates. Second, the turbine will convert more or less energy due to the changing mass flow. Thus, if such mass flows are controlled effectively, an increase in converted energy may be possible.

In this section, some general control types will be introduced. Then the parameters that may be controlled in a OWC-WEC will be explored in Section 1.4.2. In Section 1.4.3, those methods of control used for WECs in the literature will be covered. Section 1.4.4 will explore those considerations which must be taken for OWC-WEC control specifically. Finally, in Section 1.4.5, the control methods used in this thesis will be briefly described.

1.4.1 Types of control

Before discussing OWC control specifically, it is worth looking first at some generic control options. First feedforward and feedback control will be described (Leigh, 2004); then an overview of model-optimiser control will be given (Rossiter, 2003).

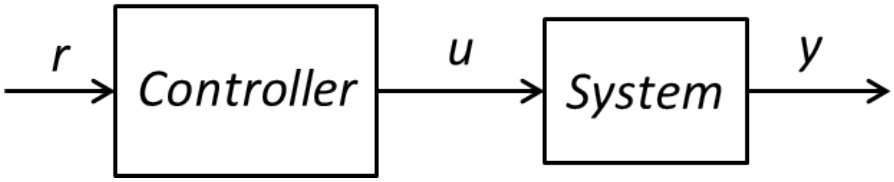

Figure 1.9: A feedforward controller

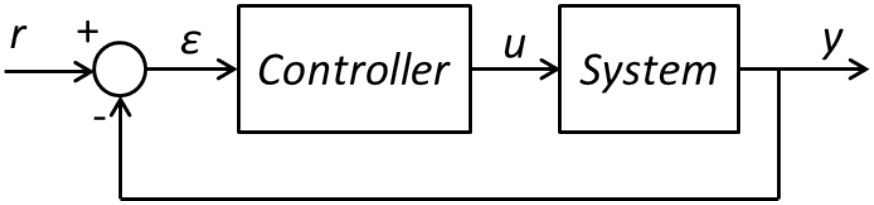

Figure 1.10: A feedback controller

Feedforward control

A very simple type of control for any system is the feedforward controller. Here, a reference input, r, is given to the controller and a rule is applied to produce a control signal, u. This control signal is then fed to the system, resulting in an output y. However, the optimality of the output (be it tracking of the reference, r, or energy maximisation) is sensitive to modelling errors and disturbances. An example of such a controller is shown in Figure 1.9.

Feedback control

If it is important that the system follows the reference with accuracy, then a feedback controller may be used. Here the controller acts to minimise the error between the reference and the system behaviour, $\epsilon = r - y$. A diagram of this controller is shown in Figure 1.10.

An example of this type of control is a thermostat. There is a desired temperature setting (r) and the heating/cooling system must change u so that the actual temperature (y) is kept at the desired point.

Model-based controllers

If the desired behaviour of a plant's output is a maximisation, for example an OWC maximising converted energy, an MPC controller can be used to calculate the best control settings to optimise energy output over some time horizon, time-step by time-step (Cretel *et al.*, 2010; Bacelli *et al.*, 2011; Li & Belmont, 2013). Such a controller is shown in Figure 1.11.

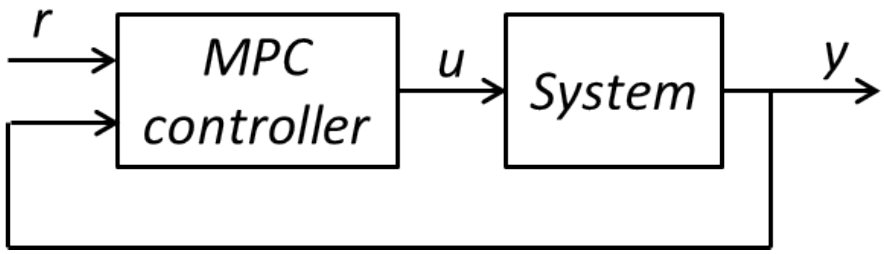

Figure 1.11: A model predictive control (MPC) controller in a system

For example, it is possible that at time, t_0, the expected inputs from t_0 to some time in the future, t_n, are known. The controller has some initial settings which will result in the unchanged outputs. The model predictive control (MPC) algorithm chooses the controller settings at each time step such that the maximum energy output is achieved overall. This would be due to the changed energies at each time step. The settings that give these changed energies will be implemented for t_0 and the next time-step, t_1. At t_1, the expected input at time t_{n+1} will be known and the process will begin again, with an initial t_1 to t_{n+1} unchanged energy set. The best overall changed energy set will again be calculated and between $t = t_1$ and $t = t_2$ (the next time-step), the appropriate settings will be used. This continues for each time step.

There are some difficulties in implementing MPC on OWCs. First, the expected input may not be known very far into the future. Cretel *et al.* (2010) tried an MPC which used the current input as the expected input over the future window. Many researchers are looking at improving the accuracy and horizon length of such predictions by using time series-based techniques or spatially distributed measurement systems (Belmont, 2010; Fusco & Ringwood, 2010).

The second major issue comes from (not) knowing the effect of the controller settings on a system such as an OWC. MPC is generally done using linear (or reasonably linearisable) systems for which there exist fast ways of performing the optimisation for such systems. For the OWC, the MPC would not be linear, although producing piece-wise linearisation could be an option. Nonlinear MPC methods do exist, but are computationally involved: they work by testing a random controller settings set and refining it into the future. The difficulty is that in order to set up the algorithm, the energy is needed as a function of the controller settings, but it is only possible to have the energy as a function of the controller settings *and* the pressure *and* the mass flow *and* the input wave. This makes the calculations take much longer.

1.4.2 Parameters for control of OWC-WECs

In order to make a controller, it is important to distinguish those parameters which may be controlled and those which such control may be based on. Control may be based upon thermodynamic parameters such as chamber pressure and mass flow, but these may not be directly manipulated. A real variable of the system should be used to change a real parameter of the turbine.

Turbine speed control

The turbine speed may be manipulated, although on a real system this would be changed by controlling generator torque. The pressure difference between the chamber and the atmosphere, for example, could be used as an input, with the turbine rotational speed as output. In order to do this, the controller must have some way of calculating the new speed.

The controller could use some fixed speed, which is chosen due to experience with the turbine, the sea states, the OWC or knowledge of their joint behaviour. A controller could also use a rule-based system. This could have some mapping developed through trial and improvement on the real system (Amundarain *et al.*, 2011), or on a model.

Valve position control

It is possible for a controller to use valve position to regulate the chamber pressure and mass flow through the turbine. For example, Monk *et al.* (2013) changed the position of a by-pass valve and Lopes *et al.* (2009) investigated a latched control method based on whether a shut-off valve is open or closed.

Combined turbine speed and valve position control

Of course, it would be ideal if the turbine and the valves could be controlled together. It would be possible to have the controller change the position of a valve relatively slowly, as in Monk *et al.* (2013), and combine this with control of the speed of the turbine. The best scenario is one in which the two controllers may exchange information about what their current settings are and what they are about to do. If one of these controllers or a master controller gives instructions to another, this would be an example of hierarchical control. Such control is beyond the extent of this thesis.

Damping control

Control of PTO "damping" is often discussed for WECs. This means controlling the $-\mu\dot{x}$ force in Equation (1.6). Some of this force is due to radiation damping and some to turbulence, but if the WEC is to convert energy, then some must be due to PTO. The damping force, f_μ, may therefore be broken down into components as

$$f_\mu(t) = -\mu_r\dot{x} - \mu_t\dot{x} - \mu_{PTO}\dot{x} \tag{1.31}$$

where μ_r, μ_t and μ_{PTO} are the damping coefficients associated with radiation, turbulence and PTO. It should be noted that these damping coefficients do not have to be scalar constants: they may be frequency dependent.

In the case of an OWC-WEC, "damping" is not a very physical parameter in comparison to the case for a floating buoy WEC where PTO may be proportional to speed. As such, it will not be used in this thesis.

1.4.3 Controller methods used for WECs including OWCs

Much of control design for WECs is concerned with the response of devices which respond smoothly across a range of frequencies, with one particular resonant period dominating the motion. (A review is given in Freeman *et al.* (2014).) For an OWC-WEC with closely packed columns, the internal water surface displacements will not change smoothly with frequency, but will be sensitive to period. Thus, control for such an OWC-WEC is likely to be different to that established for WECs with a smooth response.

The distinctions between smooth and latched control

One of the difficulties in WEC control is that sometimes power must be added to the system so as to increase the overall energy taken out. This means that the PTO equipment must allow for bidirectional power flow, which increases the cost of the PTO equipment and also may increase the fatigue cycling and thus the likelihood of failure. One way around this is to latch the WEC. This involves stopping the motion at the extreme point, which is when velocity is zero and thus no work is required. Some time later, the WEC is released and the power converted during its return in direction is greater than if the WEC were allowed to move freely. Clearly the key variable for control then becomes the moment at which unlatching occurs (Hals *et al.* (2011)).

In an OWC-WEC, this latching strategy requires a little alteration (Lopes *et al.*, 2009). Instead of latching a fixed mass buoy, the air chamber is cut off from the surrounding atmosphere by moving a shut-off valve into position very quickly. The mass of air within the chamber will then remain the same while the water around it is acted upon by the wave around the column. This leads to a greater pressure difference between chamber and surroundings, and thus greater air flow once the valve is reopened.

There are some difficulties with this set-up. The valve must not require a lot of energy to move, or to fix in place. The air pressure may fluctuate due to compressibility, which is seen at small scales in Lopes *et al.* (2009). The large fluctuations in pressure negate the beneficial effect of the latching. The turbine is entirely deprived of air-flow during large fractions of the wave cycle, so its inertia must be made very large, and its design must avoid stall and air-flow separation which could damage the blades. Also, the power taken out will not be so smoothed, which could have implications for the price of the electricity from the WEC, due to the variability and potential energy storage requirements.

Control in the frequency domain

Returning to the electrical SHO impedance matching discussion of Section 1.2.2, it is possible to find a mathematically optimal control solution for smooth control. Following Falnes (2002b), it may be stated that the speed of WEC motion is proportional to the excitation force, $F(\omega)$ and to the intrinsic impedance of the WEC, $Z_{WEC}(\omega)$ and its PTO, $Z_{PTO}(\omega)$, such that

$$F(\omega) = \left(Z_{WEC}(\omega) + Z_{PTO}(\omega)\right) U(\omega) \tag{1.32}$$

In order to increase the converted energy, total power conversion across the frequency domain should be maximised. This leads Falnes (2002b) to

$$Z_{PTO}^{ideal}(\omega) = Z_{WEC}^{*}(\omega) \tag{1.33}$$

where $Z_{WEC}^{*}(\omega)$ is the complex conjugate of $Z_{WEC}(\omega)$.

The ideal PTO settings are thus of the same magnitude as the intrinsic impedance, but with a 90° phase shift. In the OWC case, the Z_{PTO} includes the impedance due to the chamber pressure, turbine and generator. Z_{WEC} is the hydrodynamic impedance only.

In order to convert the maximum energy, therefore, the WEC must be able to have control operating at the different frequencies at any moment, and must be able to foretell

the excitation force, $f(t)$, into the future, as $F(\omega)$ has information based on frequency which necessarily must extend to future waves.

Tuning requires that the reference setting, based in some way on the Z^*_{WEC}, must be converted into settings for the real system. Fundamentally, the "damping" value must be converted into something in reality.

Control of multiple units

If there are the five OWCs described in Chapter 2, they interact in the sense that the water moves differently around each individual purely owing to the presence of the others, whether they are converting energy or not. Other multiple unit formations are possible, for example, a spaced array of single buoys, some line of pitching flaps, or some attenuators along a coast line. Thus if the interactions between the WECs may be understood, then the PTOs may be controlled so that the greatest energy is converted (Westphalen *et al.*, 2011).

Presumably the objective is to extract the maximum energy from the group overall. If the WEC which sees the wave front first extracts the maximum energy that it can, those behind it may find that they are operating at low efficiencies and thus not converting very much energy. In effect, each WEC is an agent in a free market. This does not necessarily lead to a good overall energy conversion. Also, WECs deployed as free agents do not share wave information that might be able to improve performance in the others.

Considering the breakwater OWCs again, it might be beneficial under certain wave conditions in the breakwater to switch off some of the WECs according to their linked motions - increasing the motion in the ones which are on and getting them to work in an efficient range. Looking to economics or biomimicry may also be of benefit in having the WECs work together. It could be possible to give each individual simple rules and a little information about the others - such as occurs in flocks and shoals. Such an approach was taken by Mundon (2006) for a buoy-WEC.

Another alternative is one in which there is a master controller which gives each WEC specific instructions. However, the time delay in getting these instructions to each WEC could be a considerable hindrance.

A likely scenario is one in which there is a high level controller that gives objectives to each WEC's controller based on the amount of energy available at the site of each one, and it is up to the low level controllers to select options to achieve these objectives.

1.4.4 The purpose of OWC-WEC control and considerations for controller design

OWC-WEC control must enable a maximisation of converted energy within certain limits: the internal water surface should not be allowed to reach the turbine and the turbine should not be allowed to overspeed.

The ideal controller would also be able to respond to different sea states and incident waves, such that the power output could be smoothed.

Another scenario in which control would be useful for OWC-WECs is arrays. Here it may be possible to increase energy output over the farm by decreasing the energy converted by some OWC-WECs so as to change the waves which reach others and therefore increase their converted energy. This clearly requires the ability to control each of the OWC-WECs.

Parameters to control in an OWC-WEC

In an OWC-WEC, the parameters that may readily be controlled are the position of any valves and the rotational speed of the turbine. Some turbines allow for changes in the pitch of the blades or the angle of guide vanes (Cooper & Gareev, 2007; Takao & Setoguchi, 2012).

Method for control of an OWC-WEC

For an OWC-WEC, a feedforward controller is the most readily accessible. If the output described in Figure 1.10 is assumed to be power, there is no "path" for it to follow, so feedback control is not useful here.

(There is a place for feedback control in OWC-WECs. This is when the actuation of the turbine speed is assumed not to happen instantaneously. Then u is the desired turbine speed, from a feedforward controller, and y is the actual turbine speed.)

Given that the aim of a WEC is to convert the maximum energy over a given time-frame, it may seem strange that model predictive control (MPC) is not more commonly used. This is because any incident wave prediction will give quite a large range of possible future wave heights and the effect of changing turbine speed on pressure and mass flow is nonlinear, so the standard linearisations may not be used. This makes an MPC controller computationally intensive, which is not a good first step when simple rules may give large increases in energy conversion.

1.4.5 Control methods used in this thesis

In this thesis, tests are made for two controllers. In order to manage the calculations, the controllers are optimised offline for one sea state only, the sea state at the chosen location which contains the greatest average annual energy. The controller is assumed to be able to change the turbine speed instantaneously.

Fixed speed control

Different rotational speeds are tested on the turbine to provide a baseline and to investigate which speeds lead to good energy conversion. For the fixed speed control, the turbine speed is given (in $\mathrm{rad\,s^{-1}}$) by

$$N_r(t) = N_f \tag{1.34}$$

where N_f is the fixed turbine speed, which is not a function of time.

A linear controller

The first controller is a linear one, a proportional controller. The controller has two parameters: the base speed (or offset), N_l, and the proportional coefficient, K_l. The turbine speed is given in $\mathrm{rad\,s^{-1}}$ by

$$N_r(t) = \frac{2\pi}{60} N_l + \Delta p K_l \tag{1.35}$$

Turbine efficiency control

Because turbine efficiency has such a large effect on the transformation of wave energy to mechanical energy, a turbine efficiency controller is tested. This ensures that the turbine is always operating at its maximum efficiency by changing the speed of rotation such that the non-dimensional pressure, Ψ, is that for which turbine efficiency is a maximum. This gives a control law of

$$N_r(t) = \frac{1}{D}\sqrt{\frac{|\Delta p|}{\Psi_\eta \rho}} \tag{1.36}$$

where Ψ_η is the non-dimensional pressure at which the efficiency is greatest. The other parameters are the turbine diameter, D, the pressure difference, $|\Delta p|$ and the air density, ρ. Note that it is the *turbine* efficiency which is controlled using this rule and not the efficiency for the OWC-WEC as a system.

1.5 Thesis plan

In order to discuss a breakwater OWC simply and generically, but with enough detail to be of interest, a fixed breakwater was chosen and positioned on a flat sea bed that is in fairly shallow water. It has the sea surrounding it rather than forming a shoreline cliff.

Using the velocity potential method, an isolated device is modelled first to test the results against previously published theory, then further chambers are deployed beside it to a total of five. This enables many possible modes of resonance of the water columns, but has manageable calculations and physical comprehensibility. 1-, 3- and 5-column configurations are used so as to retain symmetry. This enables clear parallels to be drawn with the isolated column.

No PTO is assumed (no lid is included in the calculation). This is because the first step is to drive a conceptual controller rather than to model a specific PTO.

In Chapter 3 a force-displacement transfer function approach is used to model the hydrodynamics of the central column in the time-domain. This is combined with equations for the thermodynamics and turbine to give a wave-to-mechanical power model of the central column OWC-WEC.

The performance of the OWC-WEC is tested in Chapter 4 for fixed speed turbine operation for the wave climate of a site in South West England.

Finally, in Chapter 5, a linear and nonlinear control scheme are tested on the OWC-WEC for this site.

Discussion of the results of the study is done in Chapter 6, with the conclusions to be drawn in Chapter 7.

Concluding remarks

An OWC-WEC converts the energy of ocean waves into electricity via an air turbine. OWCs forming breakwaters have not been tested extensively, especially not numerically, or involving models which build up from a single device to multiple units. Because these devices are located with close neighbours, the changes seen to their response profile in comparison to an isolated device may have implications for the control system, both for the controller for an individual OWC and for control options based on multiple PTOs. Controllers for an individual WEC within the breakwater setup are tested.

Summary

- An OWC-WEC is a device which converts wave energy into electricity using the motion of a water column to force the movement of air through a turbine.
- In order to improve performance (increase converted energy), a feedforward controller may be used to change the turbine speed, and thus the mass of air flowing through the turbine and the pressure of air in the chamber.

Chapter 2

Hydrodynamics of a breakwater mounted OWC

For an OWC, clearly the waves incident upon the structure are what drives the power conversion. The motion of the water within the column of the OWC will generate radiative waves, and the waves will be diffracted by the structure. The displacement of the water surface in the OWC will therefore depend on the structures around it and the motion of the water within any other columns.

To calculate the position of the water surface and the force imparted by the waves a velocity potential method was used. The mathematical method used will be presented in Section 2.1. For any system more complicated than the very simplest geometries, a solution must be sought via a numerical software. Results are presented in Section 2.2 of the numerical modelling of the free surface response for an isolated rectangular OWC, and moving through various stages to a five-column, breakwater-mounted OWC. The responses of the isolated and breakwater cases are given in aggregate in Section 2.2 and discussed in Section 2.3.

This chapter is about the wave interacting with the OWC under the assumption that there is no power take-off (PTO). For PTO inclusion, see Chapter 3.

2.1 Velocity potential method for fluid structure interaction

In order to calculate the displacement of the internal water surface for an OWC, a velocity potential method was used. Figure 2.1 shows the relevant surfaces and directions for such a method when applied to an OWC. In the velocity potential method, the fluid flow, $\boldsymbol{u}$,

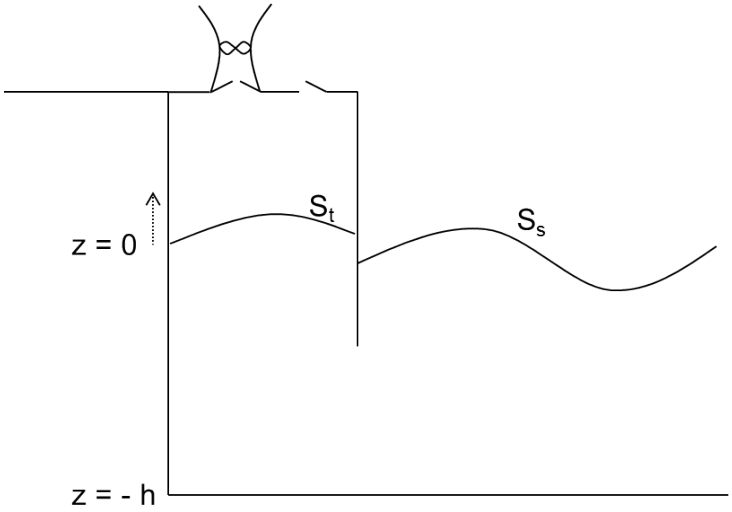

Figure 2.1: The surfaces for a velocity potential solution

is defined by a velocity potential, ϕ, using the equation

$$\boldsymbol{u} = \boldsymbol{\nabla}\phi \tag{2.1}$$

where ∇ has its standard definition as $(\partial/\partial x, \partial/\partial y, \partial/\partial z)$.

Assuming that the fluid flow is incompressible, there must be no divergence within the fluid. Thus,

$$\boldsymbol{\nabla}.\boldsymbol{u} = \nabla^2\phi = 0 \tag{2.2}$$

That is, ϕ must be a solution to the Laplace equation within the fluid.

Green's theorem may be used to simplify the calculation of these velocity potentials. Instead of calculating a velocity potential based on the full volume, the surface of the volume may be used instead.

Rather than requiring that the volume integral

$$\int_V \boldsymbol{\nabla}.\boldsymbol{A}.dV = 0 \tag{2.3}$$

be calculated, the surface integral may be used

$$\int_S \boldsymbol{n}.\boldsymbol{A}.dS = 0 \tag{2.4}$$

where V is the volume of fluid under consideration, $\boldsymbol{A}$ is *something*, S is the surface of that volume and $\boldsymbol{n}$ is the normal vector out of the volume at that surface.

Following Falnes, p91 fft, a finite region of the ocean may be considered. See Figure

2.1. Here the surface, S, that surrounds this volume is divided into five parts:

- S_s, the free water surface
- S_b, the sea bed
- S_∞, a surface connecting the free water surface and the sea bed
- S_t, the internal surface of the OWC
- S_w, the wetted surface of the structure

Now, these velocity potentials must also obey certain boundary conditions. On S_b,

$$\frac{\partial}{\partial n}\phi_{i,j} = 0 \tag{2.5}$$

and on S_s

$$\left(\omega^2 + g\frac{\partial}{\partial n}\right)\phi_{i,j} = 0 \tag{2.6}$$

2.1.1 OWC applications of the velocity potential method

Starting from very simple geometries, OWCs have been modelled using the velocity potential method. In one of the defining papers on OWC modelling, Evans & Porter (1995), assumed a 2D cliff-based OWC. The small-scale experiments performed by Sykes *et al.* (2007) are for fixed cylinder structures in the open ocean. The first structure is short, and is compared numerically with the method outlined by Mavrakos (1985). The second structure is long (deep) and thin. This structure is modelled using WAMIT and compared with experiment. Pressures (for the long structure) and forces (for the short structure) are used rather than displacements to describe the open OWC. The floating version of this structure is then described in Sykes *et al.* (2009). A similar structure was investigated by Sphaier *et al.* (2007). A fixed experiment was undertaken in deep water on a short cylinder with different sizes of openings at the base of the structure. Floating OWCs of different symmetrical shapes were also investigated using velocity potential methods for the buoy designs of Gomes *et al.* (2012) and Lopes *et al.* (2007), as was the bent duct buoy of Bull & Johnson (2013).

For fixed devices at the shoreline, a very specific model may be used which incorporates the bathymetry of the site, as in Brito-melo *et al.* (1999) or Delaure (2003). These studies are for OWCs which are cliff-mounted and sloshing plays a major part in the dynamics. Martins-rivas & Mei (2009) studied a cylindrical OWC forming part of a cliff and also saw sloshing modes, thus the sloshing is assumed to come from the way that the incident wave

interacts with the back-board formed by the breakwater, rather than from the shape of the water column.

As well as single, fixed devices, arrays of OWCs have been investigated using velocity potential methods. An array of four fixed cylinders in the open sea was investigated by Nader *et al.* (2012). A configuration in which multiple water columns exist at a shoreline-type site is the breakwater configuration. Here the columns are packed next to one another forming a wall. This has been described for one device by Hong & Hong (2012) with two neighbouring columns the future part of their set-up. According to Pontes *et al.* (2005) a study was made for the proposed Duoro breakwater OWC plant in Portugal, but no details are given.

2.1.2 Opportunities for use of the velocity potential method

The velocity potential method has therefore been used to model the water interaction with a structure under a variety of operational conditions. The difficulty in implementation lies in the incorporation of the PTO.

A study of multiple water columns in a breakwater configuration is ripe for investigation, particularly if the results may directly be compared to a similar single column design with no breakwater around it. Such comparison would enable testing of the PTO model, as well as enabling an evaluation of the back-board effect of the breakwater. It would also give an insight into the way the individual columns combine motion to form coupled modes.

2.2 Water surface study

In this section, the method and results of a water surface study will be presented. The interaction of the water column and the PTO forcing will be investigated in Chapter 3. For the water surface study, no PTO damping was included. Thus, it is the behaviour of moon pool-like structures which are modelled and investigated, a moon pool being a structure with a completely open roof.

A breakwater OWC structure was the ultimate aim of the modelling campaign, but in order to check the PTO system against known responses, an isolated OWC of the same dimension as the breakwater chambers was also considered. The breakwater structure was built up systematically. Once the isolated OWC had been considered, the breakwater itself was included. This is shown schematically in Figure 2.2. Note that the sea bed and

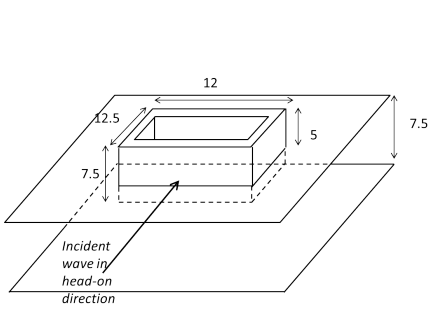

(a) The isolated moon pool

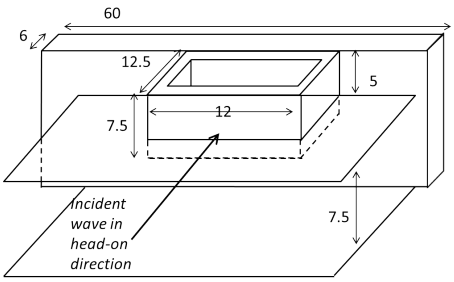

(b) The single (shallow) moon pool with breakwater

Figure 2.2: Basic geometry of the moon pool. All dimensions are given in metres and the wall thickness is 1m. Drawing not to scale.

ocean surface shown in this figure are indicative only: in fact, the sea extended 100 m from the centre of the OWC in each direction.

Chambers were positioned either side of the central one to form a breakwater with three columns. Finally two more columns were included such that a five OWC structure existed. Five columns enable the columns to act somewhat like they are in a long breakwater set-up, but for quite a simple structure which can still be understood in overview. The one-, three- and five-column structures were chosen so that the structure would be symmetrical and directly comparable to the isolated system. The size of the columns is based on that suggested for a site off the north coast of Scotland (Voith Hydro Wavegen, 2012), but is similar to that envisaged by Hong & Hong (2012).

Two extreme examples of OWC positioning may be considered in order to illuminate the choice of a five column system: these are an entirely isolated, single device and an OWC which is one of an infinite line of devices facing the sea along a coast. In the isolated case, no other OWCs interact with the WEC, while for the infinite line, no wave ever hits the edge of the structure and thus there are no interactions in which the system and wave have regions where the wave in mostly unhindered and regions where interaction is strong. Five pools was chosen as a good number, because it is odd and can therefore give simple comparisons to the isolated case through symmetry arguments, but also gives enough chambers so that the water motions no longer form the same profile as for the isolated WEC.

2.2.1 The test programme

Initially the response to waves of an isolated system is presented. This is then compared to a geometrically similar shallow-walled moon pool attached to a breakwater. Next, the

effects of deep walls are studied. The fourth step is to attach similar deep-walled columns to either side of the central moon pool to produce a three-pool system. Finally, a five-column structure is investigated. Consider two extreme examples of OWC positioning: an entirely isolated, single device and an OWC which is one of an infinite line of devices facing the sea along a coast. In the isolated case, no other OWCs interact with our WEC, while for the infinite line, no wave ever hits the edge of the structure and thus does not have an interaction in which it is partly interacted with and partly allowed to pass unhindered (or interact & be completely reflected from a cliff). Five pools was chosen as a good number, because it is odd and can therefore give simple comparisons to the isolated case, but gives enough chambers that the water motions no longer form the same profile as for the isolated WEC.

The test programme consisted of finding the (heave/vertical) response amplitude operator (RAO) and phase for each point in a grid 20 m by 20 m around the centre of the rectilinear moon pool column, for a range of waves with periods from 3.0 to 17.5 s. The RAO is the ratio of displacement seen with the structure, to the displacement seen without the structure (i.e. the ratio to that for an undisturbed wave). For example, if the displacement of the internal water surface of the column were 2 m, for an incident wave with amplitude 1 m, the RAO would be 2. The response is analysed first for waves incident head-on, then for waves incident at 30 °, 45 °, 60 ° and 90 ° to this direction.

To begin with, the column is assumed to be isolated (i.e. not part of a breakwater), but still of the same size and draft as it would be if there were a breakwater. It is also assumed that the water depth is the same as for the columns with breakwater. Next, a breakwater is included immediately behind the column. The breakwater has a length of 60 m. Thus the water may flow around the breakwater. The breakwater is assumed to extend from the sea floor to 5 m above the surface (the same height as the air chamber). This is different to the structures investigated by Ruol *et al.* (2011) and by Koo (2009), which are formed from floating breakwaters.

The assumption of water deep enough for OWCs but shallow enough for walled breakwaters is true in many parts of UK waters as well as in Northern Spain and South Africa (Vögler & Morrison, 2013; Heath, 2007; Joubert & Niekerk, 2013). Of course, for a wall structure, the tidal range will also be important as this will affect the draft of the columns during operation. Tidal range was not taken into account owing to the nature of this study being an initial exploration. In order to incorporate tidal variation, the velocity

potential calculations should be conducted using a range of different water depths, and the outcomes incorporated into the time domain model.

The model of the water at the base of the breakwater is not ideal. The real-world system would have turbulence that cannot be modelled using a velocity potential method. The lowest 1 m of wall to the sea bed is therefore assumed to be non-diffracting. This means that it is not fully included in the calculations.

2.2.2 The numerical solver

For a grid of points around geometrically similar structures, this study used ANSYS™ AQWA® to produce the response amplitude operator (RAO) and the phase at which this response occurs. This meant that the displacement seen for the water surface around moon pools, breakwaters and multi-column systems could be quantified.

The software solves the standard velocity potential theory given in Section 2.1 (see Falnes (2002b), ANSYS (2012)) with a mesh of panels. The mesh is generated automatically, based on defined maximum and minimum element sizes. Depending upon the frequency of the waves that should be considered, the size of the mesh should be chosen such that the features of the structure may be resolved: a shorter wavelength wave will require a finer grid so as to interact with the correct forces. The smallest element dimension of the chosen mesh is 0.5 m and the largest is 2 m. This enables a range of periods of regular waves, from 4.0 s waves to 17.5 s waves, to be investigated with confidence, based on the wavelength and how the structure is divided into the mesh panels.

Because a breakwater-mounted OWC is likely to be influenced by its proximity to the sea bed, such a sea bed must be specified. An ocean with horizontal bathymetry was used, with 7.5 m water depth. The water motions near the sea bed can be difficult to handle numerically. As such, the panels representing the structure nearest to the sea bed are assumed to be non-diffracting.

As the range of periods of interest for an OWC is 3.0 s to 20 s, and some of the structures are 2 m wide, a maximum element size was chosen as 1 m. The extent of the ocean around the structure was chosen to be large because the proposal was to look at how the water moves rather than how the structures move, thus a 200 m by 200 m ocean was chosen.

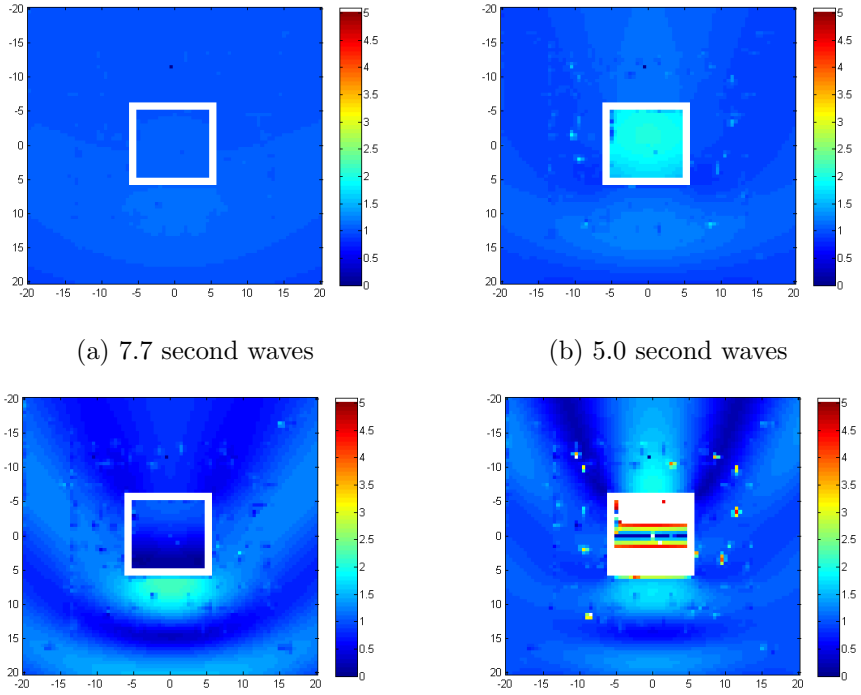

(a) 7.7 second waves

(b) 5.0 second waves

(c) 4.03 second waves

(d) 3.38 second waves

Figure 2.3: The RAOs (response amplitude operators) for an isolated moon pool with short walls in shallow water (dimensionless units). The regular wave is heading up the page. The x and y axes show the position from the centre in metres.

2.2.3 An isolated shallow moon pool

First, an isolated moon pool in shallow water with short walls is considered. This is the case shown in Figure 2.2a. The wall is fixed at the sea surface with thickness 1m, length 10.5m, breadth 10m and draft 2.5m. The wall is semi-submerged, with 5m above the waterline. The incident waves have a height of 1 m (amplitude 0.5 m).

Figures 2.3 and 2.4 show a bird's eye view of the OWC, with the amplitude and phase of the response of the free water surfaces to regular wave incident head-on to the structure given by the colours. The numbers on the left side and at the bottom of the maps are the distance in metres from the centre of the OWC. The response amplitude operator (RAO) over the whole wave cycle is shown as a colour from blue (0) to red (5). The structure is shown as white, with any wave motion larger than an RAO of 5.0 also shown as white. The same convention continues throughout the rest of this chapter. An RAO of 0 means no water motion no matter the amplitude of the wave, while an RAO of 5 means that the resultant displacement is five times as great as the incident wave.

For low frequency waves the motion of the water surface moves with the same amplitude and phase within the pool as it does for the wave outside the pool. This is shown in Figures

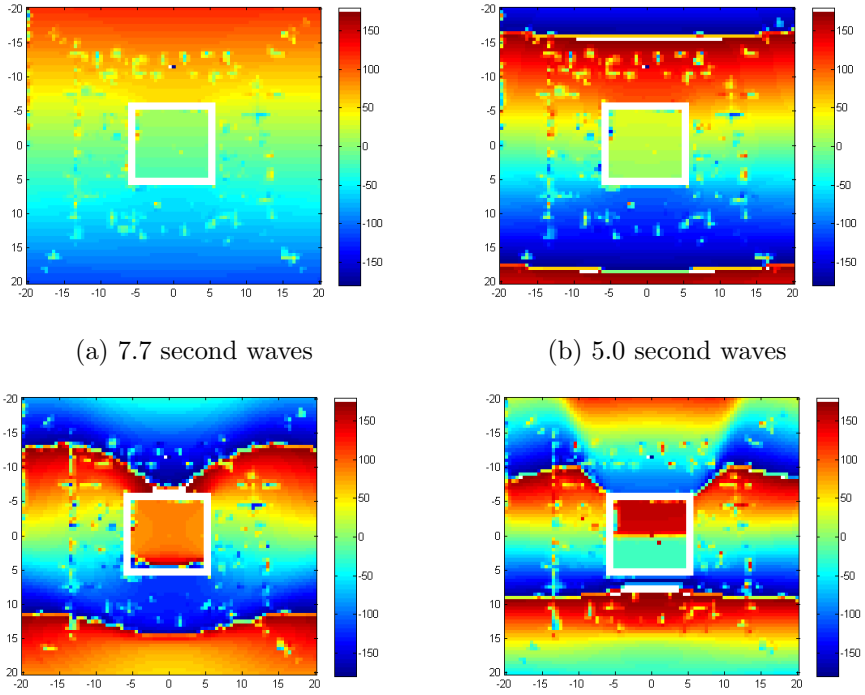

(a) 7.7 second waves

(b) 5.0 second waves

(c) 4.03 second waves

(d) 3.38 second waves

Figure 2.4: The phases (in degrees) for an isolated moon pool with shallow walls in shallow water.

2.3a and 2.4a. For waves with 5.0 s periods (Figure 2.3b), however, the water in the moon pool appears to be amplified with an RAO of 2. That is, movement twice that of the incident wave. This motion is not out of phase with the motion of the water around it (Figure 2.4b), as would be the case for motion at the resonant frequency. The phase for resonant motion is 90 °. This must occur for periods between 5.0 s and 4.03 s because in Figure 2.4c, the phase has reached 100 °.

Note that the numerical calculations here assume that the motion is linear. Thus, for a wave of 1 m amplitude (2 m wave height), an RAO of 2.5 will produce a motion with 2.5m displacement, which in the case of the moon pool under discussion would result in the column surface falling below the front lip of the column. This is clearly not within the linear regime, so such RAOs must always be used with caution. Such RAO is viable for small amplitude waves.

Figures 2.4a-2.4c show that the motion of the water surface in the moon pool is piston-like. The phase across the whole area is the same, so the surface is moving as one unit. For the high frequency 3.38 s waves in Figure 2.4d, this is clearly not the case. Here the motion between the front and the back of the pool is in anti-phase, with the surface pivoting about the centreline. When the water at the front is up, the water at the back

is down, and vice versa. The motion in the middle is very small (Figure 2.3d). The water surface at the front and back is given an RAO above 5, which is very large. A wave with amplitude 0.5 m (height = 1 m), such as that used to generate these figures, would produce motion in which the water surface would drop below the lip of the column. The motion described by Figure 2.4d is sloshing motion, which is not good for energy conversion in an OWC. While the water surface moves, the volume of air above the chamber does not and therefore air would not be pushed through the turbine. This type of motion should be avoided in OWC design. Here it is only seen for high frequency waves.

2.2.4 A shallow moon pool with breakwater

Section 2.2.3 described the response of the free water surface around an isolated fixed moon pool. This is only part of what an OWC would really be like. Fixed OWCs are very likely to form part of a breakwater structure, which has different hydrodynamics, particularly with regard to diffraction or scattering. As such, the first step taken to modelling an OWC which forms part of an array of OWCs along a breakwater is to model the hydrodynamics around a single OWC, but still one which is fixed to a breakwater.

Figure 2.2b shows the layout of the breakwater system now considered. As for Figures 2.3 and 2.4, Figures 2.5 and 2.6 show the RAO and the phase, respectively, for the water surface around a structure consisting of a single, shallow moon pool and a breakwater. Again, the structure is shown whited-out in the surface contour plots.

A crucial difference between the responses of a circular moon pool that formed part of a breakwater and those of an isolated system was described by Martins-rivas & Mei (2009). They saw that the piston mode (with high RAO and uniform phase within the pool) was dominant in the case of an isolated moon pool, but that this mode was not achieved for a moon pool as part of a breakwater. In fact, the sloshing modes were seen to be significant. The angle of incidence of the incoming wave also affected the motion, with sloshing modes more apparent for angles further from the head-on angle.

For the low frequencies, Figures 2.5a and 2.5b, the motion within the pool has an RAO larger than one. Note that the incident waves shown here are of longer period than those shown in Figures 2.3a and 2.3b. Now the breakwater prevents the wave from flowing through the domain and means that the water backs up at the centre of the breakwater. As this is within the moon pool structure, this amplification is captured within the chamber. However, it should be noted that the amplitude of motion of the wave on either side of

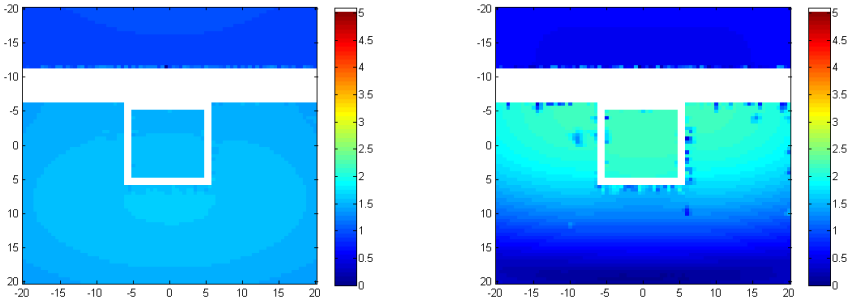

(a) 17.49 second waves

(b) 9.54 second waves

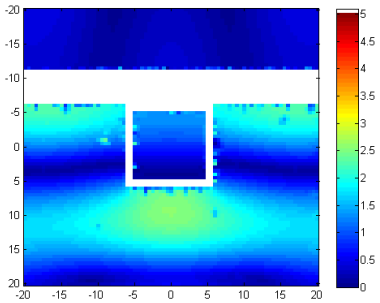

(c) 5.0 second waves

Figure 2.5: The RAOs for a single, shallow moon pool in front of a breakwater

the pool is also made large, so the difference is not due to the presence of the moon pool structure itself. (Note that this is the case for the shallow moon pool. The deep moon pool shall be covered in Section 2.2.7.)

Note the case of Figure 2.5c. For the case of an isolated structure with no breakwater, as seen in Section 2.2.3, 5.0 s was the wave which resulted in the greatest amplification. With the inclusion of the breakwater however, the RAO drops below 0.5 within the moon pool. The increased displacement ahead of the structure produces an RAO there of 2.5. Presumably the decreased response within the pool is due to the reflections from the breakwater interfering destructively.

2.2.5 The effect of the angle of incidence of the regular wave

Although the coastline position of a breakwater will lead to waves being incident with a prevailing direction, this will not be always 0 °. Thus, the effects of different angles of incidence were investigated.

For the isolated moon pool, it was found that almost no change in response is noticeable for changing the angle of incidence of the incoming wave. This is not the case for a system with a breakwater. While Figures 2.5 and 2.6 show the free water surface response to waves incident head-on to the breakwater and moon pool structure, for waves at an angle,

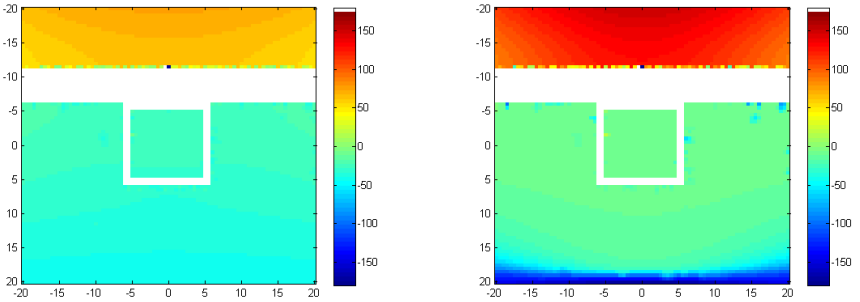

(a) 17.49 second waves

(b) 9.54 second waves

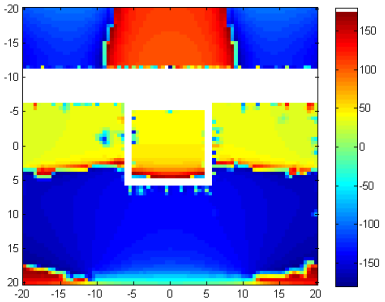

(c) 5.0 second waves

Figure 2.6: Phase response for a single, shallow moon pool in front of a breakwater

the response may be somewhat different, as in Figures 2.7 and 2.8, where the response to waves incident at 30 ° to the normal is shown. Consider Figures 2.5a and 2.7a, which both show the RAO for 17.49 s waves. In the case of waves incident perpendiular to the breakwater, the motion is very small, but when the wave is incident at 30 ° from that plane, the motion is very large: larger than the largest motion observed for the normal alignment (0 °) case. The phases are now different, with the water surface bulging around the structure, as can be seen on the right hand side of Figure 2.7b. As well as leading to asymmetry along the length of the breakwater in terms of increased amplitudes to one side of the column, there are also changes to motion prependicular to the breakwater. In Figures 2.7c and 2.8c, the motion of the free water surface within the moon pool is observed to have a phase which is uniform across the column, but an amplitude which is greater at the back of the column than at the front.

As the angle of incidence increases, modes form which are along the line of the breakwater. For a 45 ° angle wave, the greatest amplitude mode within the chamber is still seen at 5.0 s, however the greatest RAO occurs in the lee of the column.

One way of imagining the different behaviour under waves incident at different angles to the breakwater is to consider the OWC from the direction of travel of the wave. The structure may be considered to be stretched with respect to the wave at angle of incidence

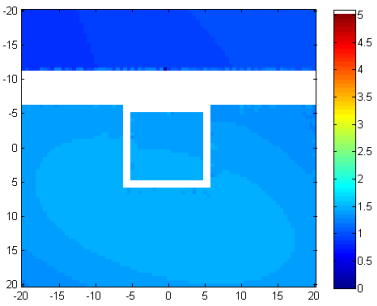

(a) 17.49 second waves

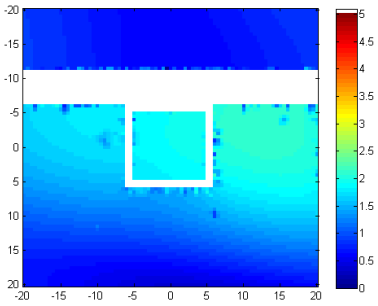

(b) 9.54 second waves

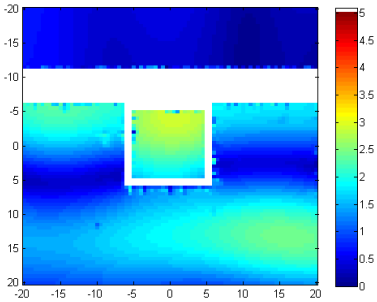

(c) 5.0 second waves

Figure 2.7: The RAOs for a single, shallow moon pool in front of a breakwater with 30° incident waves. The waves are incident from the bottom right.

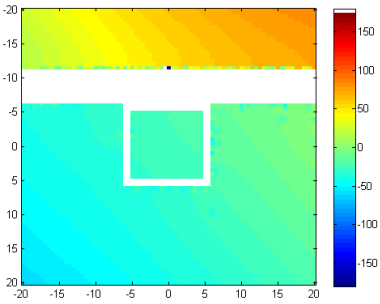

(a) 17.49 second waves

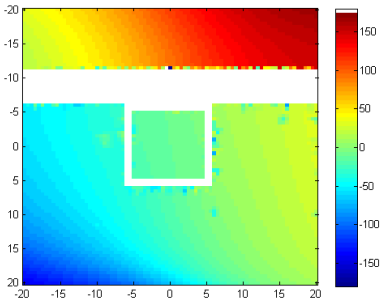

(b) 9.54 second waves

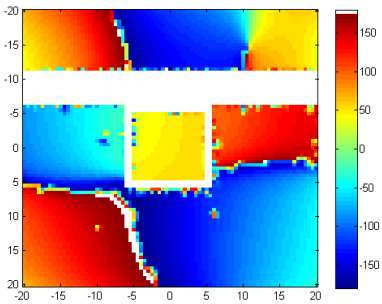

(c) 5.0 second waves

Figure 2.8: Phase for a single, shallow moon pool in front of a breakwater with 30 degree angle incident waves

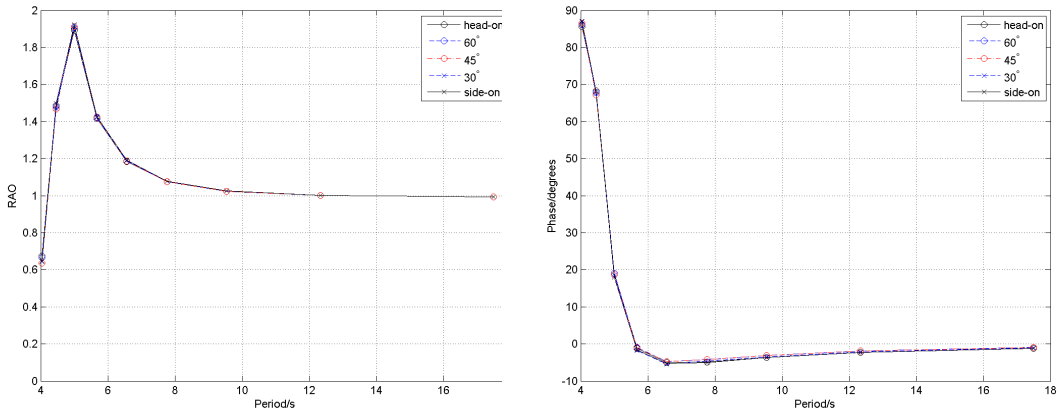

(a) Magnitude (b) Phase

Figure 2.9: Magnitude and phase for the RAO of the isolated moon pool system for waves of various incident angle

which is not head-on. This would mean that some of the response is down to the apparent shortening of the fraction of the wave covered within the extent of the pool. Thus, it is as though the pool is experiencing longer waves.

2.2.6 Aggregate motion for the isolated moon pool system

If a simple average is taken over the area of the water column, the mean displacement and phase shift of the free water surface of the column. The average free surface magnitude and phase responses are shown in Figure 2.9. The magnitude is quite smooth for changes in period longer than 4 s, with a peak RAO of 1.9 for a period of 5.0 s. For periods longer than 7 s, the displacement is approximately in-phase with the incident wave. The resonant phase response (90 ° phase shift) occurs for a period just shorter than 4 s.

Note that the angle of incidence makes barely any difference for the average surface response of the isolated water column.

2.2.7 A deep moon pool with breakwater

Sections 2.2.4 and 2.2.5 concerned a shallow moon pool structure. The walls of the moon pool structure may be extended to the sea bed on either side of the front lip. This makes a structure which is more easily built than the cantilever moon pool. Applying the same analysis as in the preceding sections shows that the most obvious difference in comparison to the shallow-walled moon pool is that the motion at 6.56 s is more pronounced, having a flatter internal water surface, moving to a greater amplitude of oscillation. The amplification of the free water surface outside the pool, ahead of the structure, is also

a little larger. No RAO or phase plots are presented here because they do not serve to particularly illuminate the water surface responses.

The deep-walled, single column structure may also be observed under different angles of incidence of the waves. At the 30 ° angle of incidence, the flat surface, high amplitude response is even more pronounced than for the 0 ° waves, with a calculated RAO of 4.0 for the 6.56 s waves. For the 5.0 s waves, however, the water surface remains very close to the still water level within the chamber. This is a very different response to that seen for the shallow walled structure, where Figure 2.8c shows a large RAO. Outside the column, a large oscillation (RAO of 3.0) is seen to the left of the pool.

These effects are caused by the interaction with the deep walls on either side of the moon pool. While the water can still access the pool under the front lip of the structure, the side walls block the flow. This means that water can be blocked from any interaction, or can build up with nowhere to go. Thus, the frequency and direction of a regular wave have a stronger effect on the more complicated structure.

2.2.8 Three moon pools with a breakwater

Having investigated the free water surface response for single columns, moon pools are added to either side of the central column. All of the surrounding walls extend to the sea floor. Only the front lips have 2.5 m drafts. For the three column system with 0 ° incident waves, the low frequency wave free water response is similar to that seen for the single block with breakwater, with a little more water concentrated in the central pool because the submerged walls between the pools prevent the water from escaping around the edges of the breakwater very easily. For the medium length waves, the amplification of the free water surface in the central pool is more pronounced. The largest RAO for any pool occurs for a longer wave than in the case of the single pools, both shallow and deep: 7.7 s rather than the 6.56 s of the deep, single pool case or the 5.67 s of the shallow single pool case. This geometry appears to be very good at cancelling the wave immediately ahead of the structure in the 7.7 s wave case, where the free water surface is observed to be very flat, but this is only true for that particular incident period wave.

Rather than show the free water surface figures as for the single pool cases, in this section schematic diagrams for the column water surface responses are shown. This is because when there are three moon pools, there are more options for the arrangement and phase of the motions and thus the free water surface figures are not so easy to read. (The

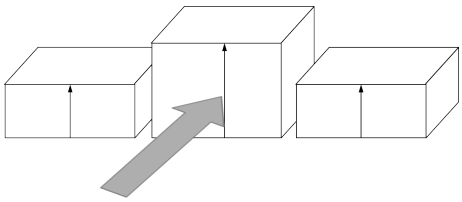

Figure 2.10: Schematic diagram of three column free surface motion for 7.7 s waves incident head-on to the breakwater

free water surface diagrams can be found in Section A.2 for completeness.) Figures 2.10 to 2.12 show schematic diagrams for how the motion can now occur in the three column case. For 7.7 s waves incident head-on to the breakwater, Figure 2.10 shows that the motion of the free water surfaces in the columns is similar to that seen in the case of the single moon pool with breakwater. The central column has the largest amplitude of motion and all three columns move in phase with one another.

For the same frequency, Figure 2.11 shows the response when the wave comes from a direction 30 ° from the perpendicular. The free surfaces in the columns are no longer symmetrical. The column that first experiences the wave has the highest amplitude, and the amplitude falls off along the length of the breakwater. The motion is now a wave which moves along the breakwater (the motion is no longer in phase).

If instead of the 7.7 s wave, the 5.67 s wave is investigated, the motion becomes more like that shown in Figure 2.12. Here the right-most column surface moves 90 ° ahead of the central one, with the phase of the left-most surface half-way between the two (i.e. at 45 °). The amplitude of motion is highest for the left-most surface, with the central surface having a very low amplitude of motion. The highest amplitude is in fact seen in the lee of the left-most column, as was the case for the single column with breakwater for the off-centre waves.

For the three column system, the behaviour of the free water surface in one column clearly has a large impact on the response of its neighbours, as can be seen by the very different responses shown in Figures 2.10 to 2.12. Making a small change to the motion of a column is therefore likely to make a larger change to the oscillation of the rest of the system. This is important to bear in mind for control of an OWC.

2.2.9 Five moon pools with breakwater

Finally, another chamber is placed on either side of the three in the previous section. There are now considered five water columns with a breakwater. Again, the possible motions

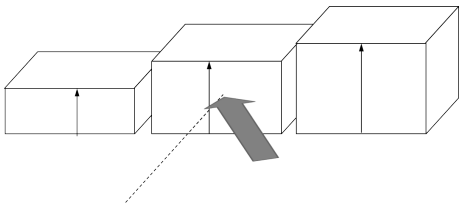

Figure 2.11: Schematic diagram of three column free surface motion for 7.7 s waves incident 30° from head-on to the breakwater

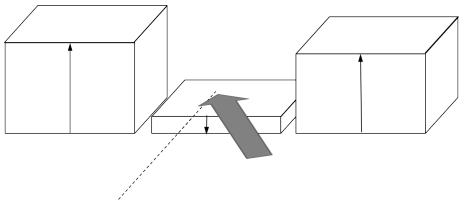

Figure 2.12: Schematic diagram of three column free surface motion for 5.67 s waves incident 30° from head-on to the breakwater

are investigated.

Figure 2.13a shows the RAOs for a low frequency wave corresponding to a 13.14 s wave incident head-on to a breakwater with five moon pools. Here the response is fairly uniform for the different pools, with the central pool having the largest amplitude response. This corresponds to the same general shape as was seen for the response of the single moon pool. In Figure 2.13c, however, with a 6.59 s incident wave, the pools alongside the central one show the greatest response. This is more like the 30 ° angle wave for three columns shown in Figure 2.12. As is the case for the three moon pool system, the five moon pool system allows for a greater number of distinct responses as the free water surfaces within the columns may move together, as a wave or as combinations of in-phase and in anti-phase.

Figure 2.15 shows these different variations schematically for three different wave periods, for wave incident with an angle of 0 °. Motion with a central peak, a double outer peak and in anti-phase is seen. This is clearly not like that observed for the isolated system.

2.2.10 Conclusions from the study of free water surface maps

For the isolated system, the response was very uniform depending upon the direction. Peak amplification occurred for a wave period of 5.0 s, with an RAO of 2. The 90° phase response (resonant motion) occurs between 4.03 and 5.0 s.

Introducing the breakwater behind the column lead to a big difference in the periods at which certain behaviour was seen. For perpendicularly incident waves, the period of greatest amplification was 9.54 s, almost twice the period as for the isolated case. At 5.0 s,

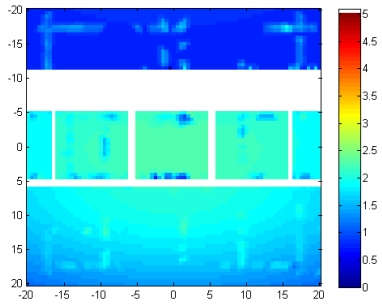

(a) 13.14 second waves

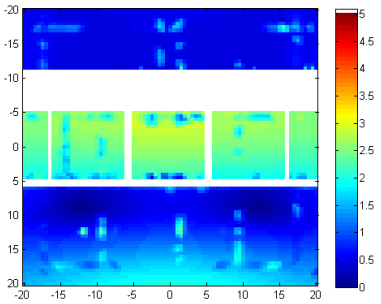

(b) 7.53 second waves

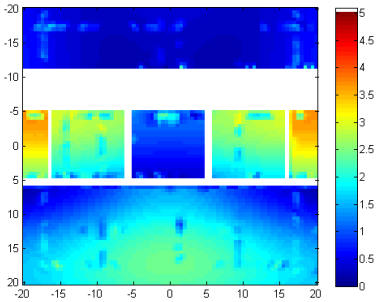

(c) 6.59 second waves

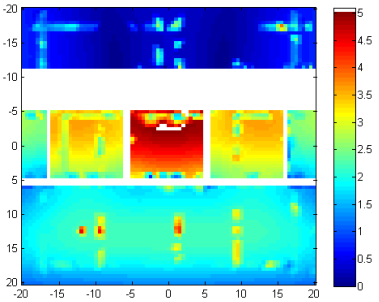

(d) 5.86 second waves

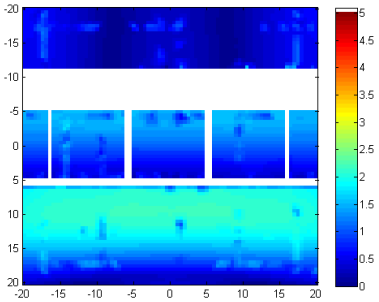

(e) 5.28 second waves

Figure 2.13: The RAOs for the five moon pool system with the inter-pool walls reaching the seabed

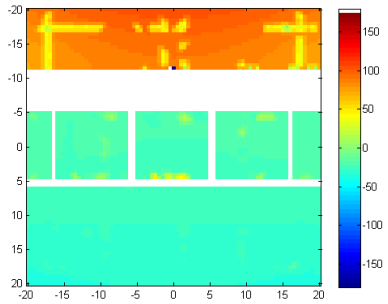

(a) 13.14 second waves

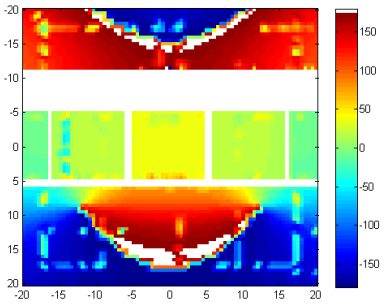

(b) 7.53 second waves

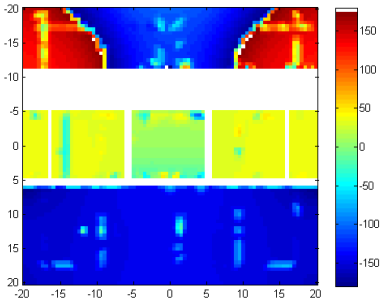

(c) 6.59 second waves

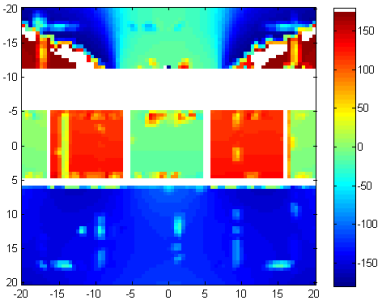

(d) 5.86 second waves

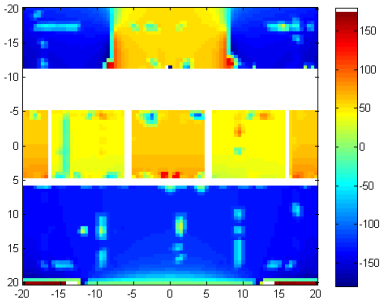

(e) 5.28 second waves

Figure 2.14: The phases for the five moon pool system with the inter-pool walls reaching the seabed

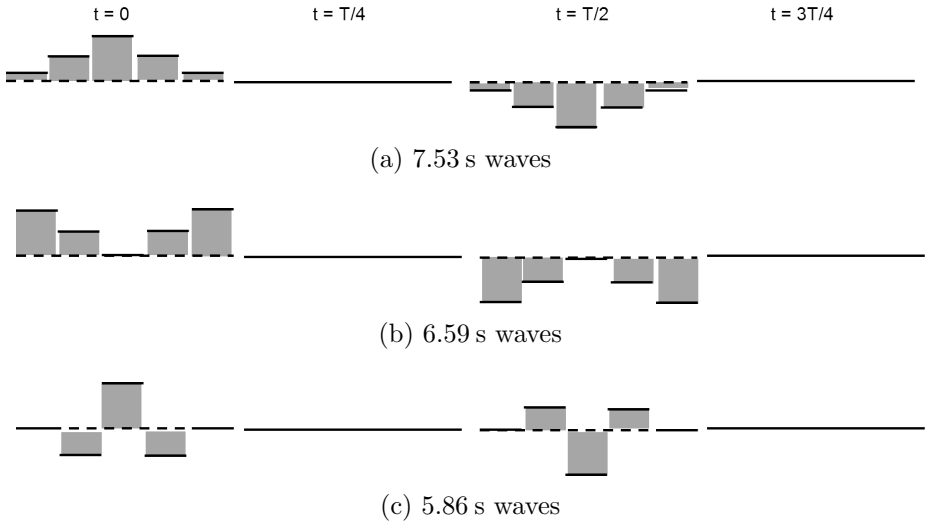

(a) 7.53 s waves

(b) 6.59 s waves

(c) 5.86 s waves

Figure 2.15: Schematic diagram of free surface water response for the system with five moon pools showing linked motion between the columns. The waves are incident head-on (0 °) and the columns are viewed from the front elevation

the RAO was less than 0.5 for the column with breakwater (suppressed motion). This is clearly very different to the isolated case. Sloshing was not seen to be a particular problem for periods longer than around 4 s, but the angle of incidence did have a large effect. For non-zero incidence angles, the periods at which amplification occurred generally became shorter. It was also observed that the maximum displacement happened in the lee of the water column.

The introduction of extra columns lead to very different possible responses. For both the three- and the five-column configurations, responses in which the maximum amplification occurred in the centre column were seen (water surface motion like that for the single column). It was also seen that there was motion where the outer columns had the greatest amplification, or where there was some kind of motion in anti-phase. Thus, it has been shown that adding in extra columns for a breakwater configuration leads to linked behaviour for the water columns. This should be taken into account for modelling and control of such breakwater OWCs.

2.2.11 Aggregate motion for the five moon pool system

In Figure 2.16, the aggregate motion is shown for the central column of the five-column with breakwater configuration. The most notable differences between the five column system and that of the isolated system is that the behaviour is less smooth and the angle of incidence does now make a difference to the response.

The peak amplification is larger for the central column of the five-column configuration

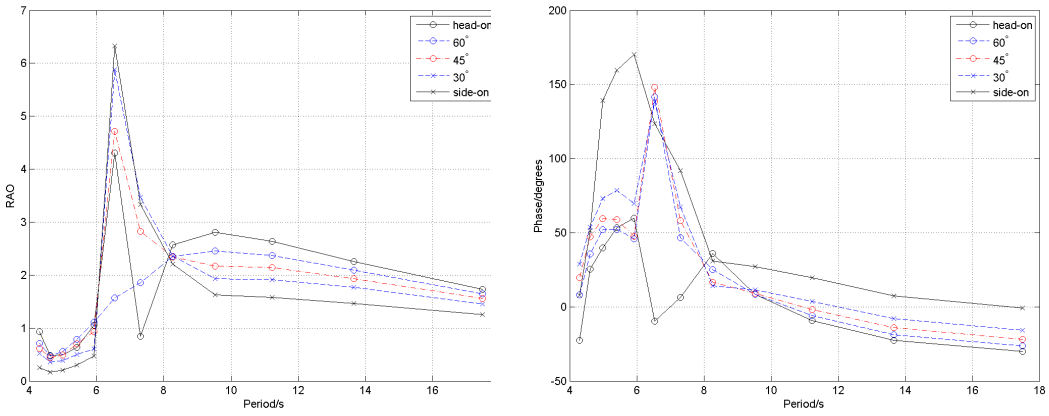

(a) Magnitude (b) Phase

Figure 2.16: Magnitude and phase for the RAO of the five moon pool system with breakwater for waves of various incident angle

than for the isolated system, but the sensitivity to period is large, so the water column can respond with very different phase and magnitude for seemingly very similar waves. For waves of long period, at all incident directions, the RAO is larger in the five-column case, with an RAO somewhat greater than 1.

The phase of the response tends to move from approximately in-phase for the long period waves, to phases which are not in-phase with the higher frequencies.

The aggregate internal water surface displacements are shown in Section A.11 for the other structures described in Section 2.2.

2.2.12 Discussion of aggregate results

As for the single cliff-based cylinder of Martins-rivas & Mei (2009), the angle of incidence made a difference to the response for a water column with breakwater in a way that is not seen for an isolated column. This is assumed to be due to the back-board effect in which the wave oscillates against the breakwater.

Note that for a high RAO, a wave of only moderate height is required to force the motion of the surface in such a way that the water surface may drop below the lip of the OWC, totally invalidating the linearity assumptions. This will clearly be noticeable for the 6-8 s range of periods.

2.3 Discussion of hydrodynamic results

The major finding of this velocity potential water surface study is that the response of a multi-column breakwater system is very different to that of an isolated system, as it

can show linked modes of motion, unlike in the case of a single column with breakwater. The single column cannot demonstrate displacements coupled to those of neighbouring columns because there are no neighbouring columns.

2.3.1 Findings of the free water surface study

For an isolated single OWC, it was seen that the heave (piston) mode is the only one that is significant in the response of the free water surface. The response is thus similar to that seen by Sykes *et al.* (2007) for the fixed cylindrical moon pool.

It was also seen that for a column which is part of a breakwater, the response is very dependent on the angle of incidence of the wave. This corresponds to the finding of Martins-rivas & Mei (2009).

It has been shown that in the case of columns that form part of breakwater systems, the neighbouring columns play an important part in the hydrodynamic response of any individual column. Behaviour in which the water surface of the central column oscillated with greatest amplitude and the outer columns had a lower amplitude was seen, as was behaviour in which the opposite was true. It was also seen that modes exist in which the water surfaces of the columns move in anti-phase.

As for the single-column breakwater system, the role of angle of incidence has also been described. It was shown that for the same frequency of incident regular wave, a change of angle can completely change the behaviour of the system, shifting it from one type of resonant behaviour to another. Thus, for a breakwater more than for an isolated system, the directionality of any given sea state will have a strong effect.

2.3.2 Relevance of the findings

The major finding, that the behaviour of a column is strongly influenced by its neighbours, even in the head-on incident angle case is very important for the modelling of OWCs. This is particularly true where control of OWCs is concerned, as any damping applied to one water column will very much influence the response of another. From the shapes of the excitation modes, it seems that it may be prudent in some conditions to turn off the PTO of either the inner or the outer OWCs. In certain conditions, alternating the on/off status of the PTO for the OWCs along the length of the breakwater could result in increased energy conversion.

2.3.3 Limitations of the free water surface study

Any velocity potential method would struggle to give relevant responses for highly non-linear behaviour, for example that for high amplitude motion within the moon pool. This is true for both large waves impacting upon the device (including those which over-top) and for highly resonant motion within the chamber.

In addition, the ANSYS™ AQWA® software is designed for ship hulls rather than for actively damped moon pools. This means that the software is not generally structured such that interaction with the sea bed is fully incorporated. Thus, in order to include precise bathymetry for a specific project, another set-up should be used.

Additionally, ANSYS™ AQWA® has not traditionally been used for port design, thus configurations in which the sea surface does not extend around the whole system are not straightforward to model.

This model does not take viscous or turbulent damping into account. The results are therefore applicable to the linear regime, but more detailed study would be required for nonlinear motion.

2.3.4 Extensions to this study

The major task for extension is the inclusion of an appropriate PTO and damping model for the system. This can be done using the open chamber displacements in chapters 3 and 4. If a direct calculation in ANSYS™ AQWA® is required, then this would involve the inclusion of a lid above the column that acts to damp motion within the chambers. Of course, in order to estimate this damping, a first test should be made that does not include the lid.

Future work could study this type of structure under irregular waves. The time-domain solutions obtained using ANSYS™ AQWA® are only appropriate for wave spectra with long period waves, but another velocity potential solver or a different method could be used to investigate an irregular sea interacting with such a multi-column breakwater structure.

Using the same ANSYS™ AQWA® software, it would be fairly straightforward to extend this model to a floating device, including looking at its use at different angles, as for Ruol *et al.* (2011). However, again, the inclusion of the PTO is the limiting factor.

Conclusions

The hydrodynamics of a single OWC as part of a breakwater-mounted structure was investigated using regular waves in the potential flow solver ANSYS™ AQWA®. The hydrodynamics are significantly more complicated than for an isolated structure as there are many possible interacting motions of the different chambers. Some of the observed coupled modes were described, including large central column motion, large outer column motion and alternate columns in anti-phase.

Due to the complex possible hydrodynamic interactions, when modelling OWCs with such near neighbours as may be found in a breakwater, the complete system should be modelled rather than assuming that the response will be the same as for the isolated case.

In order to extend this study to an OWC rather than neighbouring moon pools, the PTO damping should be included.

Summary

- ANSYS™ AQWA® was used to find the internal water surface response of an isolated moon pool, as well as for a single column with breakwater and three- and five-column configurations.
- It was observed that the behaviour of the OWC as modelled using these simple assumptions is very different when there is an isolated device in comparison to when the column is backed by a breakwater.
- The effect of angle of incidence is very small for an isolated column. For a breakwater-mounted system, the effect of angle of incidence is large.
- When columns neighbour one another, it is possible to excite different types of motion for the internal water surfaces: coupled modes. For example, the central column may have amplified motion in comparison to the outer ones, or vice versa. Another example is motion with relative anti-phase between the columns.

Chapter 3

A time domain model for an OWC-WEC

In Chapter 2, the response of an OWC was investigated for a system with its column open at the top. In this chapter, the turbine of the OWC-WEC will be included so that the air is constrained by the chamber and the modelled OWC-WEC is capable of converting energy. Due to the nature of the power take-off method, the numerical model should be developed in the time-domain. This means that the frequency-dependent behaviour described in Chapter 2 should be transferred into the time-domain. In Section 3.1 the system identification method for modelling the OWC will be described, which will give the description of the OWC behaviour in the time-domain without power take-off. Then, in Section 3.2 the power take-off will be included and the OWC-WEC behaviour explored for regular waves.

3.1 OWC-WEC behaviour in the time domain without PTO

In order to model the air in the chamber as described in Section 1.2.3, the OWC-WEC model must be in the time-domain. This means that a model is needed in which the motion described in Chapter 2 is captured. The system identification method used is described in Section 3.1.1. In Sections 3.1.2 and 3.1.3, the method will be applied to the isolated OWC and the central OWC of five, respectively. The PTO will then be introduced in Section 3.2. In the interests of simplicity, only waves incident head-on to the structure were considered.

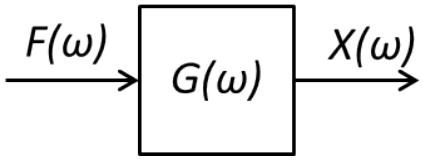

Figure 3.1: A force to displacement transfer function

3.1.1 System identification

If it is assumed that for the frequencies between those tested in Chapter 2, the magnitude and phase of response change smoothly, it is possible to take a wave frequency and make a response $X(\omega) = \hat{X}e^{i(\omega t+\sigma)}$, where $\hat{X}$ is the magnitude and σ is the phase.

For each frequency, $\hat{X}$ and σ will have different values. Thus,

$$X(\omega) = (\hat{X}(\omega)e^{i\sigma(\omega)})e^{i\omega t} \tag{3.1}$$

and $(\hat{X}(\omega)e^{i\sigma(\omega)})$ gives the response to the wave $e^{i\omega t}$. If instead of $e^{i\omega t}$, the force of the wave is used, a new function, $G(\omega)$, can give the effect of the system:

$$X(\omega) = G(\omega)F(\omega) \tag{3.2}$$

where $F(\omega)$ is the incident wave force and $G(\omega)$ is a function yet to be identified. This setup is shown diagrammatically in Figure 3.1 and is called a transfer function.

If some set of $F(\omega_j)$ and $X(\omega_j)$ are known for discrete values of frequency, ω_j, then $G(\omega_j)$ may be calculated and $G(\omega)$ may be estimated. It is important that both the amplitude and the phase match in the resulting estimation.

In order to find $G(\omega)$, the incident wave force at each of the frequencies used in Chapter 2 needs to be calculated, as this is the input to the function. The magnitude of this force is given by

$$\hat{F}(\omega_j) = A_w\rho_w g\frac{\cosh k(d-h)}{\cosh kd}A_E(\omega_j) \tag{3.3}$$

where $A_E(\omega_j)$ is the amplitude of the wave at each frequency, g is gravitational acceleration and k is the wavenumber (Gervelas *et al.*, 2011). There is zero phase difference associated with this incident force and k is defined as

$$k\tanh kd = \frac{\omega^2}{g} \tag{3.4}$$

The other variables used in Equation 3.3 are given in Table 3.1.

Variable	Value
Water density, ρ_w	$1025\,\mathrm{kg\,m^{-3}}$
Water column area, A_w	$105\ \mathrm{m}^2$
Water column draft, h	$2.5\,\mathrm{m}$
Water depth, d	$7.5\,\mathrm{m}$

Table 3.1: Values for the variables used in the numerical modelling

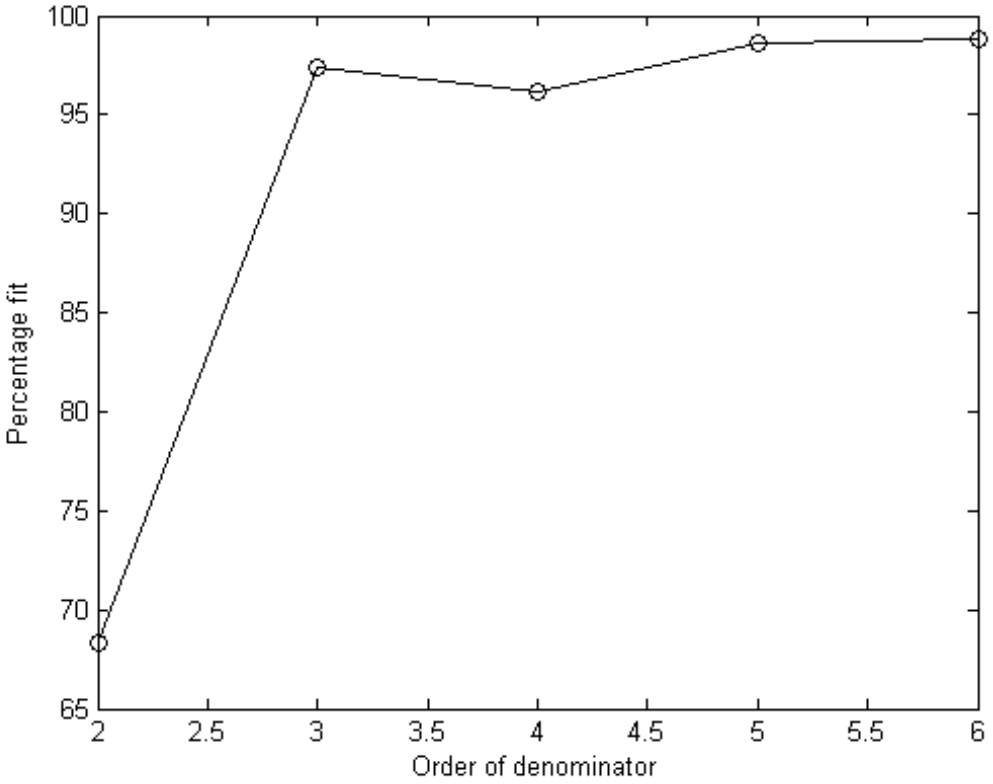

Figure 3.2: Fit for various orders of transfer function for the isolated OWC

3.1.2 Force to displacement transfer function for the isolated moon pool

Using the magnitude of the incident wave force at the different frequencies, and the subsequent phase and magnitude displacement, the MATLAB® System Identification function "`frd()`" was used to create a system from the frequency response data. That is to say, using the frequency of the incident wave and the magnitude and phases responses associated with this, a transfer function may be estimated which will produce such a response, in effect estimating a transfer function from the Bode diagram of the system.

For the isolated OWC, the 9 longest period wave responses from the model of Chapter 2 were used to come up with a transfer function of order n_z/n_p, where

$$n_z = n_p - 1 \tag{3.5}$$

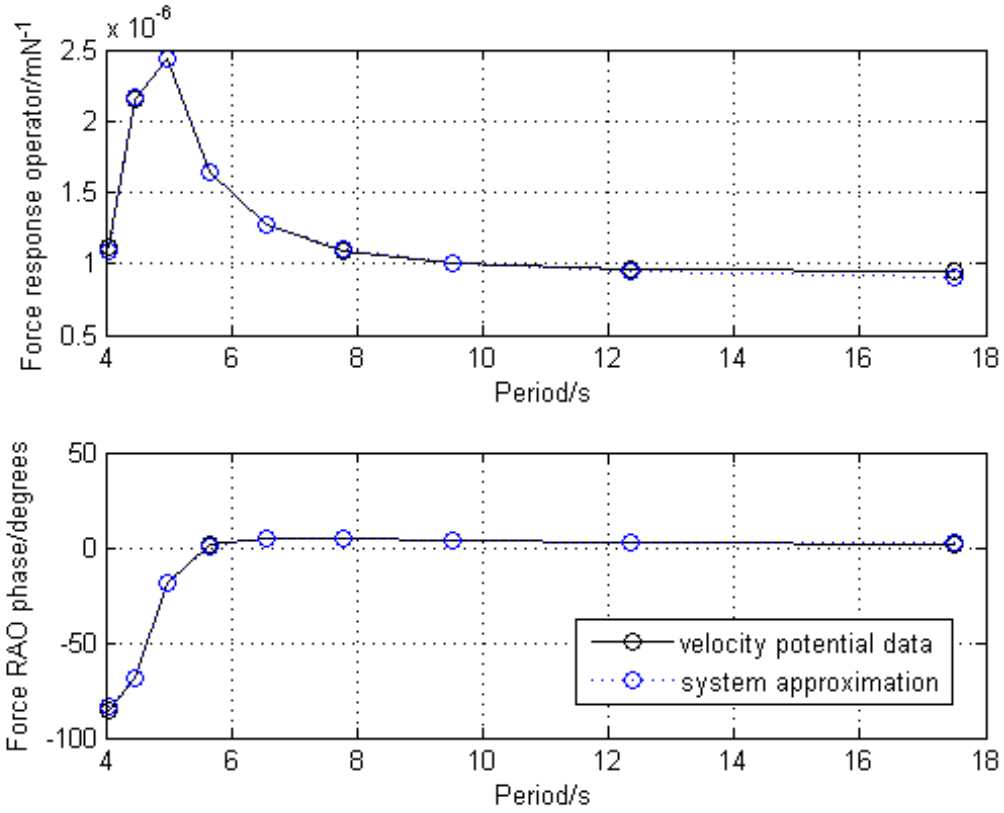

Figure 3.3: Magnitude and phase match for the force to heave transfer function approximation for the isolated column

and n_z is the number of zeros and n_p is the number of poles. The percentage fit of the tested transfer functions is shown in Figure 3.2. A three pole, two zero system was found to give a good match in both magnitude and phase, with a 97.4% fit. The transfer function which links force to displacement is then

$$G_{iso}(s) = \frac{8.829 \times 10^{-6}s^2 + 7.842 \times 10^{-6}s + 2.601 \times 10^{-5}}{s^3 + 16.63s^2 + 5.904s + 29.68} \tag{3.6}$$

and the resulting force to heave transfer function match is shown in Figure 3.3.

The transfer function was then converted to a state space model and the wave force implemented in the time-domain using MATLAB® Simulink (as for Jayashankar *et al.* (2000); Taylor *et al.* (2009), etc.). The resulting heave response is given in Figure 3.4. A fixed time-step of 0.005 s is used for all of the runs to ensure that the model is able to calculate effectively for the most extreme cases, whilst being numerically comparable. 300.0 s (5 min) is simulated for the regular waves. The solver is an ode3 Bogacki-Shampine.

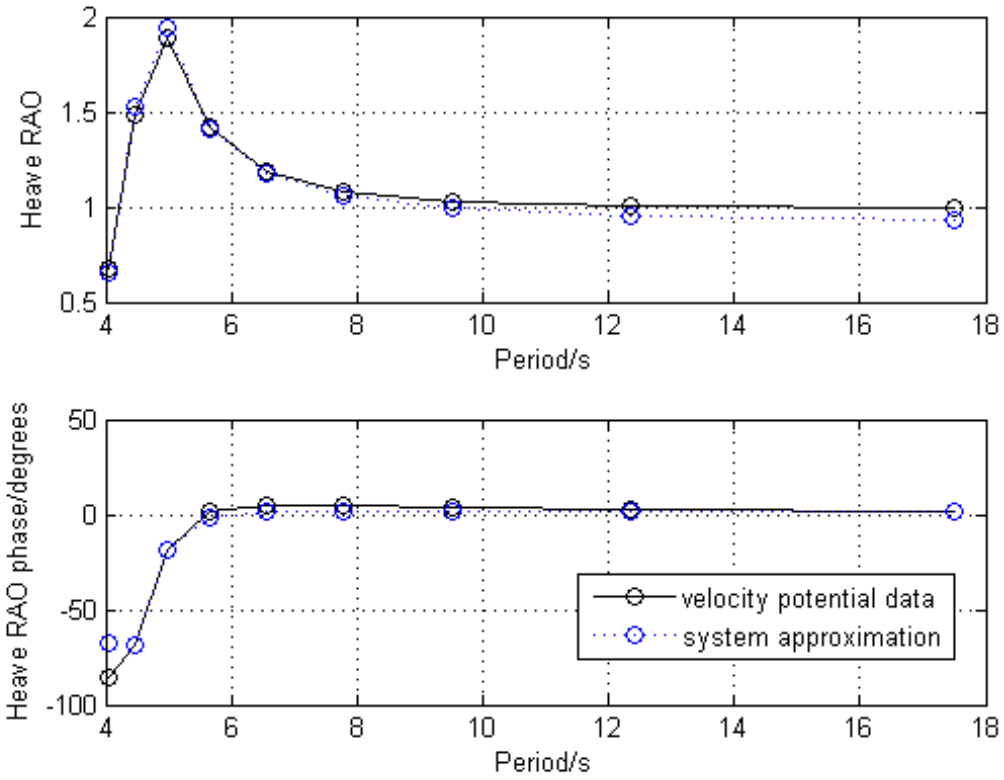

Figure 3.4: Heave response for the time domain model of the isolated column without PTO

3.1.3 Force to displacement transfer function for the central column of five

For the central column of five the same method was used to find a function that takes incident wave force as input and estimates the heave displacement output. The function chosen as a good approximation is of higher order than that for the isolated OWC, with 8 poles and 7 zeros. This is necessary due to the complicated nature of the internal water surface response. The fit of the various tested transfer functions is shown in Figure 3.5. The 8 pole, 7 zeros solution has an 88.5% fit and the chosen transfer function is

$$G_{cen}(s) = \frac{N_{cen}(s)}{D_{cen}(s)} \tag{3.7}$$

where

$$\begin{aligned} N_{cen}(s) =& 0.0001822s^7 + 7.587 \times 10^{-5}s^6 + 0.0007244s^5 + 0.0002273s^4 \\ &+ 0.0008901s^3 + 0.0001603s^2 + 0.0003348s + 1.749 \times 10^{-5} \end{aligned}$$

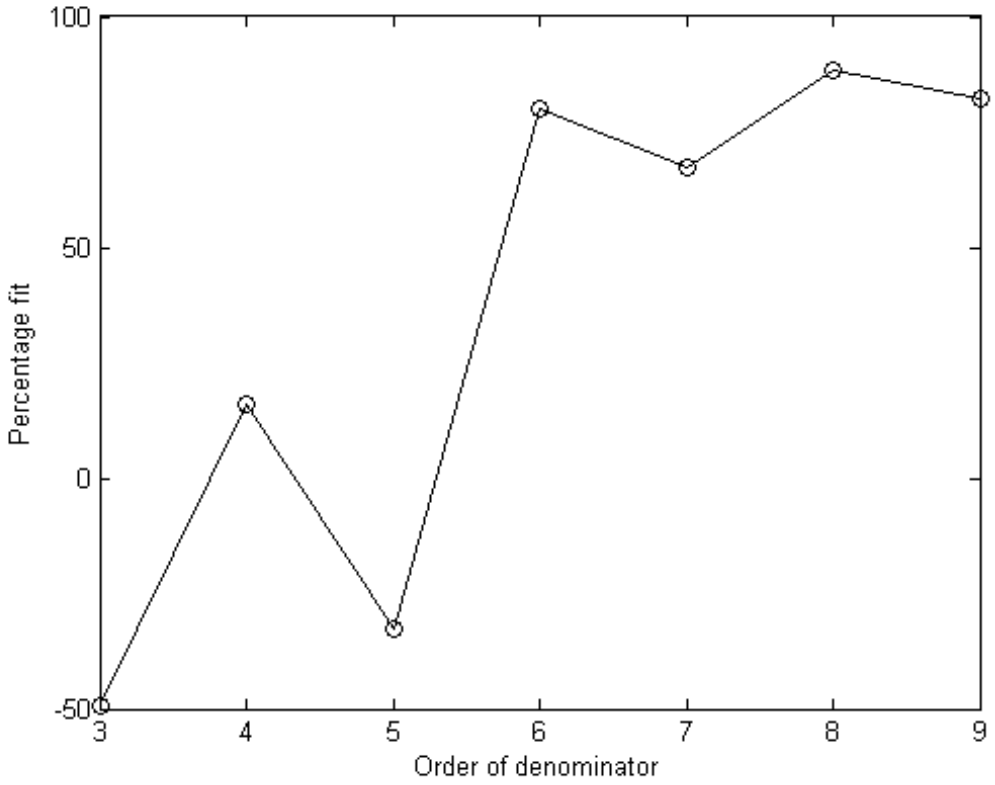

Figure 3.5: Fit of various orders of transfer function for the central column of five

and

$$D_{cen}(s) = s^8 + 135.5s^7 + 86.99s^6 + 498.2s^5 + 270.3s^4 + 535.8s^3 + 227.9s^2 + 173.8s + 48.01$$

An alternative relationship between the number of zeros and poles was also tested: $n_z = n_p - 2$ but was found not to give as good a fit.

The response using the 8 pole, 7 zeros transfer function from force to displacement is shown in Figure 3.6. Clearly the match is not perfect, especially in phase, but the approximation is good across the range of periods considered.

This transfer function leads to a heave (rather than force) response amplitude operator as shown in Figure 3.7.

3.2 OWC-WEC behaviour in the time-domain with turbine PTO

In order to have a WEC, the energy of the waves must be converted to electricity. The OWC model should therefore have a power take-off (PTO) stage which models this con-

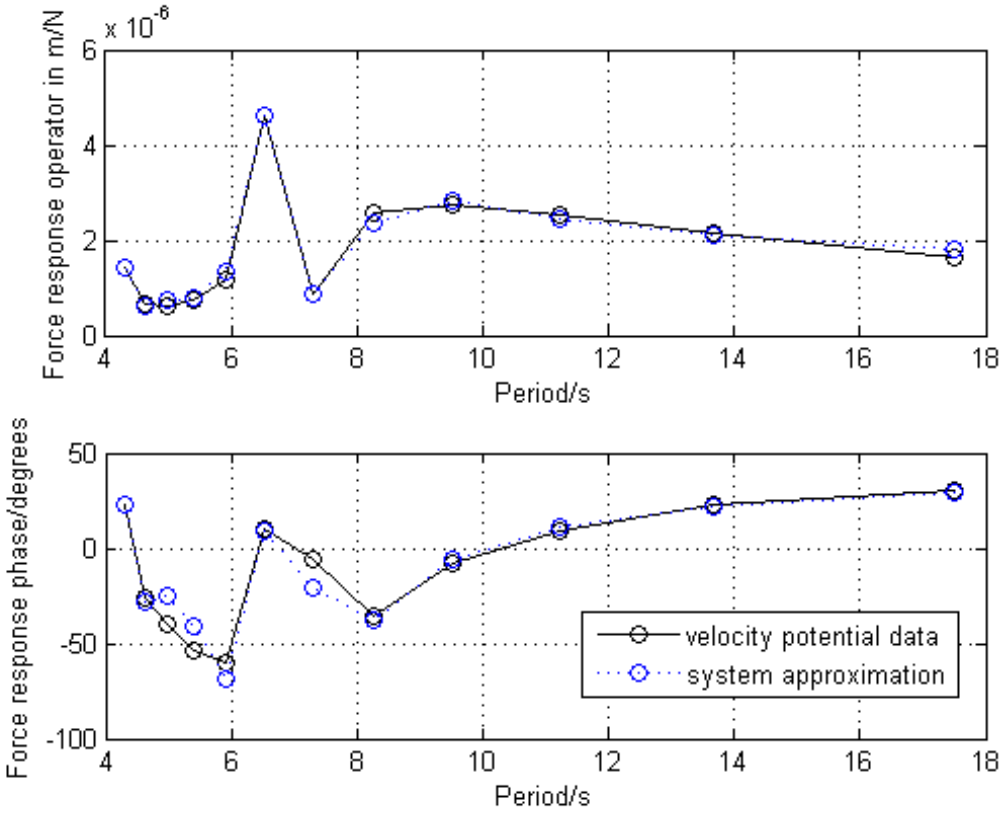

Figure 3.6: Magnitude and phase match for the force to heave transfer function approximation for the central column of five

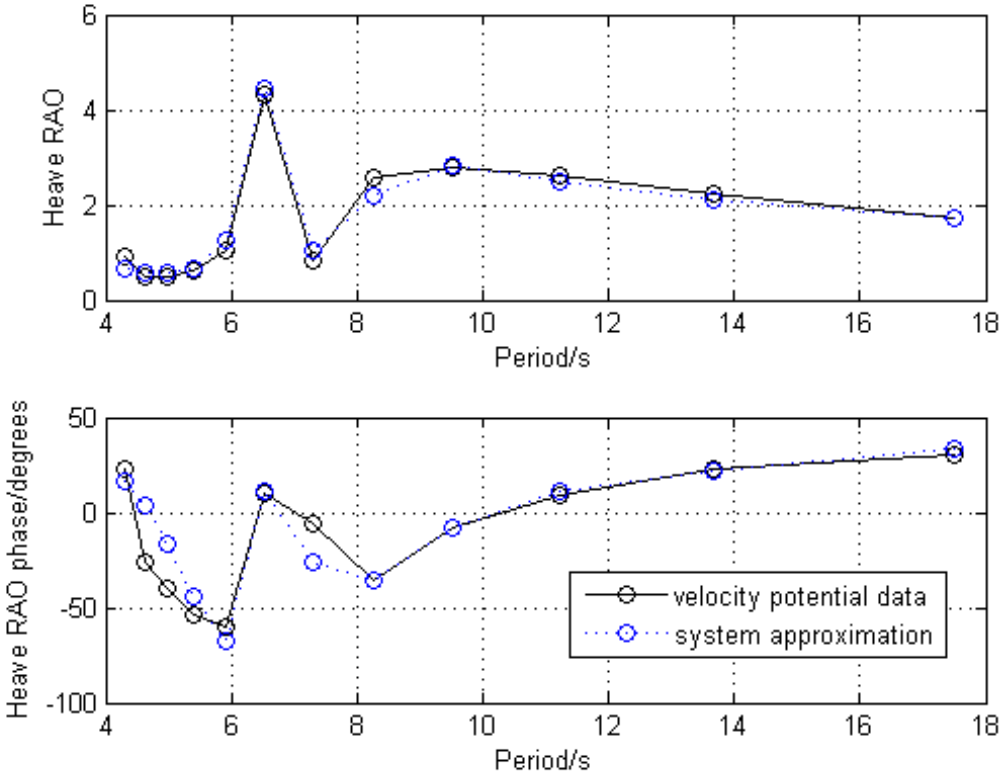

Figure 3.7: Heave response for the time domain model without PTO for the central column of five

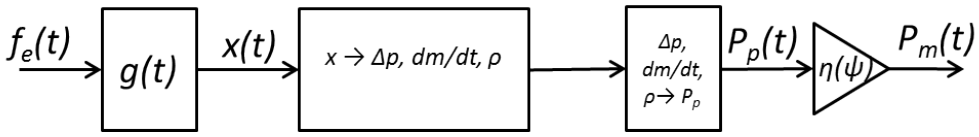

Figure 3.8: Schematic diagram of the force to mechanical power calculation

version. A turbine model is therefore included.

3.2.1 Thermodynamics for the turbine

For the inclusion of a turbine, as suggested in Section 1.2.4, the thermodynamic properties for the chamber are calculated using Equations 1.24, 1.25 and 1.28. Putting together the wave force, the impedance model and these thermodynamic properties, the movement of the water and changes in the air may be calculated. For a WEC, however, the crucial value is the amount of energy that is converted.

Figure 3.8 shows how each step in the calculation is linked. The incident wave force is supplied as input to the state space model, $g(t)$, which gives the mean displacement of the water surface of the OWC. That displacement is then used to calculate the pressure difference, air flow and air density of the OWC-WEC. From these thermodynamic properties, the pneumatic power may be calculated, then the efficiency may be used to give a measure of the mechanical power as described in Section 3.2.2.

3.2.2 Energy conversion

In any WEC, the purpose is to convert the maximum amount of energy (within some limits). This means that the power converted at any instant should be calculated. Instantaneous pneumatic power, is given by

$$P_p = -\frac{\Delta p}{\rho_{atm}} \frac{dm}{dt} \tag{3.8}$$

However, the efficiency of the turbine is not the same over all operating conditions. The difficulty in modelling the energy converted is then that the most reliable way of testing the efficiency of the turbine is to make experimental measurements and these must be converted into something that can be used in the numerical model.

In the model described herein, a curve is made which maps non-dimensional pressure, Ψ, to turbine efficiency, η, after the turbine described in Falcão & Rodrigues (2002).

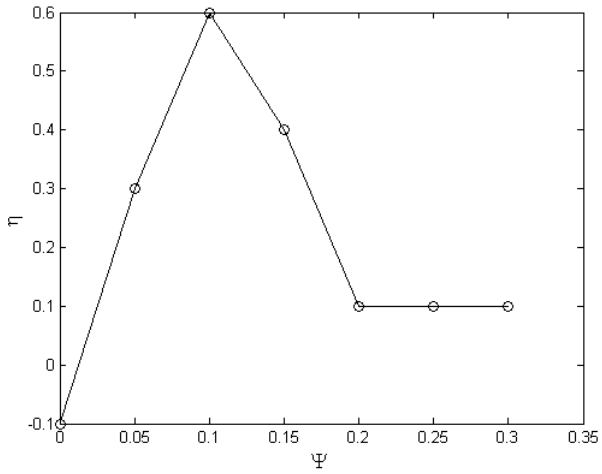

Figure 3.9: The efficiency of the turbine

Ψ	0	0.05	0.1	0.15	0.2	0.25	0.3
η	-0.1	0.3	0.6	0.4	0.1	0.1	0.1

Table 3.2: Coefficients to describe the efficiency of the turbine based on non-dimensional pressure

Non-dimensional pressure is defined here as

$$\Psi = |\Delta p|/(\rho_{atm} N_r^2 D^2) \tag{3.9}$$

where D is the diameter of the turbine and N_r is its speed of rotation in $\mathrm{rad\,s^{-1}}$. The non-dimensional pressure difference, Ψ, is used rather than the pressure difference, Δp so that different turbine speeds may be included in the same categorisation.

This turbine was used due to the availability of its data, rather than because it is the most perfect and suitable turbine for this particular application. The mapping is shown in Figure 3 of that paper and the coefficients that were used in this thesis to describe this mapping are given in Figure 3.9 and Table 3.2. The paper notes that this mapping has a great deal of effect on the resultant performance of the turbine and that therefore great pains should be taken to ensure that the mapping is a correct one. While this is indeed true, for the purposes of this thesis, the particular mapping has been considered less important than the opportunity for exploring control methods to exploit the more efficient regions of operation identified by any such mapping.

Using this efficiency method then, the instantaneous mechanical power conversion is

$$P_m = \eta(\Psi) P_p. \tag{3.10}$$

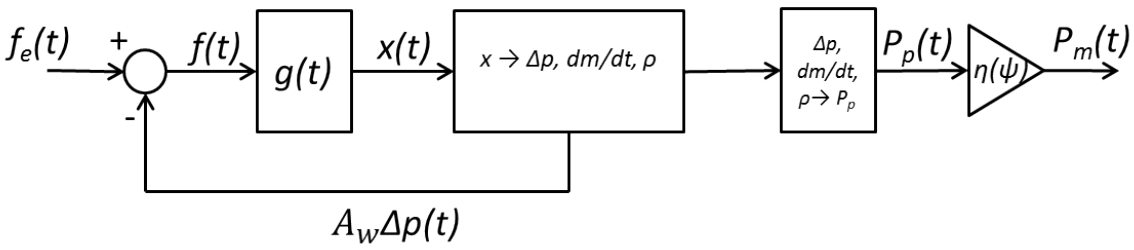

Figure 3.10: Schematic diagram of the TDM including power

where η is the function which describes the efficiency of the turbine. Note that this power estimation does not include electrical losses. The total energy converted over time may be found by solving the equation

$$E = \int_0^t P_m.dt \tag{3.11}$$

The equations of this section may thus be solved numerically to find the mechanical energy converted under different conditions.

3.2.3 TDM response with turbine PTO

In order to test the system numerically, the driving force which maps incident wave force to displacement is updated to include the pressure force on the water surface. This is shown schematically in Figure 3.10, which is an updated version of Figure 3.8. The force which drives the input to the transfer function is now

$$f(t) = f_e(t) - A_w \Delta p \tag{3.12}$$

where $f_e(t)$ is the excitation force and is defined at each frequency as in Equation 3.3.

The inclusion of the PTO is first tested for the isolated column, then for the central column of five. For both systems, a turbine speed of 632 rpm is used and the diameter of the turbine is 2.5 m. This is due to the performance optimisation of Chapter 4.

Response of the TDM for the isolated OWC with turbine PTO

The motion of the water column can be seen in Figure 3.11 for the case with the turbine. The feedback from the pressure forces suppresses the motion of the surface of the water column. The turbine is significantly damping the motion of the system and this has the effect of suppressing the amplification of the motion for short periods. For long waves, the RAO tends towards 1, but is still below this. It should be remembered that these turbine

properties are those which are the optimum for the central column OWC rather than for the isolated column.

The magnitude of the pressure response (that is, the mean amplitude of the pressure oscillation) to regular waves of 0.5 m amplitude is shown in Figure 3.12. The pressure variation follows more the trend of the displacement of the system without the PTO, than that of the displacement with the PTO. The chamber pressure difference, rather than the displacement, is what increases for the OWC with turbine. A magnitude of around 2500 Pa is seen for the long period waves and 3000 Pa for the 6.0 s ones. In comparison to atmospheric pressure, 3000 Pa is not very large (atmospheric pressure is around 100,000Pa), only around 3%. This pressure difference is around half that estimated by Amundarain *et al.* (2011) as a likely driving pressure, but the pressure here is taken as the mean absolute difference, so the pressures seen are very similar to those elsewhere.

The same pattern is seen for the mass flow in the same figure, as mass flow is proportional to pressure difference by equation 1.28. The magnitude of the mass flow is around 15-25 $\mathrm{kg\,s^{-1}}$. This corresponds to a volume flow of around 25 $\mathrm{m^3\,s^{-1}}$. For a wave with period 8 s, the movement of the water surface is such that around 25 $\mathrm{m^3}$ is displaced each second, so the mass flow is certainly close to that expected from the volume flow, although of course some change due to the pressure fluctuation should be included.

The power plot in Figure 3.13 shows that the power follows this pressure difference. There is a peak for waves with period 7 s. The magnitude of this response is around 20 kW, although the turbine properties are not optimised for this column, and the wave height is low, at 1 m. Clearly the incident period is important in the conversion of this power, as for high and low frequencies, the power is lower, at around 4 kW.

Response of the TDM of the central column of five with turbine PTO

The same analysis may be presented for the central column of the five column system. Figure 3.14 shows the internal water surface displacement for the OWC-WEC operating with a fixed speed turbine. For waves with period below 12 s, the heave motion is very suppressed in comparison to the case with no PTO.

For the pressure and mass flow, shown in Figure 3.15, the shape from the displacement with no PTO is visible, as it was in the isolated OWC case. Pressure and mass flow both show very uniform behaviour for waves where the period is 8-16 s. This could be useful in a real sea, where a strong dependence on wave period may not be favourable to energy

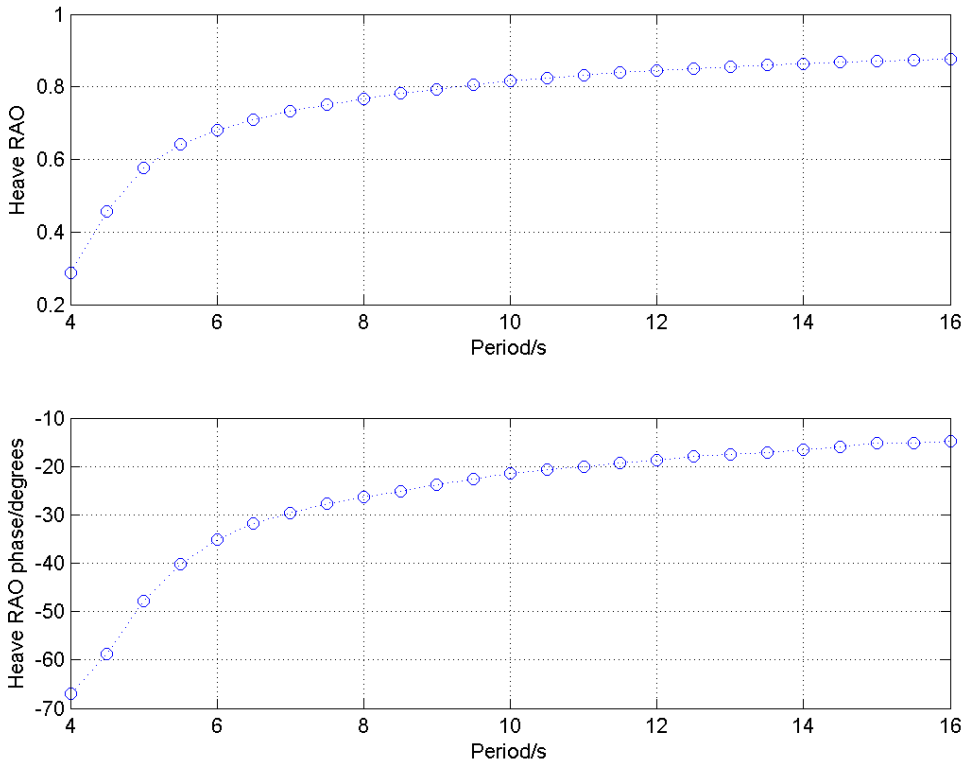

Figure 3.11: RAO for the internal water surface displacement for the isolated OWC with turbine PTO in regular waves, plotted with respect to period

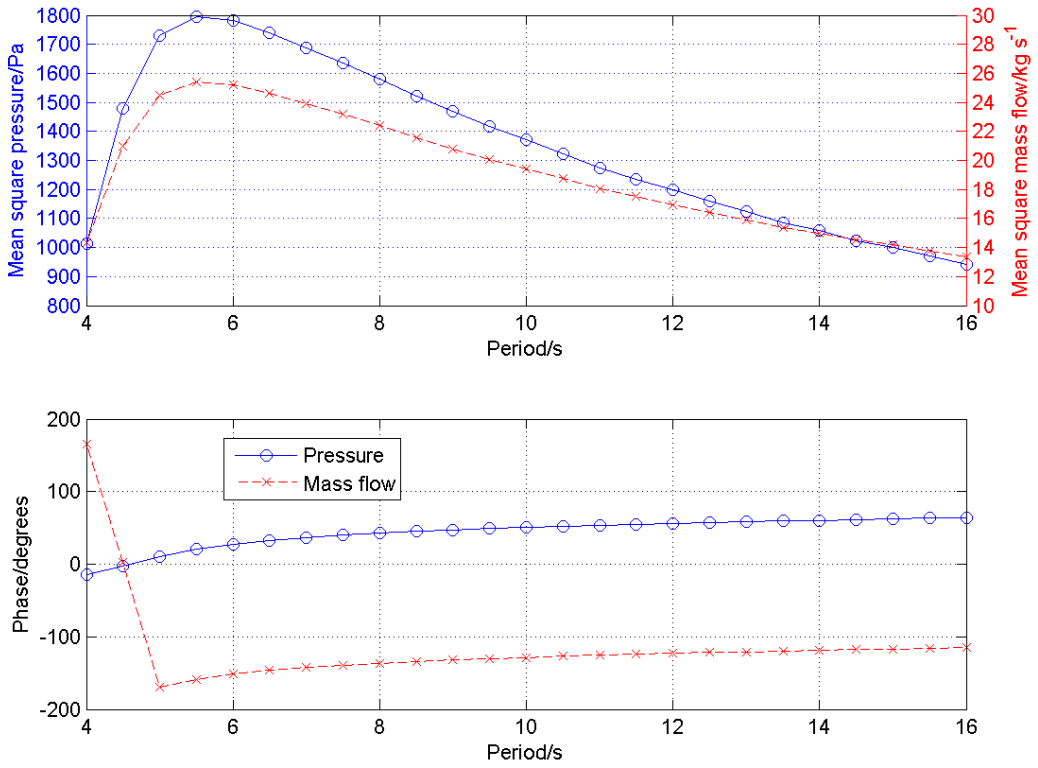

Figure 3.12: Pressure and mass flow for the isolated OWC with turbine PTO in regular waves, plotted with respect to period

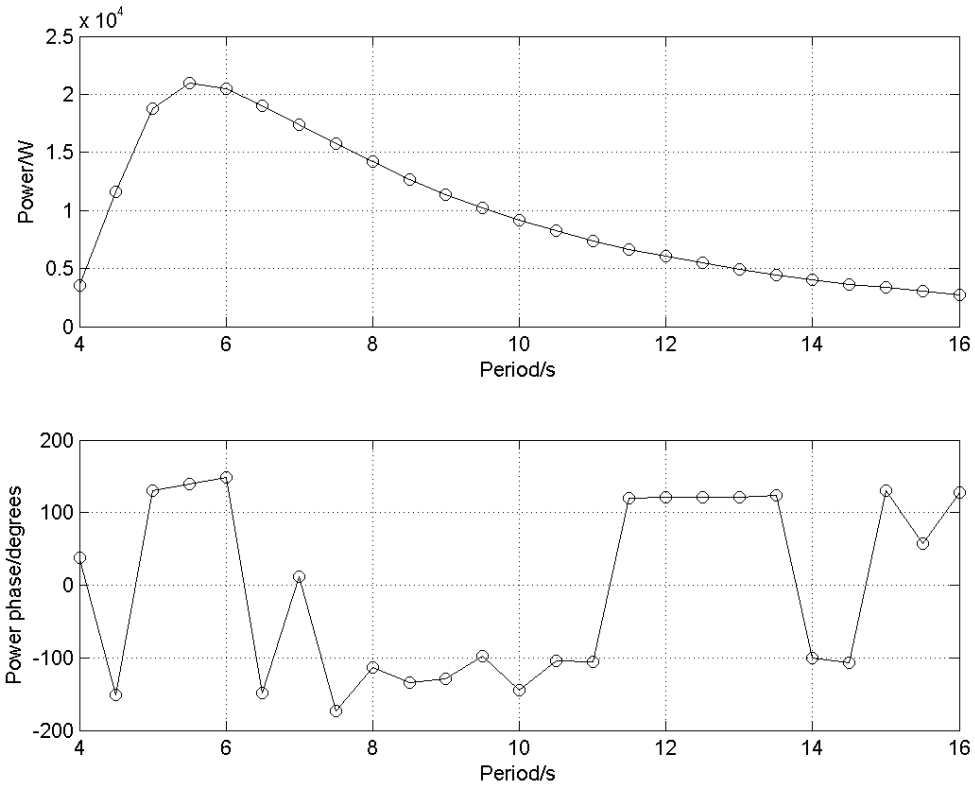

Figure 3.13: Power for the isolated OWC with turbine PTO in regular waves, plotted with respect to period

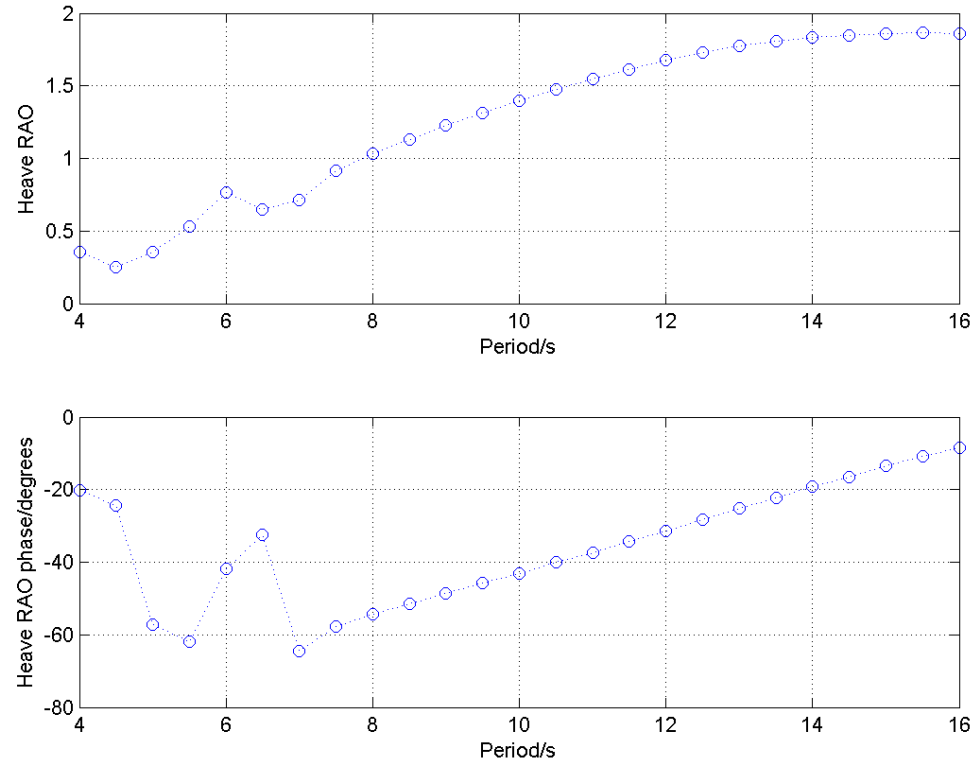

Figure 3.14: RAO for the internal water surface displacement for the central column of five with turbine PTO in regular waves, plotted with respect to period

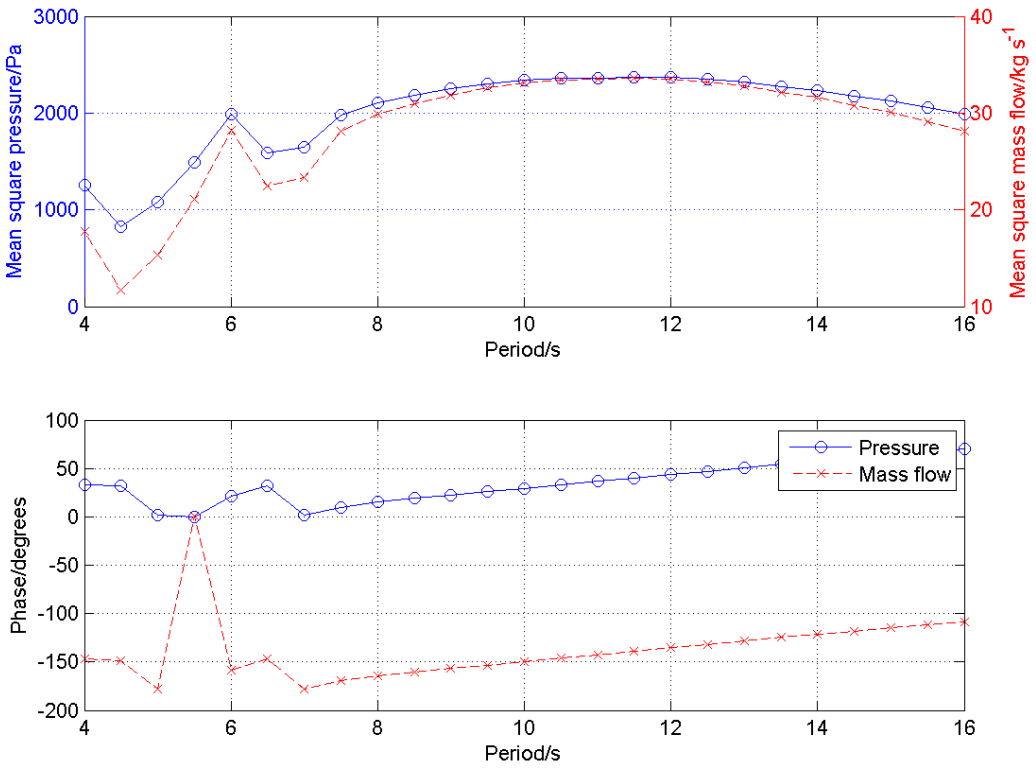

Figure 3.15: Pressure and mass flow for the central column of five with turbine PTO in regular waves, plotted with respect to period

conversion. The magnitude of the internal water surface displacement is higher for the central column of five than it is for the isolated OWC, thus pressure values of 2000-2500 Pa, and mass flows of 30 kg s^{-1} seem to be in line with those seen for the isolated case.

The resulting average power is shown in Figure 3.16. Because power is based on multiplying the pressure difference and the mass flow, the magnitude of the power response is less uniform than the pressure and mass flow were themselves. In fact, there is a noticeable, if not large, domed pattern for wave periods from 8 to 16 s, with a peak at 11-12 s. Over this domed region, the average power varies from 30 to 40 kW, which is a reasonable value for an OWC-WEC of this size.

3.2.4 Comparing the TDM results of the different OWCs

The pressure and power plots show that for the model with the turbine under regular waves for both the isolated and the central system, the power is concentrated at those frequencies which are associated with maximum pressure difference, which is not necessarily the same as that of maximum displacement of the internal water surface. Maximum displacement in fact shifts to the longer period waves when the turbine is included. For the central

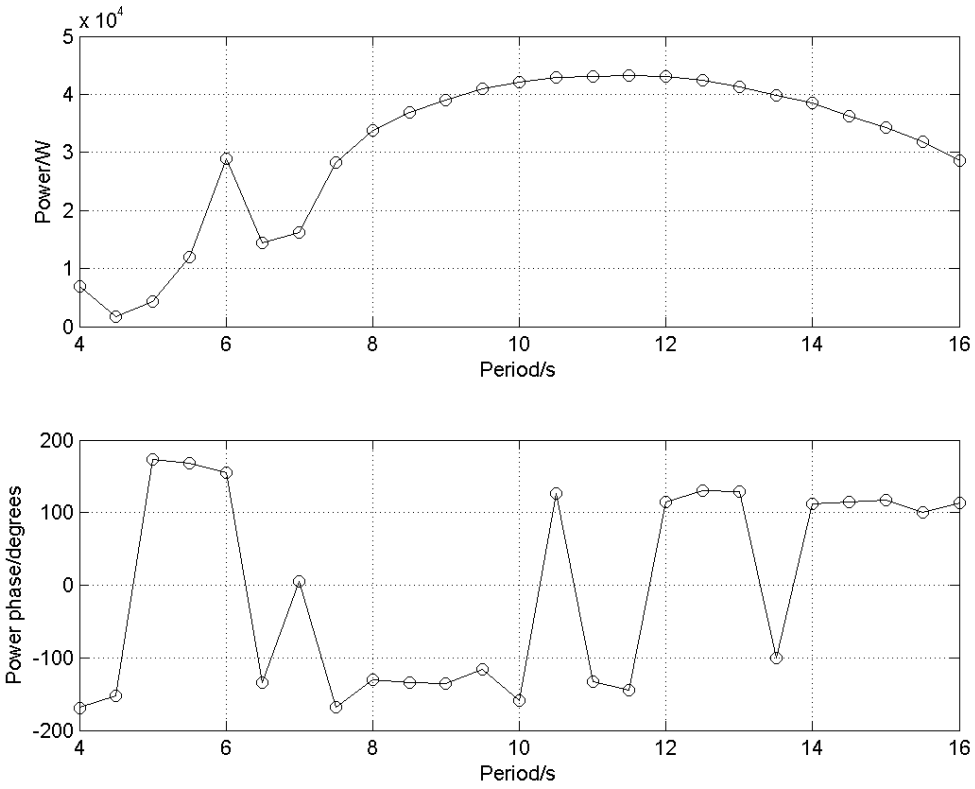

Figure 3.16: Power for the central column of five with turbine PTO in regular waves, plotted with respect to period

column of the five column system, the open column response has a peak at 6.5 s. This peak is important for the power output of the column, but waves of this frequency lead to the same level of power conversion as for those with longer period waves.

3.3 Discussion of the OWC-WEC time-domain model

In this chapter a numerical time domain model was made of an OWC-WEC forming the central column of a five column breakwater structure.

3.3.1 Effectiveness of the time domain model of the OWC

In order to develop a numerical time domain model of an OWC-WEC forming the central column of a five column breakwater structure, a mapping was made to take the force of an incident wave and turn this into the expected displacement of the internal free water surface. This mapping suitably matched the behaviour calculated using the velocity potential method in Chapter 2. Because the mapping looked at force, the force caused by the chamber pressure difference could be incorporated in the internal water surface estimation.

A turbine with diameter 2.5 m, coefficient, $K_t = 0.375$ and fixed speed of 632 rpm was used to test the response. Inclusion of the turbine lead to significantly suppressed displacements for both the isolated and central columns in comparison to the open case.

The system identification force-displacement mapping model recreates the displacements of the water surface seen in the velocity potential study very well. The method seems able to handle a pressure force (feedback) caused by the PTO. This means that the effect of control decisions are not tested in a vacuum - the thermodynamic properties and the expected hydrodynamics can also be fed into the understanding.

This pressure force feedback is not small. When using ANSYS™ AQWA®, for example, the lid damping can be any value from 0 (no damping) to 1 (total damping). From looking at the displacements seen for the isolated column and the central column of five, it seems that a value of around 50% would give the right level for waves with periods less than 10 s, and ranging to 0% for waves with periods of 16 s. For a greater level of detail, different damping values could be tested for waves of different incident frequency. However this could prove to be quite time consuming.

Comparison of the central column behaviour to that of the isolated column

Both the isolated and the central columns have thermodynamic properties with shapes somewhere between those of the displacement of the internal water surface with turbine and the displacement for the open case. The pressure is high for the short period peaks seen for the open case in both the isolated and the central column of five.

For longer period waves in the isolated system, the pressure level falls away, but for the central column of five, it does not. The central column shows behaviour which changes quickly with small period changes, as it did for the open case, while the isolated column has smooth behaviour. The output power reflects these trends.

3.3.2 Importance

This particular time domain model features a model for an OWC with near neighbours. Even though the neighbouring columns do not have PTOs of their own, they still affect the displacement of the water surface as a function of wave period, and so they affect the expected energy conversion (Chapter 4) and the best control systems (Chapter 5).

The existence of the time domain model means that such performance can be estimated and such control options explored. The resulting chamber pressures may then be incor-

porated into the velocity potential model so as to estimate the response of the chambers when a PTO is incorporated into each one.

3.3.3 Relation to other work

In order to look at how this time domain model relates to other models of OWCs, the comparison will be split into two parts: first, the force-to-displacement model; second, the model with PTO.

Comparison to other system identification models

The transfer function model of Nunes *et al.* (2011) maps incident waves to pressure and mass flow such that power could be calculated quickly. The wave height was also matched to displacement so that extreme motions could be eliminated. The initial data to match was generated by a standard forced-based approach in which the radiation, buoyancy and so on were estimated individually using a WAMIT velocity potential model.

Stappenbelt *et al.* (2013) looked at a mechanical oscillator model and did small scale physical experiments, using free and forced vibrations, to estimate the parameters. Again, this work assumed a specific list of forces and tried to estimate each parameter separately.

In the work described in this chapter, the whole system was modelled as a single mapping.This simplifies the process and, importantly, allows different pressure-mass flow relationships to be tested.

Comparison to other PTO models

The work by Gervelas *et al.* (2011) and Nunes *et al.* (2011) both use the same turbine model as is used here, that of Falcão & Rodrigues (2002). The output pressures fit within the range seen by these studies, and with the estimation from Amundarain *et al.* (2011), in which the pressure is used as a driving quantity, rather than a specific wave. The power is quite low, at around 10 kW. However, this is average power rather than the peak value.

It would be possible to model a different type of turbine, for example an impulse turbine with a smoother efficiency response.

3.3.4 Limitations of the time domain model

The time domain model does not contain five OWCs, but only one WEC with a PTO. In order to make an estimate of the PTO's effect on the other OWCs, it could be possible to

do a nonlinear system identification from the velocity potential data: mapping the water surface displacement from one column to another.

A time domain model has only been made for the central column in the five column system. It would be interesting to compare this to a similar model of the other columns.

No allowance is made in the time domain model for incident angles other than head-on. A model which used a fine range of incident angles could give a much more realistic model of the system. Methods for achieving this are discussed in more detail in Section 4.4.3.

3.3.5 Extensions to the time domain model

A major step is to apply irregular waves to the time domain model and investigate the resulting performance. This will be covered in Chapter 4.

As well as testing control strategies, as will be done in Chapter 5, it would be possible to test the response for different turbine types or properties using this model.

Concluding remarks

The magnitude and phase responses of the various columns of the velocity potential study (Chapter 2) were turned into a mapping from the incident wave force to the resultant average displacement of the surface of the water column.

Rather than using the displacements estimated by the force to displacement mapping as a changing volume to drive all of the changes in the air, the mapping was used as a bridge between the wave forcing and the thermodynamic equations. It is the *difference* of the excitation force and the air pressure force which is used as input to the force-displacement mapping. Thus, not only does the wave excitation force affect the displacement of the internal water surface and therefore the air pressure in the chamber, but the air pressure in the chamber effects the internal water surface. This means that different pressure and mass flow relationships can be tested (and will be tested in Chapter 5).

The time domain model has been shown to be good enough to test out the expected performance of the central column of a breakwater mounted OWC system, assuming that the other columns are open, or at least almost not damped.

Summary

- OWC-WEC time domain models take frequency domain hydrodynamics and turn these into the time domain, then combine them with thermodynamic and turbine descriptions to model the system from wave to wire.
- A force-displacement transfer function was used to make a time domain model for an OWC-WEC in the central column of a five-column breakwater OWC system.
- The time domain model used regular, single frequency, plane waves with an amplitude of 0.5 m.
- The time domain model uses a Wells turbine with $D = 2.5\,\text{m}$, $N = 632\,\text{rpm}$ and $K_t = 0.375$.

Chapter 4

Performance of the breakwater OWC-WEC in a real sea

The most important factor for a WEC is the amount of energy that it converts. In order to know this for the breakwater OWC-WEC, the device should be tested under real sea conditions. This means that it should be tested in irregular waves and for a particular wave climate.

In Section 4.1, the methods for such describing such sea states and wave climates, as well as ways of testing a WEC in them, will be discussed. The central column of the breakwater system will then be tested in irregular waves with different sea states in Section 4.2. Finally, in Section 4.3, the annual performance of this OWC-WEC will be estimated for a site in the south west of the UK. This performance will be discussed in greater depth in Section 4.4.

4.1 Describing real seas

In order to describe a real sea in which to test the OWC-WEC, the spread of frequencies in the different sea states must be specified and an estimation of how often the sea states occur should be used to calculate an expected rate of energy conversion.

4.1.1 The real sea

In the open sea, the waves look quite different to those produced in most (numerical) wave tanks. The waves come from many directions and have a large spread of frequencies and phase shifts with respect to one another. The waves with different frequencies travel with

different speeds, which makes the ocean surface a compelling structure to watch. In order to describe this structure, the spread of directions and frequencies may be approximated by some distribution, and a sum may be taken over the frequencies and directions.

The methods by which such distributions are created come from measurement of the water surface by buoys (Saulnier *et al.*, 2011), radar and ADCPs (Strong *et al.*, 2012) and by calculations involving the measurement of wind speeds, followed by subsequent statistical manipulation.

The speed of a wave is influenced by the depth of the ocean and this depth has an impact on the shape of the water motion and the amount of energy contained within the waves. There is more energy in the deep ocean than at the shore where energy in dissipated.

There is also a difference between the distribution of the wave frequencies between waves which come from local and distant winds. Swell waves come from distant storms and tend to have longer wavelengths than wind-driven waves which are more local. It is obviously possible (and usual) to have two types of waves superimposed at a given site. For example, off the north coast of Devon, a swell-sea may see waves coming from Atlantic storms to the south-west, while the local winds may be driving waves from the north-west.

As well as varying in space, these wave fields vary with time: storms build, move and die and winds change in strength and direction. Thus, there is quite some variation in the waves that a WEC will experience hour-to-hour, day-to-day and season-to-season as well as year-to-year. The differences occurring over these time scales are large, thus, in order to convert energy effectively a WEC must be able to adapt to such changes.

All of these spatial and temporal effects mean that the waves at any point, say that of a measuring buoy, can be very different to its near neighbours in both mean statistics and distributions (Saulnier *et al.*, 2011). Thus, although a WEC may be designed in its geometry and expected PTO range for a certain area, each WEC (or collection of WECs) must be able to adapt its operation to the specific environment in which it finds itself.

4.1.2 Frequency domain models of the real sea

If it may be assumed that the wave field is made up of several superposed waves of different frequency and magnitude, then the relative proportions of different wave frequencies observable in a given sea may be described by a spectrum. There are different ways of approximating spectra mathematically.

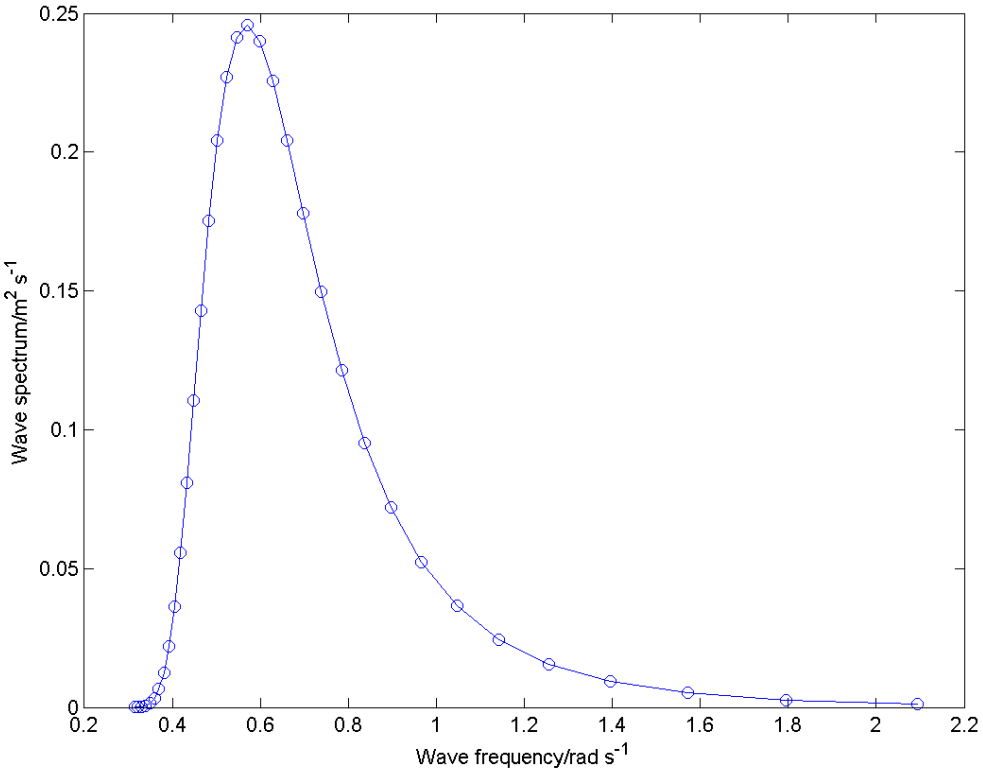

Figure 4.1: Wave spectra for waves with $T = 8.5\,s$ and $H_s = 1.25\,m$

The width of the spectral band may change such that there is a greater or lesser range of wave frequencies represented within the sea state. As the waves are produced by different atmospheric effects, different spectra result. Seas produced by local winds tend to produce shorter crested seas with a narrower range of frequencies in comparison to swell seas.

A Pierson-Moskowitz spectrum (Kiprakis *et al.*, 2009) describes a sea based on winds, which has become fully developed. This is the spectrum used to approximate the sea states seen by the buoy in Section 4.3. The spectral density is given by,

$$S_{PM}(\omega) = H_s^2 \frac{0.11 T_1}{2\pi} \left(\frac{\omega T_1}{2\pi}\right)^{-5} \exp\left(-0.44 \left(\frac{\omega T_1}{2\pi}\right)^{-4}\right) \tag{4.1}$$

The units of spectral density are $\mathrm{m}^2\ \mathrm{s}^{-1}$, which seems unphysical, but is defined such that

$$E = \int_0^\infty S(\omega)\omega d\omega \tag{4.2}$$

gives the total energy in the spectrum.

Following Kiprakis *et al.* (2009) as above, for the amplitudes, A_E, of the components

within the spectrum at each frequency, ω_j

$$A_E(\omega_j) = \sqrt{2S(\omega_j)\Delta\omega} \tag{4.3}$$

where, $\Delta\omega$ is the frequency band that is covering ω_j.

4.1.3 Time domain models of the real sea

In order to make a time domain model, the spectral amplitudes must be turned into a force. This force is dependent on the area of the structure, the depth at which the force is acting, the frequency of the wave component and the depth of the ocean.

For waves which are formed from a spectrum, the total force in the time-domain is given by using the amplitude of the waves at a given frequency, as in Section 3.1.1. Now, there are many frequency components, so the force is given by the sum over all of these frequencies:

$$f_e(t) = \sum_j \delta(k_j) A_w \rho_w g A_E(\omega_j) \sin(\omega_j t + \phi_j) \Delta\omega_j \tag{4.4}$$

where $\Delta\omega_j$ is the weighting for each section of the spectrum and $\delta(k)$ is defined as

$$\delta(k) = \frac{\cosh k(d-h)}{\cosh kd} \tag{4.5}$$

where d is the ocean depth and h is the depth at which the force acts (here the draft of the water column).

Note that in Equation 4.4, the phases ϕ_j are random. This describes a sea which does not have interactions between its spectral components. Note also that this is a sea state with all of the waves moving as a planes perpendicular to the breakwater (cross-shore/beam-sea). The assumption of plane waves is obviously a simplification of the real sea, although for a breakwater, the wave alignment is likely to be closer to this than would be the case for an isolated WEC.

4.2 Performance in irregular waves (seas defined by spectra)

Chapter 3 showed the behaviour of the OWC in regular waves. However, this is not the performance that would be seen in a real sea. In this section, the model of the central column of the five column OWC-WEC will be tested using irregular waves, and with different sea states.

4.2.1 Testing the time domain model of the OWC of the central column of five in the breakwater set-up for spectral waves

A fixed time-step of 0.005 s is used for all of the runs. 900.0 s (15 min) of model time is run for irregular waves (the regular waves use only 300.0 s). Each irregular wave run takes around 5 s to complete. As for the regular waves, the solver is an ode3 Bogacki-Shampine. In the spectral waves, there are 81 frequency components, ranging from 0.31 rad s^{-1} to 1.57 rad s^{-1}. Higher frequencies were not included owing to the range of frequencies for which the impedance model is valid. The assumption is that the higher frequency response would be low in the real sea situation.

4.2.2 Internal water surface displacement in irregular waves

Using the time-series of a spectral sea, the displacement can be investigated. An example is shown in Figure 4.2. The magnitude of the internal water surface motion is similar to that seen for the incident wave. There is a slight lag, and the amplification is positive for longer waves, while shorter waves have a lower amplification. This reflects what was observed for the regular waves in Figure 3.14.

4.2.3 Thermodynamics in irregular waves

Figure 4.3 shows that the pressure follows the same pattern as the displacement of the internal water surface. The magnitude of the peaks at around 2000-4000 Pa is a little larger than that for the regular waves, which is 2500 Pa for a 1 m high wave. It should be noted that the regular wave figure comes from the mean of the the absolute variation, and the the peak values of the variation are higher than this. The pressure variation is a little smoother than the displacement.

The mass flow obviously follows the same pattern as the pressure difference. This is also shown in Figure 4.3 so that the phase relationship is clear. The magnitudes are similar to those seen under regular waves (around 20 kg s^{-1}). Clearly, the mass flow is in anti-phase with the pressure. This is because, for fixed turbine speed, Equation 1.28 leads to $dm/dt \propto \Delta p$.

4.2.4 Power output in irregular waves

The power output is shown in Figure 4.4. The peaks come twice as frequently as for the pressure and mass flow because the power shows conversion for both the in- and out-flow

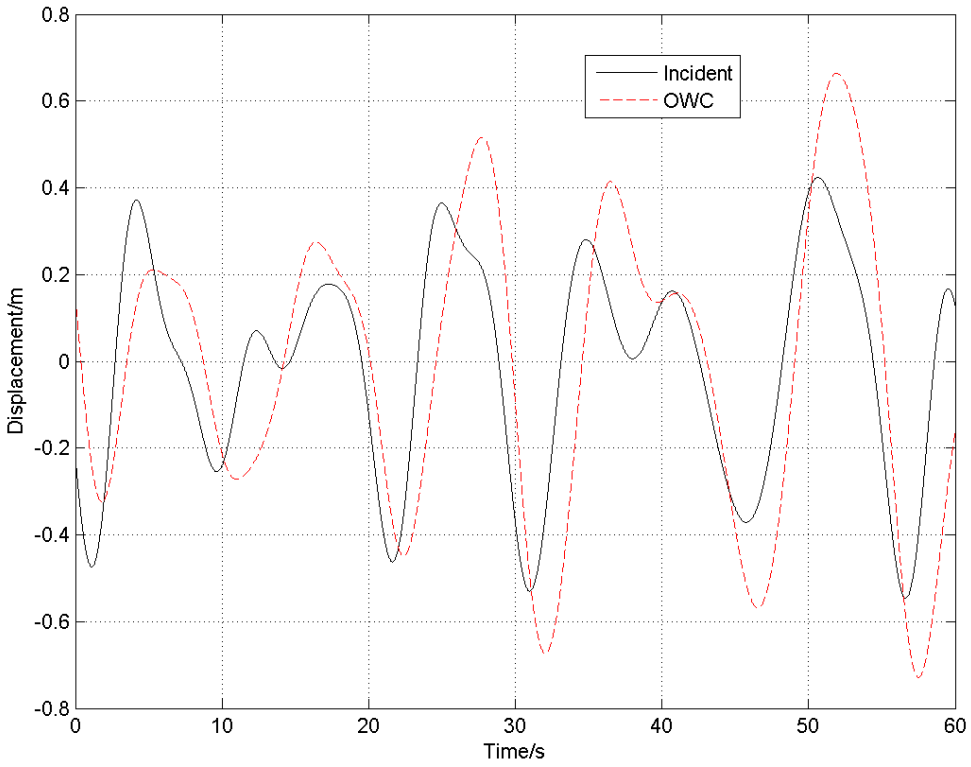

Figure 4.2: Displacement for the internal water surface, with H_s =1.25 m and T_e =8.5 s. (Turbine constant, K_t, is 0.375, fixed turbine speed, N_f, is 632 rpm and the diameter of the turbine, D, is 2.5 m. These parameters are given in Section 4.3.2)

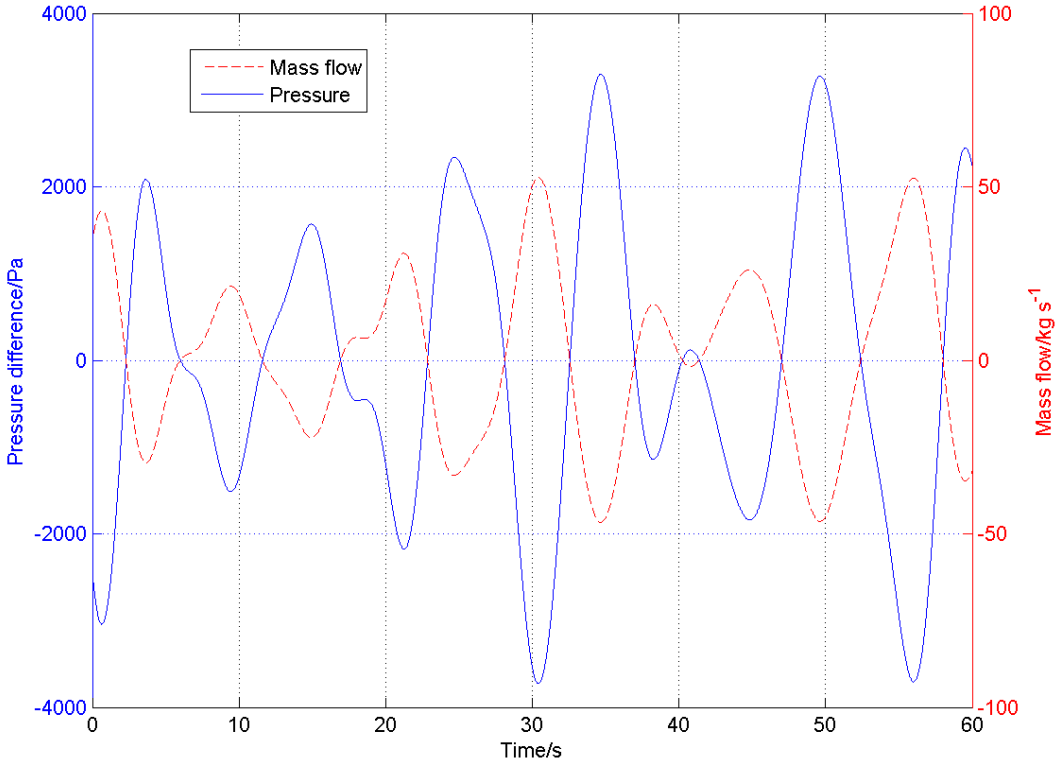

Figure 4.3: Pressure and mass flow for the same wave as in Figure 4.2

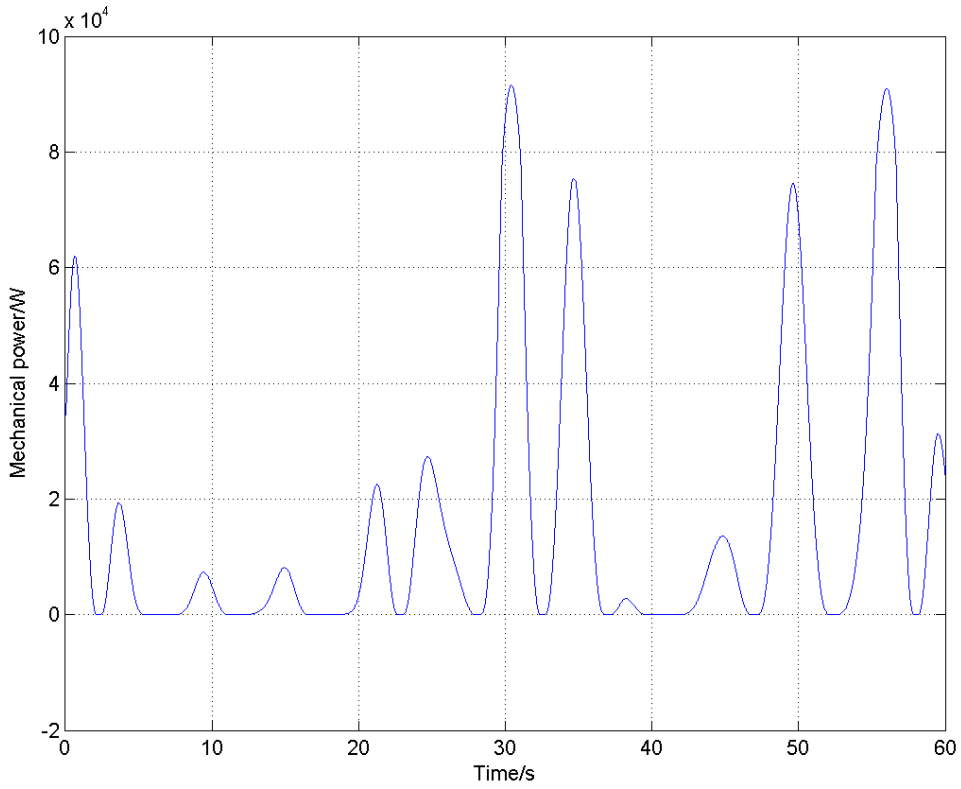

Figure 4.4: Power trace for the same wave as in Figure 4.2

parts of the wave cycle. Note that for much of the time the power converted is *much* lower than that at the peaks. For this particular sea state, with $H_s = 1.25$ m and $T_e = 8.5$ s, the average power output is 24.8 kW. The maximum power is 118 kW in the test section, which occurs at stalling conditions. The standard deviation of the power is 33.0 kW, so clearly there is a lot of variability in the power output. This can have implications for generator design: because the generator has to be able to handle very large powers, the generator will need to be over-rated, but will also need to be efficient at low powers.

The power output may be calculated like this for several sea states. The result is shown in Figure 4.7, with the values given in Table C.1. The power converted is clearly highly dependent on wave height, with most of the variation as a function of wave height. However, the period also makes a difference. For a given H_s, it is clear that the power converted will have a maximum for some period, with the 7-10 s periods the most effective for energy conversion. The power outputs for the large wave heights, of 60-70 kW, are much larger than the 30 kW seen for sea states where H_s is lower than 1.5 m.

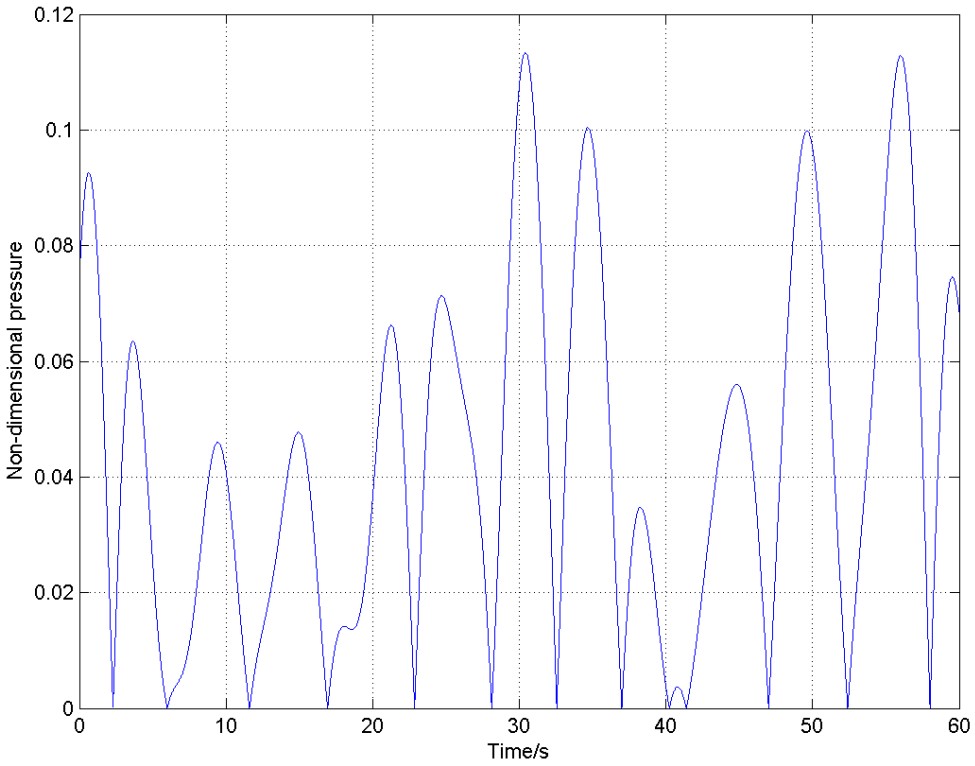

Figure 4.5: Non-dimensional pressure for the same wave as in Figure 4.2

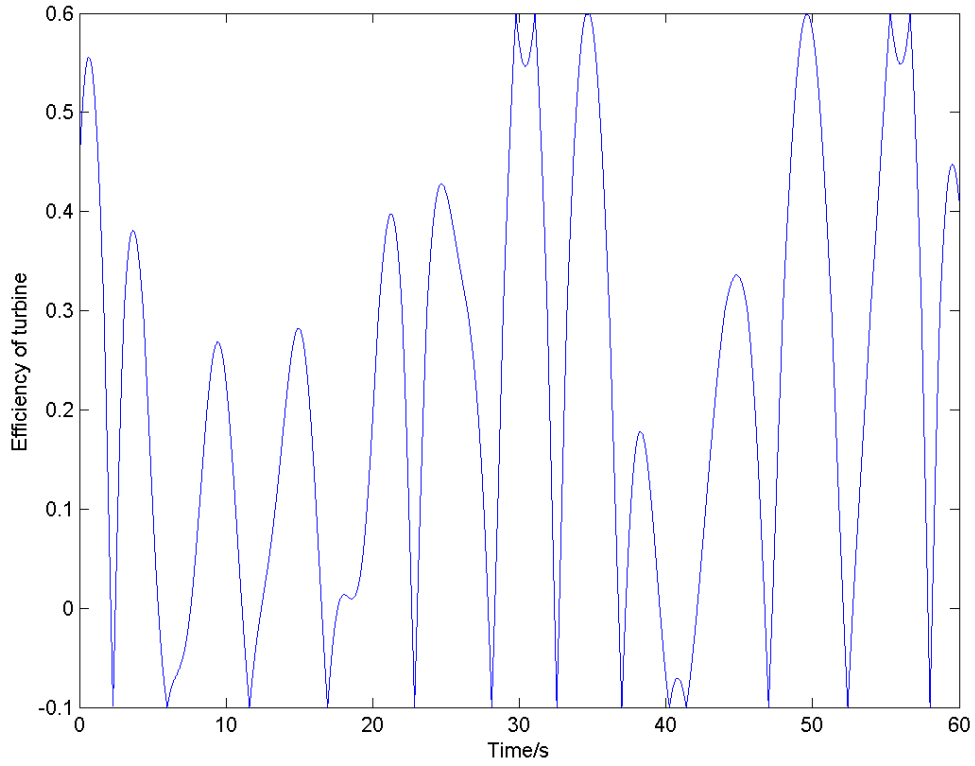

Figure 4.6: Efficiency of the turbine for the same wave as in Figure 4.2

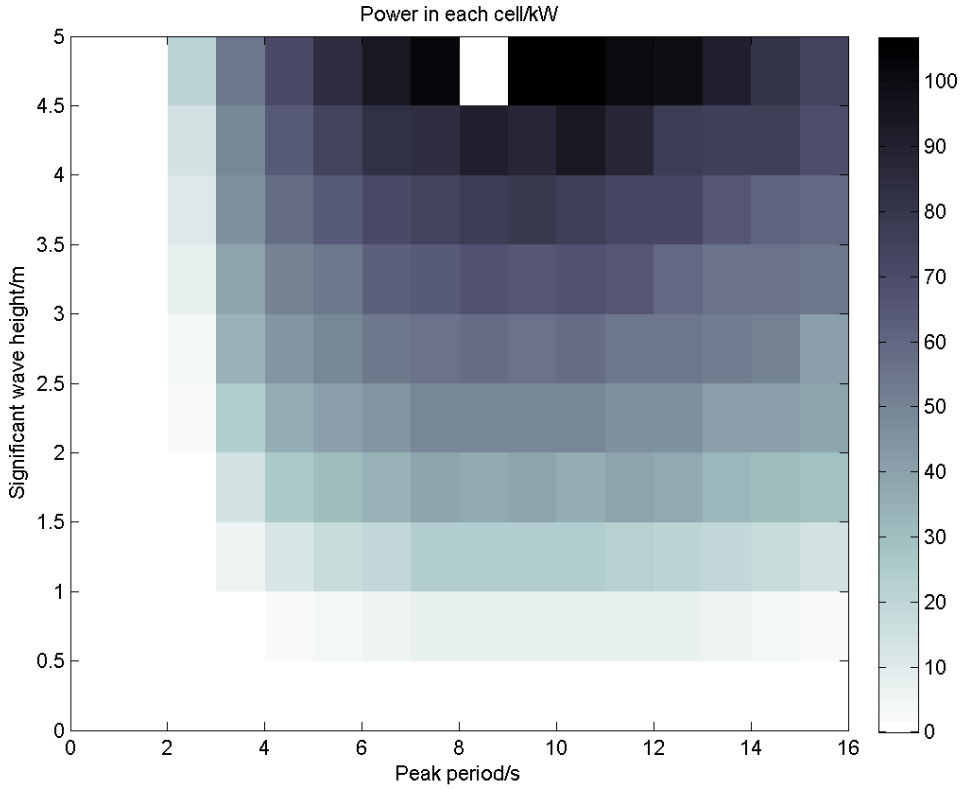

Figure 4.7: The power output from the central OWC for various sea states using a Pierson-Moskowitz spectrum

4.2.5 Power output in various sea states

The estimated average power converted by the OWC-WEC in various sea states is shown in Figure 4.7. This shows that the power increases with wave height, with a peak for sea state wave period of around 10 s. Note that for the sea state with $H_s = 4.75$ m, and $T = 8.5$ s the power is 0 as the internal water surface was found to reach the top of the water column and it is therefore assumed that the OWC-WEC will be shut-off when such sea states occur.

Note that the internal water surface reaching the top of the column is assumed to cause shut-down, but it may fall below the OWC lip without causing shut-down. This is because it is assumed that the OWC-WEC may continue to convert energy in such situations. If the internal water surface has fallen this far, the behaviour is therefore far from linear, so the assumptions regarding the wave-structure interaction will no longer hold. This means that another method of modelling the OWC-WEC should be used in this nonlinear regime. Further details are given in Section 4.4.2.

4.3 Annual performance

To estimate annual performance, a specific site should be selected and representative frequency of occurrence of spectra used to calculate overall energy conversion.

For the fixed breakwater, a coastal sea is envisaged and so the Channel Coast Observatory data was used to select a suitable site. The coastal sea is considered to be that of the Bideford Bay buoy and the frequency of occurrence are shown in Figure 4.8. Bideford Bay is on the north coast of Devon, where the Atlantic Ocean reaches towards the Bristol Channel. The site is in 10 m water depth and the coastline faces west towards the Atlantic, although is somewhat sheltered from full South-Westerly storms.

The range of periods seen is very similar to that of deeper water sites as swell waves are a prominent feature, but the wave heights are decidedly lower, being confined to spectral wave heights of 3 m or so, rather than ranging to spectra with H_s of 8 m.

4.3.1 The chosen wave climate

The yearly average sea is composed of mean data from the four years 2009-2012. The joint occurrence is shown in Figure 4.8. The Environment Agency buoy situated in Bideford Bay off the North Devon coast. The wave spectrum is measured in each 30 minute interval and a Pierson-Moskowitz spectrum is fitted to this. The joint occurrence is then the fraction of the year in which joint H_s and T_e pairs occur. The most frequent joint occurrence is that of H_s of 1-1.5m and T_e of 8-9s. This sea state was observed to occur for 7.2% of the time.

4.3.2 Selection of the parameters for baseline performance

A range of possible values for the diameter and speed of the turbine were tested in the irregular waves. The energy outputs were calculated for different combinations of N and D and for each combination of H_s and T. The energy output was assumed to be zero where the water surface reached the chamber roof or where the turbine operated in stalled conditions such that non-dimensional pressure, Ψ, was greater than 1. The energy estimations were made on the basis of 15 minutes of spectral waves for each sea state. These energy estimations for the given sea states were then multiplied by the frequency of occurrence over the year to come up with an estimation of the total annual energy.

The resulting converted energy is shown in Figure 4.9 for various combinations of turbine speed, N_f, and turbine diameter, D. Only combinations of 1, 1.5, 2, 2.5 m diameters

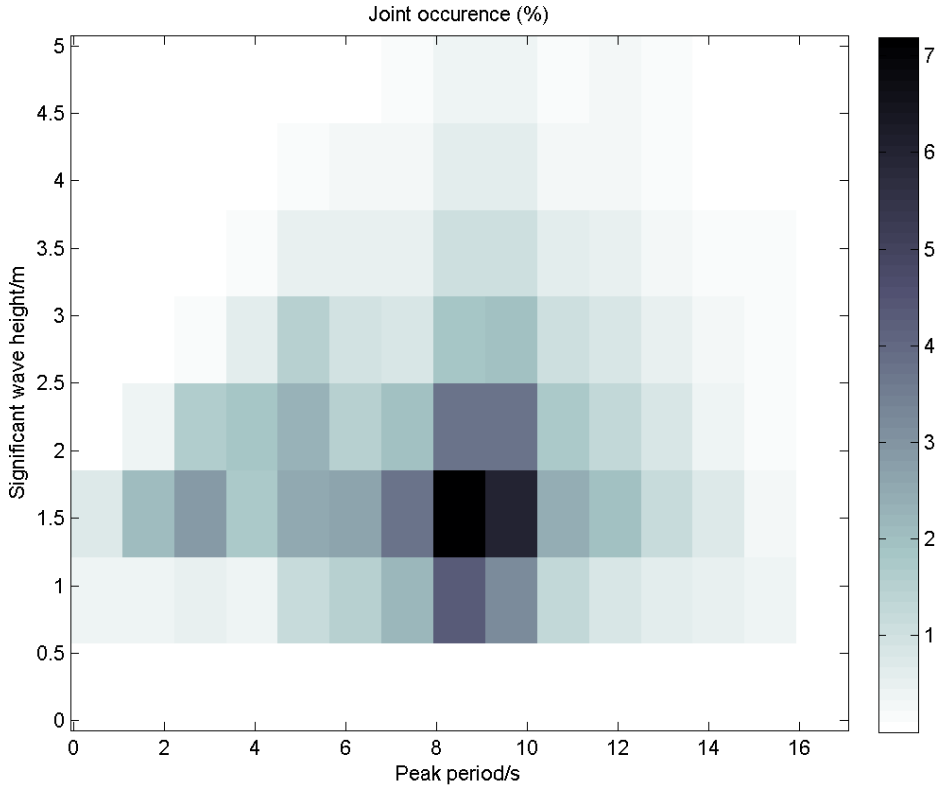

Figure 4.8: H_s and T_e joint occurrence (sea state occurrence) at Bideford Bay in percentage of the mean year

and 500, 1000, 1500, 2000 rpm were tested due to a full wave climate test taking around 20 mins. The peak occurs for a turbine diameter of 2.5 m and a turbine speed of 1000 rpm.

The diameter was chosen to be as large as was deemed physically possible (2.5 m) due to the shape of the contour figure. However, the fixed turbine speed could have its maximum anywhere between 500 and 1500 rpm, so the MATLAB optimisation function `fminsearch()` was used to optimize the turbine speed.

In order to reduce the computational time for this optimization, the different fixed speeds were tested in the Pierson-Moskowitz sea state with $H_s = 1.25$ m, and $T = 8.5$ s. Figure 4.10 shows the average power for the OWC-WEC for various values of turbine speed (and using a turbine diameter of 2.5 m). The turbine speeds shown are those that the `fminsearch()` function chose to search. This optimisation function uses a Nelder-Mead simplex direct search and was started at both 500 rpm and 1000 rpm based on the values suggested from Figure 4.9. The greatest converted energy is achieved using a turbine diameter of 2.5 m and a turbine speed of 632 rpm.

The baseline performance for energy conversion therefore comes from the turbine size and speed combination applied across the whole average year. This performance is shown

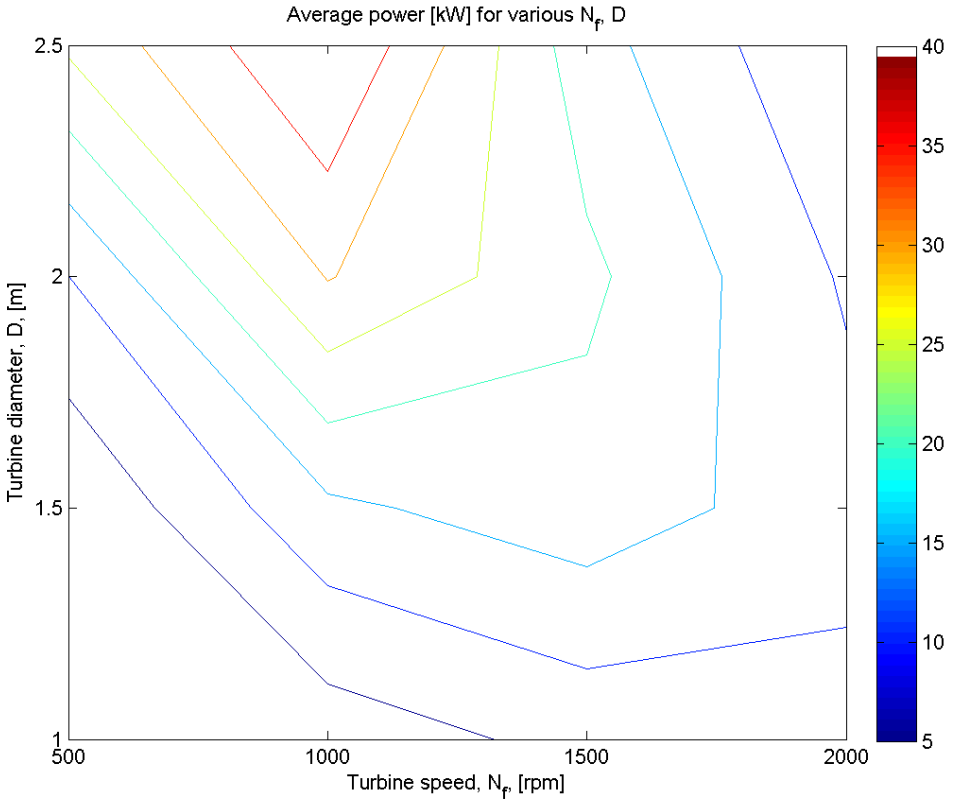

Figure 4.9: Power estimated for various turbine diameter and speed combinations for the central column of the breakwater system assuming that it was positioned in the Bideford Bay wave climate

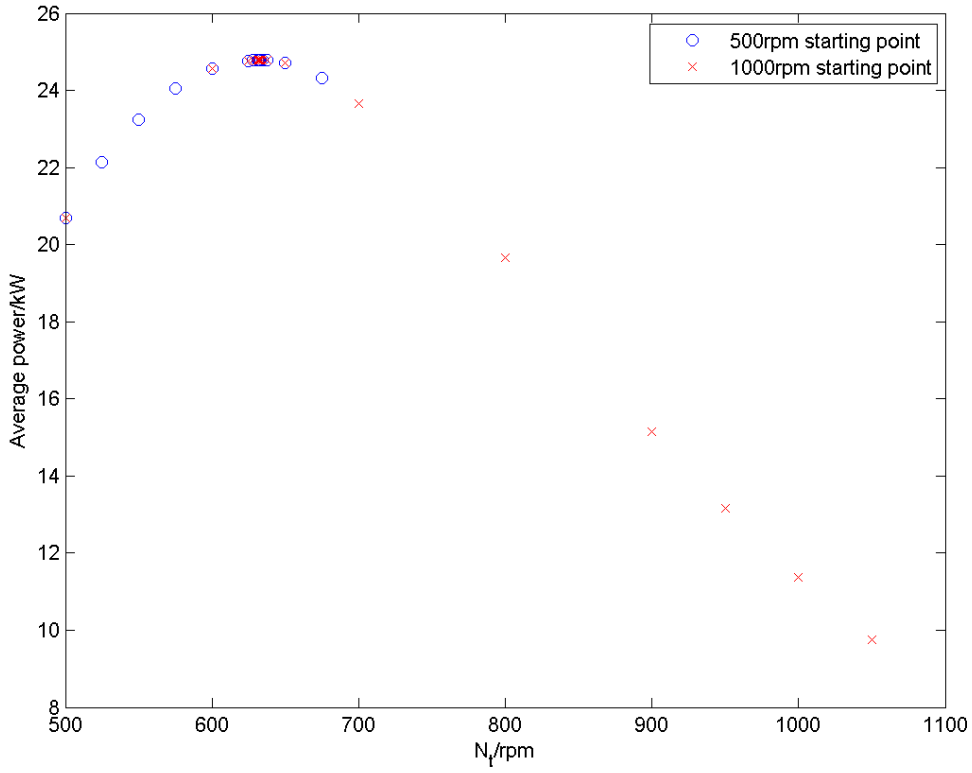

Figure 4.10: Selection of fixed turbine speed

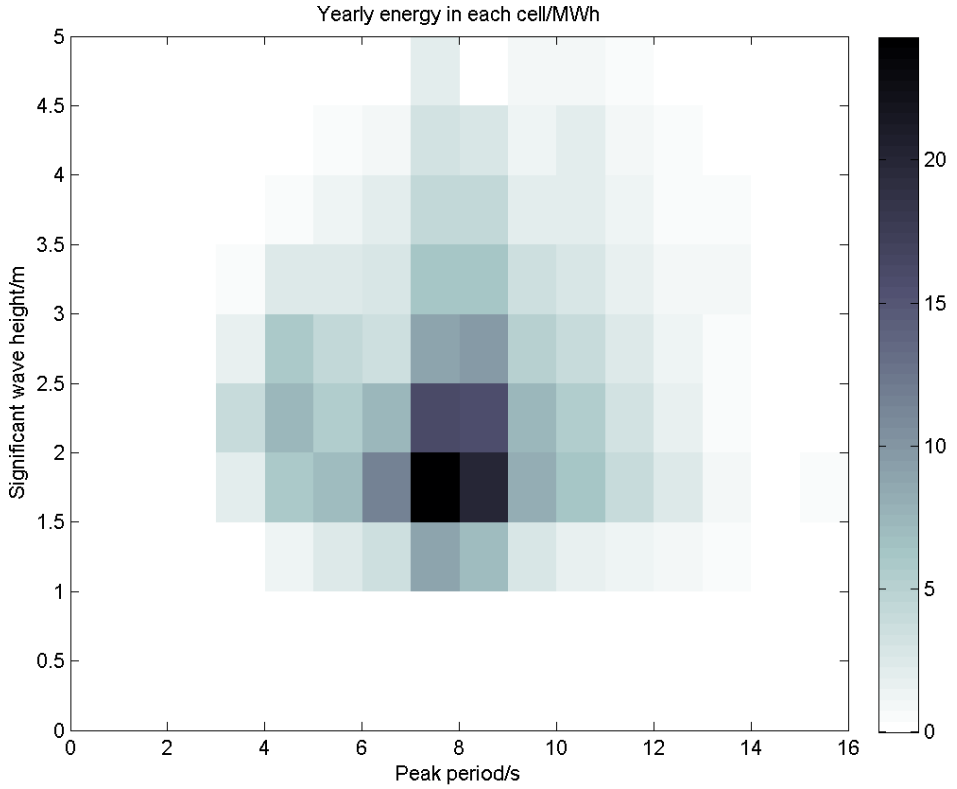

Figure 4.11: Energy output over the average year for a turbine with $D = 2.5\,\text{m}$, $N = 632\,\text{rpm}$

in Figure 4.11. Total energy converted is estimated to be 318 MWh, for waves incident head-on, with no PTO for the surrounding columns and with no unexpected down-time. If this were provided uniformly across the year, the power output would be 36.3 kW. Note that this is lower than that calculated when a fixed speed of 1000 rpm was used. This is because the lower speed is more effective for the smaller sea state, with the 1000 rpm version converting more energy in the larger sea states.

4.4 Discussion of the modelled performance

The purpose of modelling the performance of the OWC-WEC with five columns and a single PTO over the central chamber is to estimate the amount of energy converted by the OWC-WEC in real sea conditions. This enables an estimation of the amount of damping which a PTO applies to the internal water surface. It also enables the testing of different control strategies on realistic seas. This in turn gives a better idea of the kinds of damping which will be observed on the internal water surface and whether this happens steadily or in a very time-varying manner. This will be covered in Chapter 5.

4.4.1 Comparison of estimated energy conversion to published work

The pressure differences seen for an OWC are obviously vital to the estimation of converted power. The magnitude of the pressure difference which Amundarain *et al.* (2011) assumed to be driving the energy conversion is 7000 Pa. This is around twice as high as those seen here, but is certainly of the same order of magnitude. This produced a power output of around 20 kW, which is lower than anticipated here.

For operation at a fixed speed, Nunes *et al.* (2011) found an average power over the whole year of 29 kW. This was for a single device deployed in the open sea and for a 7 m diameter variable pitch Wells turbine, with turbine coefficient $K_t = 3.6$. The pressures and mass flows described for their OWC-WEC are around twice those seen here: 10,000 Pa and 50 kg s^{-1} for regular waves. (A 1.5 m wave height was assumed by Nunes *et al.* (2011) in the case of irregular waves, so it is assumed that a similar value was used for their regular waves.) The power output of the Nunes *et al.* (2011) OWC-WEC could be increased to 98 kW by choosing a good fixed speed of rotation for each sea state.

4.4.2 Limitations to the performance estimation

Variation between years means that the estimation of annual energy is not necessarily accurate. The estimation of which turbine speed would give best results in each sea state is well characterised though, albeit only for waves incident head-on. However, such characterisation is limited by the initial time domain model, in that the status of the neighbouring devices have influence only as open chambers and not as WECs with PTOs of their own.

These sea states themselves also provide a limitation, as they are defined by spectra and thus are only approximations to real seas. No account is taken of seas which are not single moded, nor of seas in which the waves do not all travel from a single head-on direction. However, clearly the waves can come from alternative directions, and certain wave groups within a prevailing sea can come from a greater spread of angles.

The temporal variability of the wave climate suggests that the system needs to have a controller which can change the plant's behaviour to match the sea. Optimisation which assesses parameters fixed over a year will not use a good criterion for assessment. The different years are as different as the different seasons within them. It is assumed that any controller that is used in the real world will include switching between different rules or models to deal with the very different wave climates that may present - Nunes *et al.*

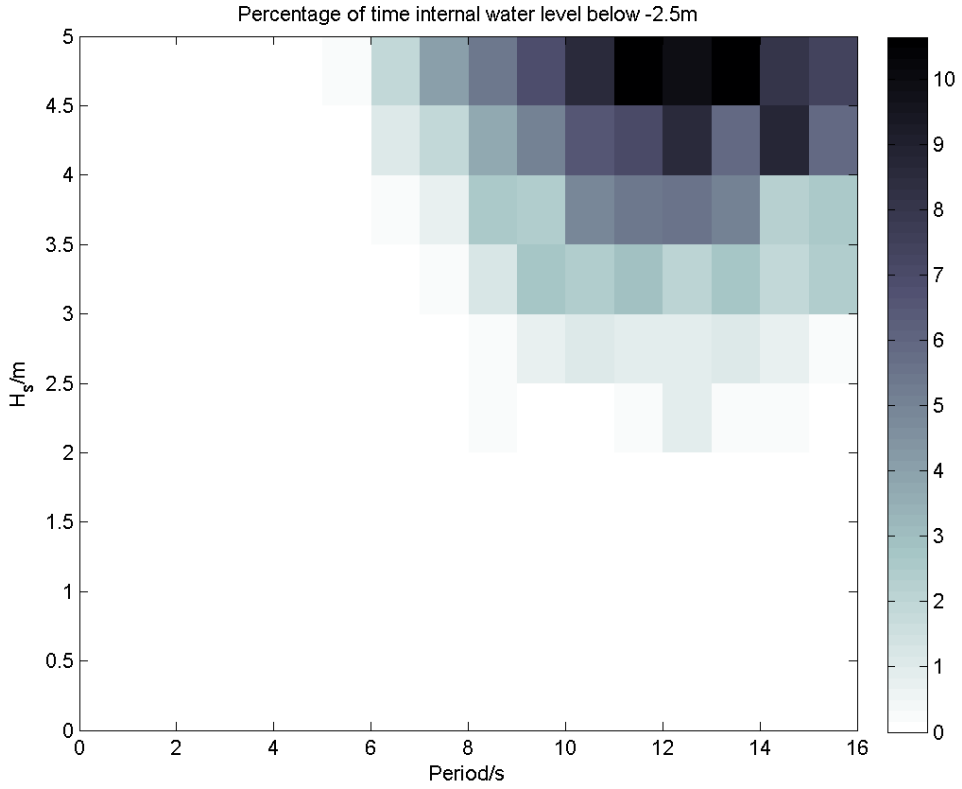

Figure 4.12: Percentage of time that the internal water level is below the lip of the OWC in each sea state for a turbine with $D = 2.5$ m, $N = 632$ rpm

(2011), for example, uses switching in the sense that for each H_s and T, a different transfer function is used to represent the TDM.

One major limitation comes from the linearity assumption of the wave-structure interaction. Figure 4.12 shows the amount of time the internal water surface is below the lip of the OWC. This may be used as an indication of when the linear velocity potential approximation will not hold. For those sea states where the water surface does drop below the front lip, the WEC may go on converting energy, but the values estimated here should only be used as indicative. Thus the estimation of energy in the sea state with $H_s = 1.25$ m, and $T = 8.5$ s is most likely a good one, but the estimation for the annual energy conversion is likely to be quite approximate with the energy converted in the larger seas likely to be lower than that shown in Figure 4.7. However, the sea states for which the internal water surface drops below the OWC lip are not very highly represented in Figure 4.11. For larger seas, a nonlinear model of wave-structure interaction should be used. This could involve the CFD or physical modelling options described in Section 1.2.2.

4.4.3 Extensions to the performance estimation

In order to extend the model and the performance measurement to include waves of different incident angles, Equation 1.2 may be used. This requires a model which responds to different angles of incidence. It would be possible to use a velocity potential method, as in Chapter 2, to produce different force-displacement mappings based on different angles of incidence, and drive them using the wave components from Equation 1.2.

A system identification method based on prevailing direction might be more appropriate than identifying each component. It would probably be faster to run and easier to handle as fewer parameters are required. The accuracy, however, would depend very strongly on the training of that model.

Another significant extension to the model is to look at how changes to the turbine speed affect power take-off. This will be explored in the next chapter.

Conclusions

Using the constant speed turbine leads to an estimated annual average power of 36.3 kW, based on operation with no extra down-time during the average year assumed from the wave buoy measurements in Bideford Bay during 2009-2012. In the sea state for which the fixed speed was chosen to be optimal, the average power was found to be 24.8 kW. This will be used as a baseline when testing control methods in Chapter 5.

Summary

- The time domain model of the breakwater OWC was generalised to include irregular waves.
- The time domain model was used to estimate energy converted in different sea states as defined by a Pierson-Moscowitz spectrum.
- The frequency of occurrence of different seas was used to estimate annual energy output for the central column OWC-WEC in a wave climate corresponding to the Bideford Bay site. For a turbine with diameter, $D = 2.5\,\mathrm{m}$, turbine coefficient, $K_t = 0.375$ and fixed speed $N_f = 632\,\mathrm{rpm}$, the energy converted was 318 MWh.

Chapter 5

Control system design

Chapter 4 clearly showed that changing the rotational speed at which the turbine operates can increase the energy converted by the OWC-WEC. In this chapter, the turbine will be tested with control rules that change the speed of the turbine during the wave cycle. To begin with, a very simple, feedforward control action is tested: the speed changes linearly with chamber pressure difference from an offset speed. In Section 5.2, a nonlinear feedforward controller is tested. This controller is designed to keep the turbine operating at the speed which gives it maximum efficiency. This was used because the efficiency of the turbine was shown to have a large effect on the effectiveness of the whole system - if the pneumatic power is multiplied by a very small factor (or by a negative one), this will reduce the energy converted in comparison to a case with a larger factor.

5.1 A simple linear controller

In order to test whether speed control could be effective, a very simple controller was tested. This controller takes pressure difference as its input and calculates a value for turbine speed. This control action was optimised by choosing the control parameters which lead to the highest average power when tested on the sea state at Bideford Bay which contained the most annual energy.

5.1.1 Definition of the linear controller

A simple feedforward linear controller may be envisaged, having two variables: an offset speed, N_l and a constant of proportionality, K_l, such that the turbine speed is given in $\mathrm{rad\,s^{-1}}$ by

$$N_r = \frac{2\pi}{60} N_l + \Delta p K_l \tag{5.1}$$

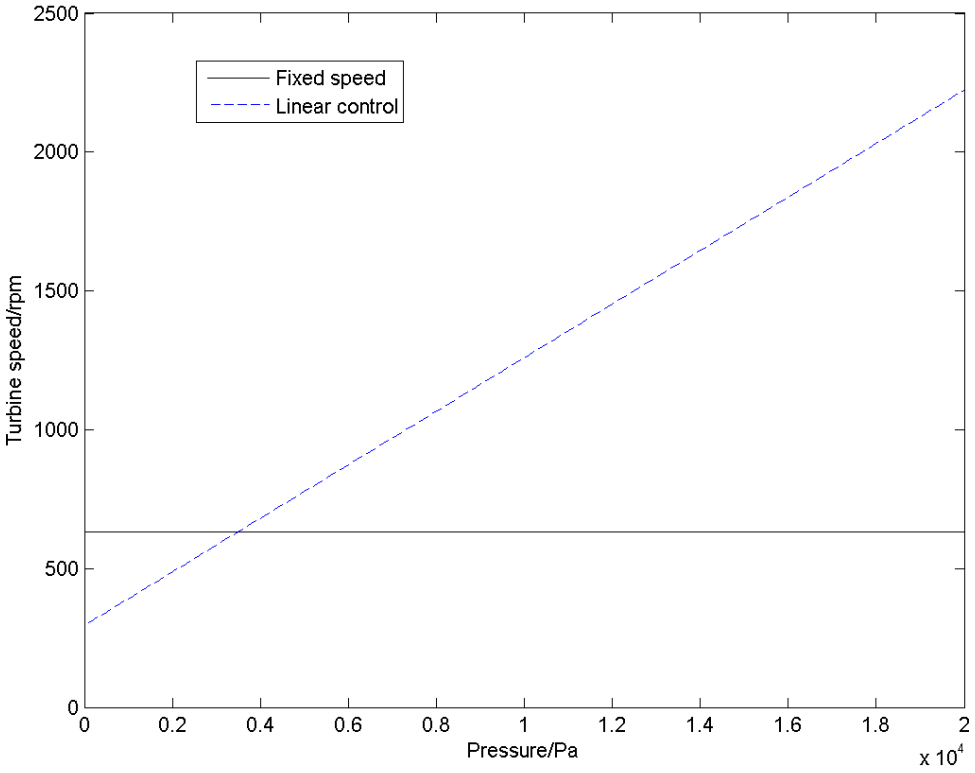

Figure 5.1: Action of the linear controller

Such a control action is shown in Figure 5.1.

5.1.2 Optimization of the linear controller

In order to choose a combination of N_l and K_l which leads to suitable performance, the controller was tested in the sea state which has the largest annual energy at Bideford. That sea state is defined as having a Pierson-Moskowitz spectrum with wave height 1.25 m and period 8.5 s.

The cost function by which the controllers were tested is simply maximisation of average power. As in Section, 4.3.2, for those combinations which lead to displacements higher than the chamber or to non-dimensional pressures, Ψ, greater than 1 a "not-a-number" value of the cost function was recorded. Here, where turbine speed is changing, turbine speeds greater than 3000 rpm also resulted in a "not-a-number" value of the cost function.

Initially, a large scale search was conducted over the N_l, K_l combinations. This is shown in Figure 5.2. Here the N_l, K_l combination which lead to the highest average power was a turbine speed offset of 250 rpm and a constant of proportionality of 0.01 rad s^{-1} Pa^{-1}, which resulted in an average power of 31.0 kW. In the upper left of the figure, there is another (lower) peak where N_l and K_l are 650 rpm and 0.0 rad s^{-1} Pa^{-1}.

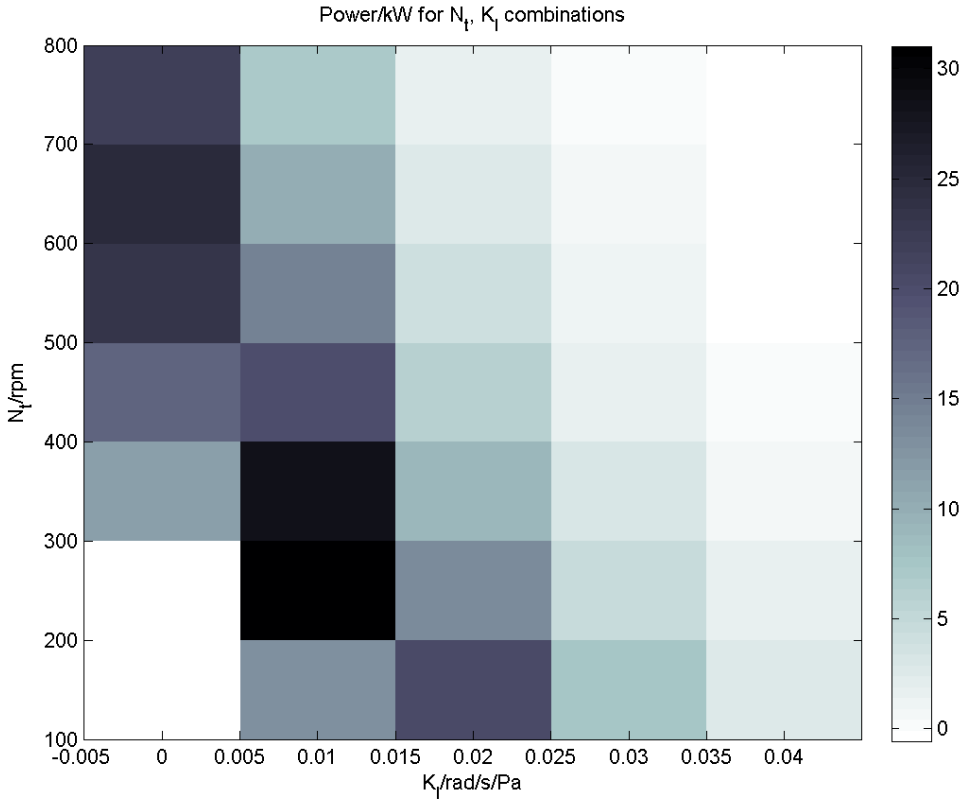

Figure 5.2: Optimisation of the linear controller coefficients

This lead to average power of 24.7 kW, and corresponds to the fixed speed control option.

These two N_l, K_l combinations were used as starting points for the MATLAB optimisation function `fminsearch()` as in Section 4.3.2. Both starting points converged on an N_l, K_l combination of 295 rpm, 0.0101 rad s^{-1} Pa^{-1}. This convergence process is shown in Figure 5.3.

This combination of speed offset, N_l, and constant of proportionality, K_l, gave an average power in the optimisation sea state of 32.9 kW, which means that 33% more energy is converted in this sea state using this linear controller than is converted when using the optimum fixed speed control.

5.1.3 Performance of the linear controller in regular waves

The performance of the system with the linear controller is tested in regular waves, as it was for the fixed speed case (Section 3.2.3). Figures 5.4 to 5.6 show how the OWC-WEC performs using the linear controller. The displacements (Figure 5.4) are higher than in the fixed speed control case (Figure 3.11), by about 0.1 at all periods.

In comparison to the fixed speed case (Figure 3.12), the mass flow in and out of the chamber increases when the linear controller is used (Figure 5.5). The pressure difference

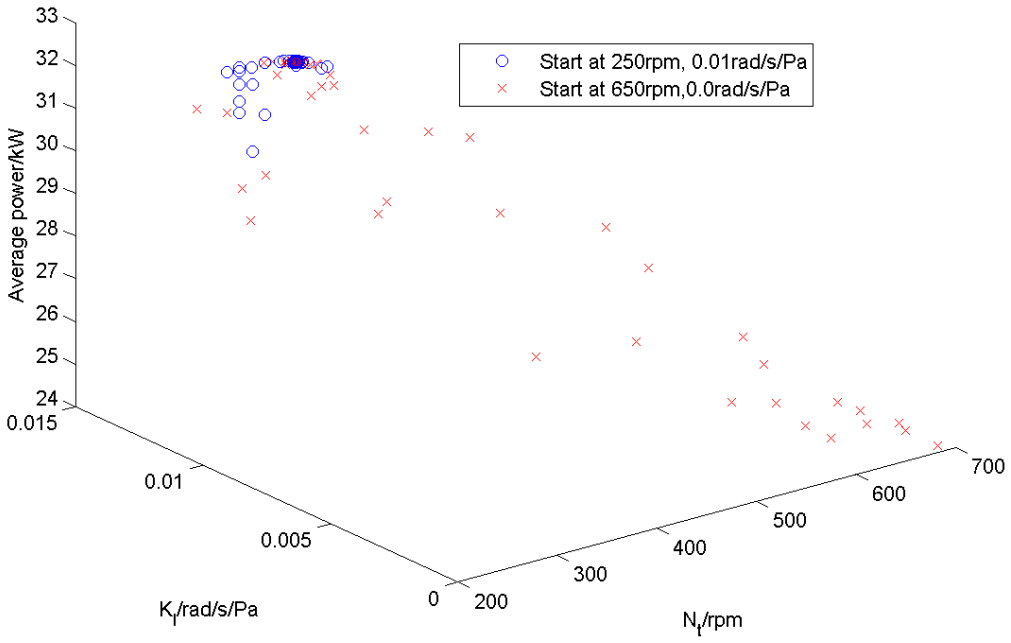

Figure 5.3: Optimisation of the linear controller coefficients

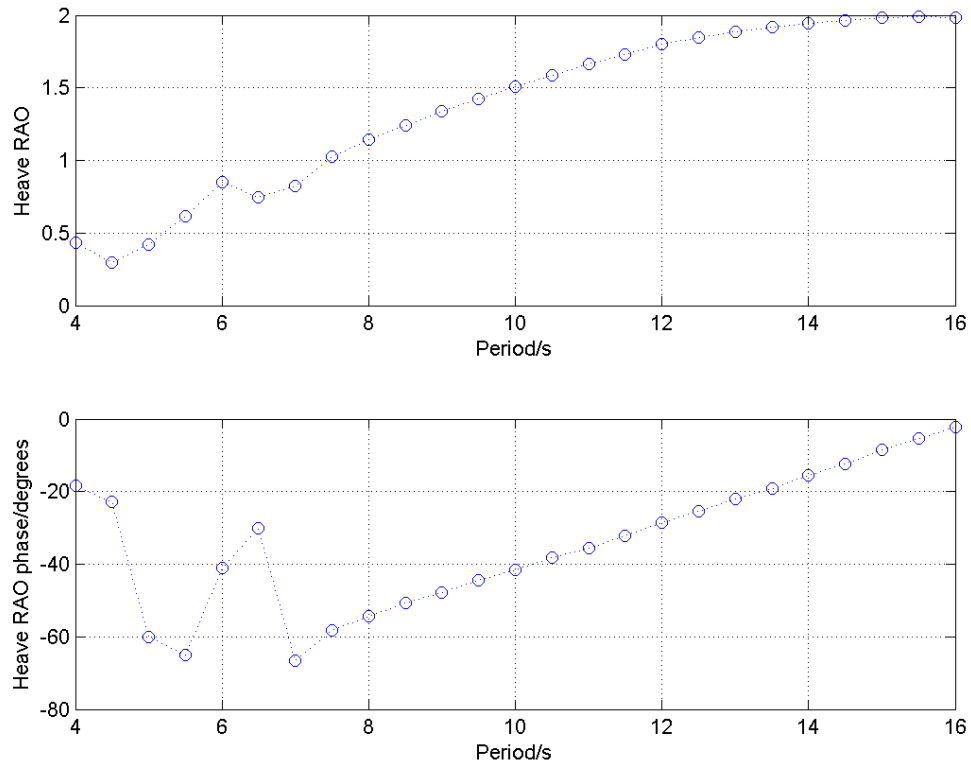

Figure 5.4: RAO of the internal water surface displacement for the OWC-WEC with linear controller for regular waves in regular waves, plotted with respect to period

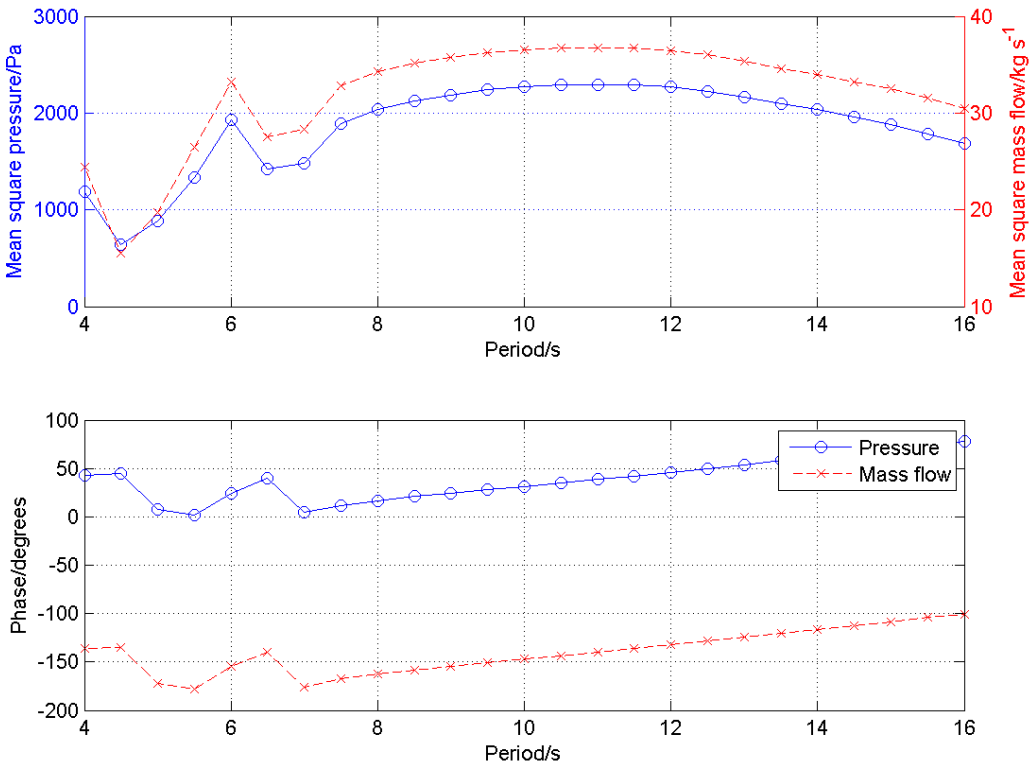

Figure 5.5: Pressure and mass flow for the OWC-WEC with linear controller for regular waves in regular waves, plotted with respect to period

is very slightly lower in the linear case than under the fixed controller. The pressure and mass flow phase trend is the same as for the fixed speed case, however the value of the phase is around 5° ahead of the fixed speed OWC-WEC.

The mass flow and pressure changes thus caused lead to increased power at all wave periods, as shown in Figure 5.6.

5.1.4 Performance of the linear controller in irregular waves

The controller must also be tested in irregular waves. Section 4.2 showed this response for the system with fixed speed controller. The same irregular waves are used here for clarity in comparison.

Figure 5.7 shows the displacement of the internal water surface seen when the linear controller is used. The peaks and troughs are slightly larger here than in the fixed speed case.

For pressure and mass flow (Figure 5.8), the pressure changes seem to be very similar to the fixed speed case. The mass flow, however, is a little larger, and the peaks are broader than under fixed speed control. This means that the power peaks are generally

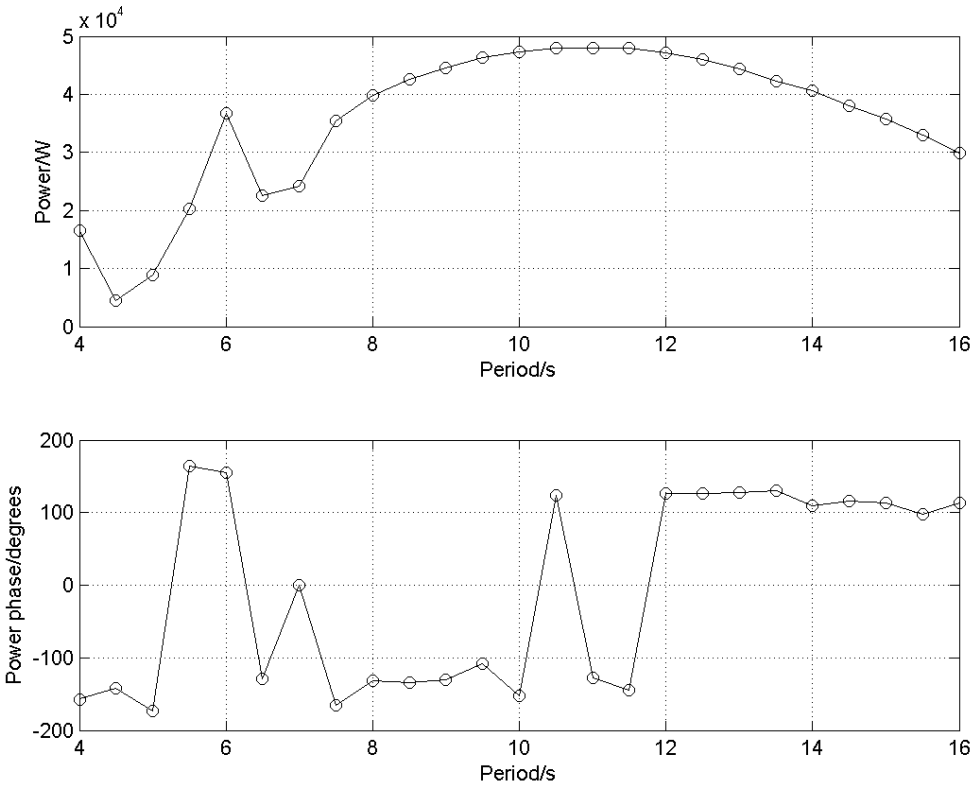

Figure 5.6: Power for the OWC-WEC with linear controller for regular waves in regular waves, plotted with respect to period

a little higher and certainly are broader in the linear controller case, as can be seen in Figure 5.9.

Figure 5.10 shows the turbine speeds which are used. The turbine's lowest speed is 295 rpm or 30.9 rad s^{-1} (4.9 Hz). It does reach the speed at which the fixed speed controller operates on two occasions, but for the most part, the turbine speed is lower for the linear controller.

The sharpest change of speed that the turbine must go through is during one of the larger peaks where the speed reaches 650 rpm within around 2 s. A change of 175 rpm in one second is the equivalent of 18.3 rad s^{-1} (or 2.9 Hz). This represents a 60% change in speed in 1 s, which is quite fast.

5.1.5 Performance of the linear controller in various sea states

The controller optimised for a single sea state may be tested in other sea states. Figure 5.13 shows the ability of the OWC-WEC to convert energy in each of these sea states using the linear controller. The resulting conversion is shown as average power for that sea state. As for the linear case, the OWC-WEC can give a higher average power in sea states where the

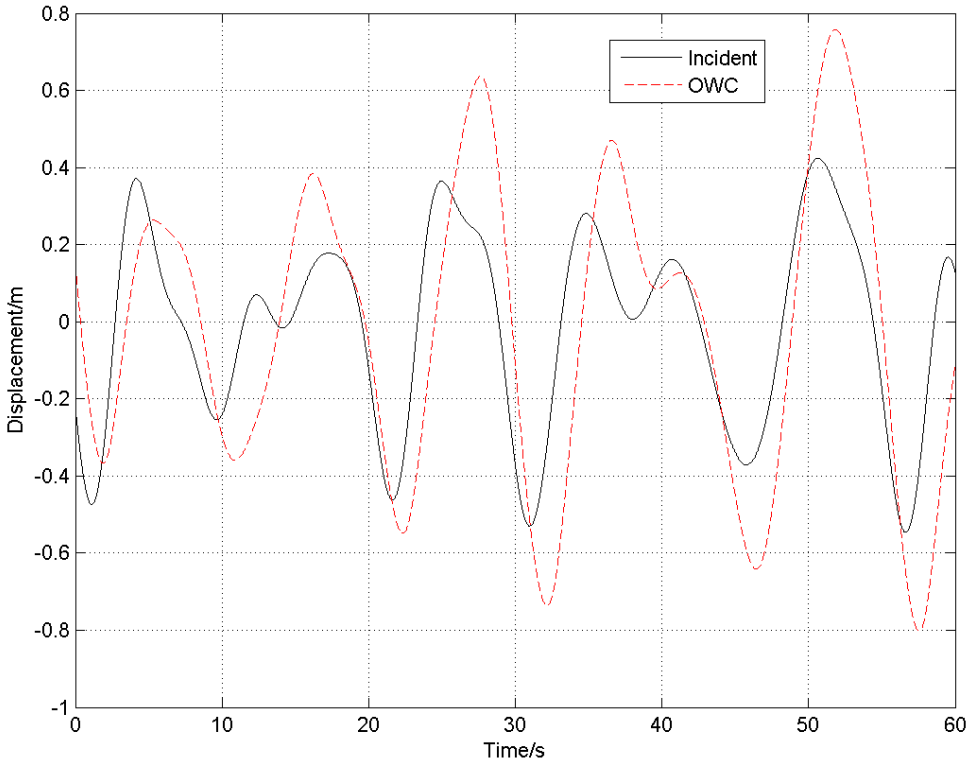

Figure 5.7: Displacement of the internal water surface for the OWC-WEC with linear controller for irregular waves, from a Pierson-Moskowitz spectrum, with 1.25 m wave height and 8.5 s peak period

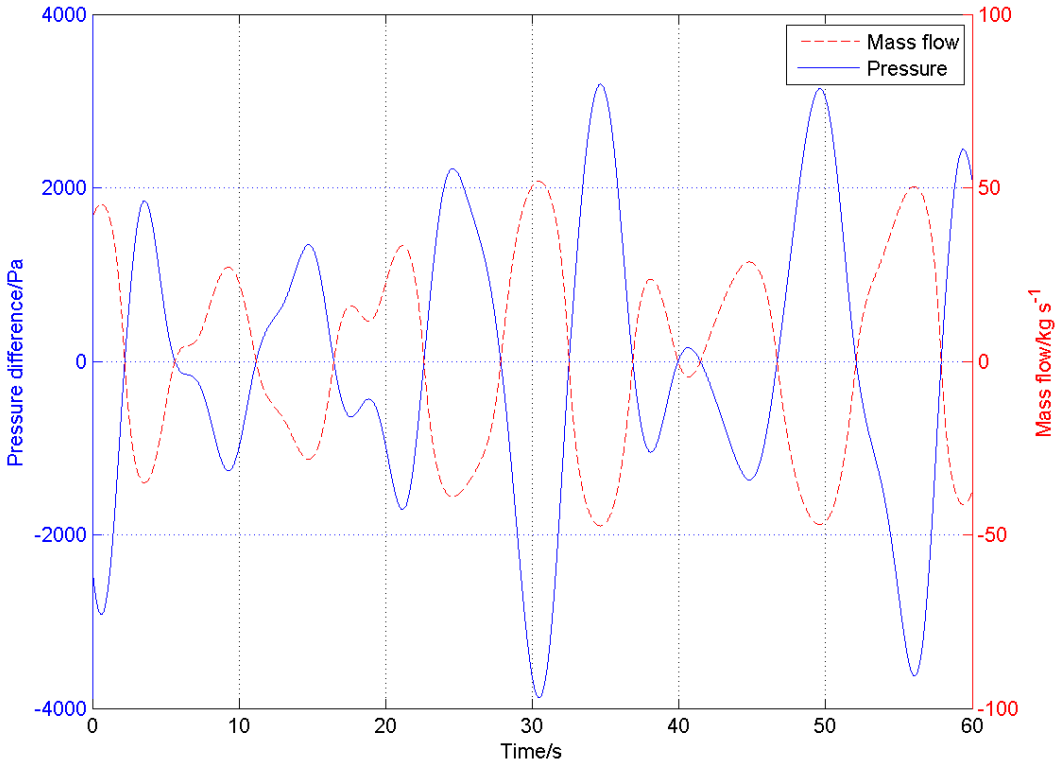

Figure 5.8: Pressure and mass flow for the OWC-WEC with linear controller for the same irregular waves as in Figure 5.7

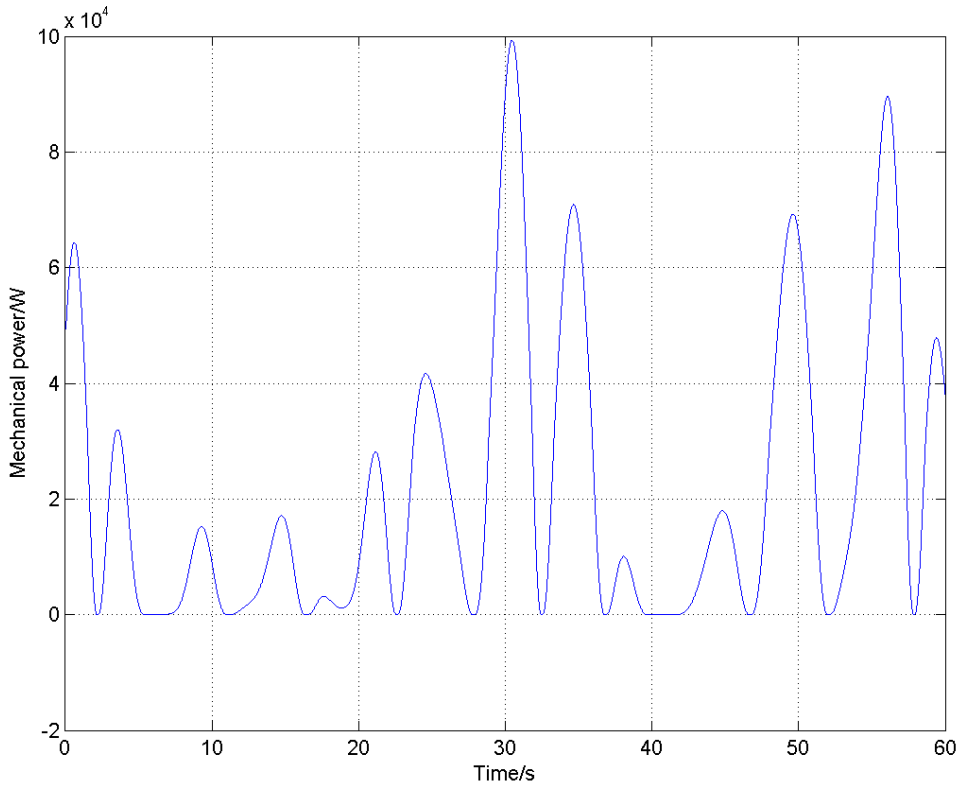

Figure 5.9: Power for the OWC-WEC with linear controller for the same irregular waves as in Figure 5.7

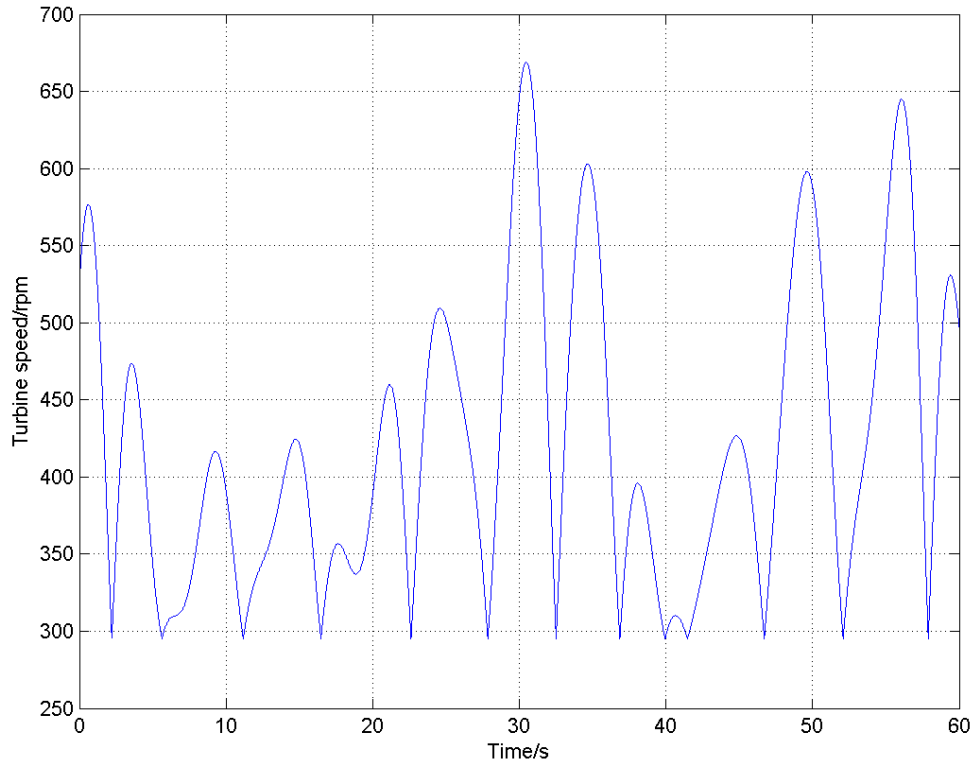

Figure 5.10: Turbine speed for the OWC-WEC with linear controller for the same irregular waves as in Figure 5.7

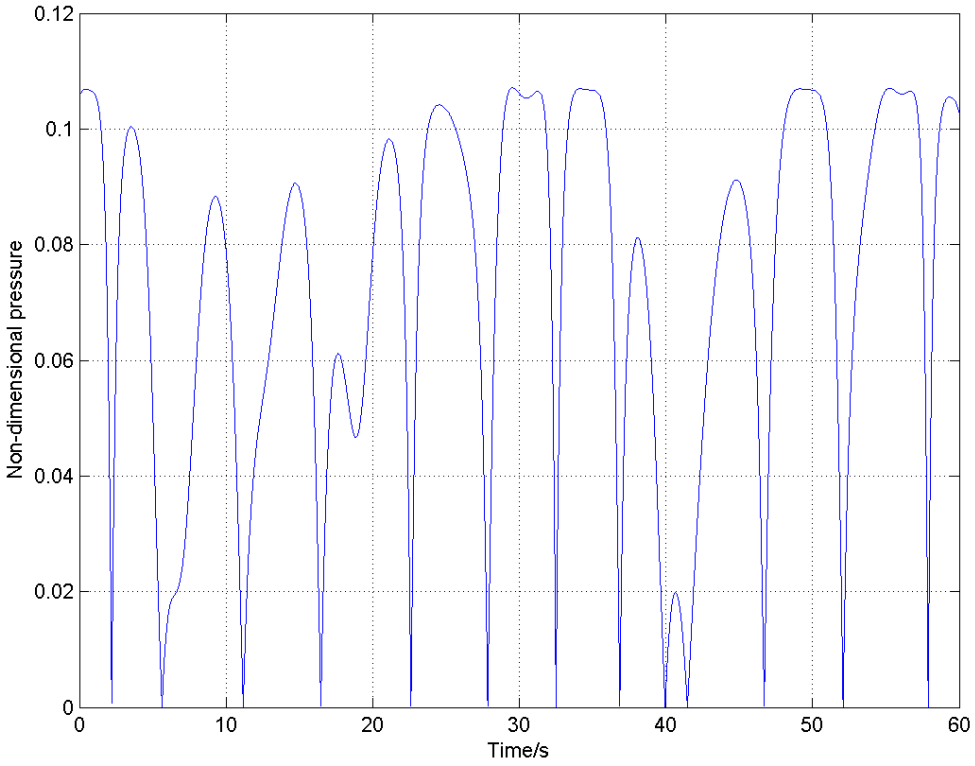

Figure 5.11: Non-dimensional pressure for the same wave as in Figure 5.7

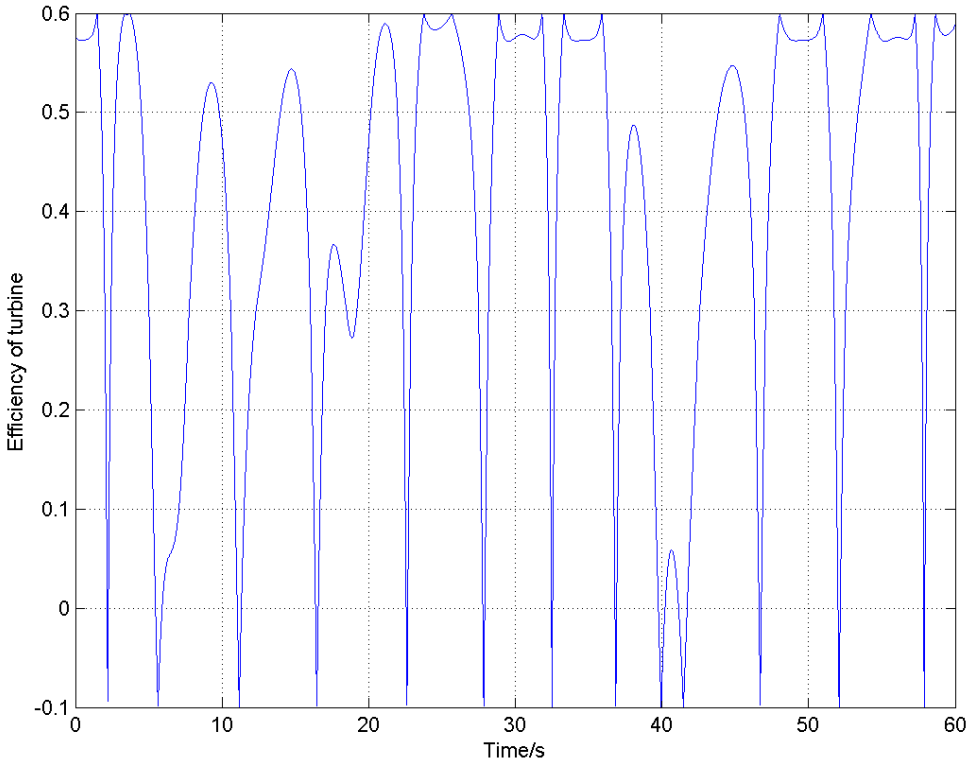

Figure 5.12: Efficiency of the turbine for the same wave as in Figure 5.7

wave height is large, but where the period is moderate, at around 8-10 s. The maximum average mechanical power available in these sea states is now 177 kW, where using the fixed speed controller, the maximum power was 107 kW. These mechanical power outputs are given in Table C.1.

5.1.6 Performance of the linear controller in the Bideford wave climate

As was the case for the fixed speed controller, the linear controller's power conversion data may be used to estimate annual energy conversion for such an OWC-WEC at the Bideford site by multiplying by the joint occurrences for each sea state. This results in a total annual energy conversion of 512 MWh, which is the equivalent of an average annual power of 58.4 kW. That is a 59.8% increase on the fixed speed case, where N_f is 632 rpm.

5.2 A controller based on turbine efficiency

From the performance of the linear controller, it seems that the efficiency of the turbine plays a major role in the power conversion. Figure 3.9 showed the relationship between non-dimensional pressure, Ψ, and efficiency, η. It is possible to invert this relationship

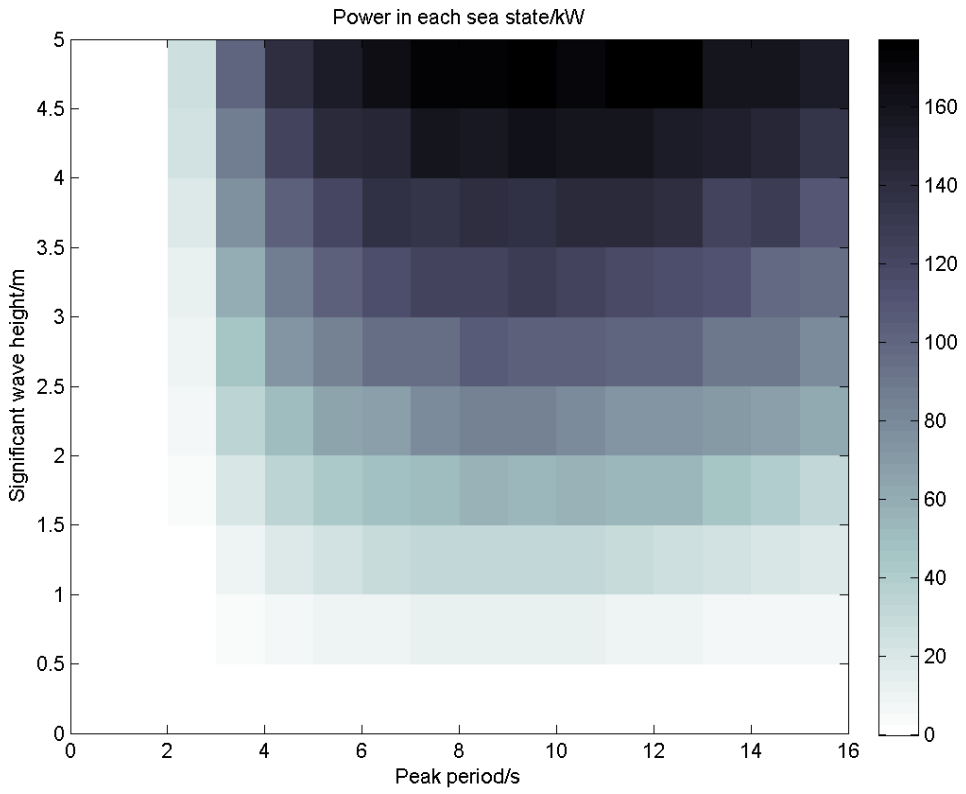

Figure 5.13: Average power in each sea state using the linear controller

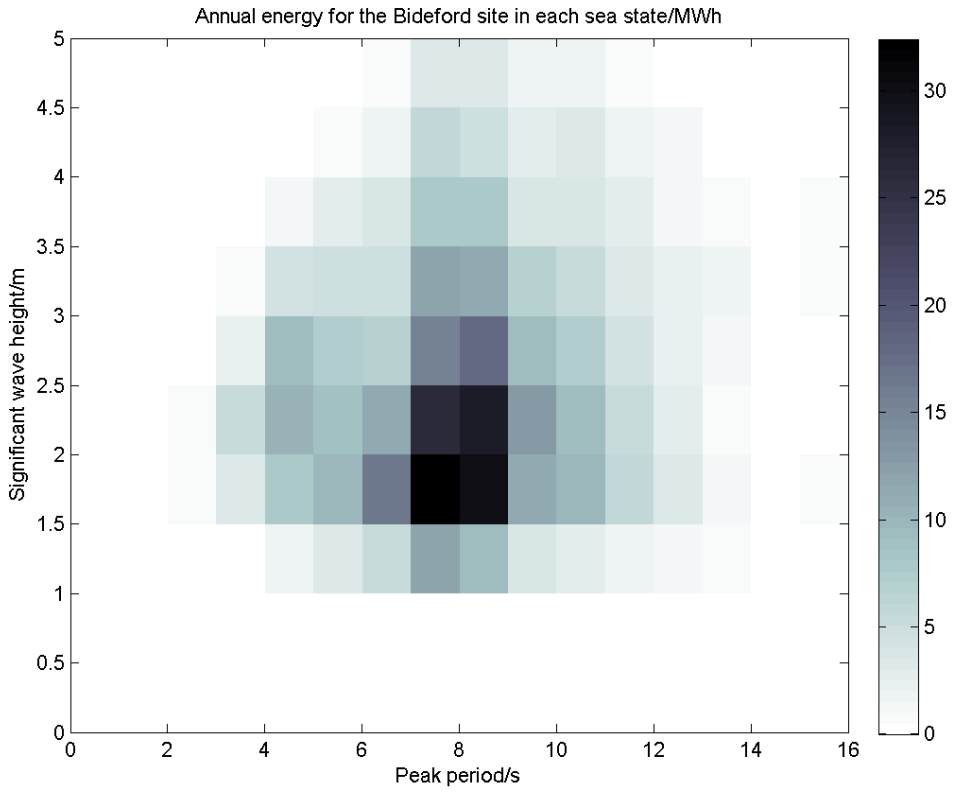

Figure 5.14: Energy converted under the Bideford wave climate using the linear controller

such that the maximum turbine efficiency is always used.

5.2.1 Definition of the turbine efficiency controller

Non-dimensional pressure is a function of turbine speed, so the speed may be changed such that the most efficient, Ψ is maintained. Thus,

$$\Psi = \frac{|\Delta p|}{\rho_{atm} N_r^2 D^2} \tag{5.2}$$

so if the Ψ at which the efficiency is a maximum is used, Ψ_{max}, can be substituted and the equation rearranged so that

$$N_{eff} = \frac{60}{2\pi D}\sqrt{\frac{1}{\Psi_{max}}}\sqrt{\frac{|\Delta p|}{\rho}} \tag{5.3}$$

The factor of 0.1 is the non-dimensional pressure at which the efficiency is greatest (Figure 3.9) and may thus be substituted for Ψ_{max} such that

$$N_{eff} = \frac{60}{2\pi D}\sqrt{\frac{1}{0.1}}\sqrt{\frac{|\Delta p|}{\rho}} \tag{5.4}$$

where N_{eff} is the speed of the turbine using this control action. For a given turbine diameter, D, pressure difference, $|\Delta p|$ and air density, ρ, the turbine speed which produces the maximum turbine efficiency may be calculated. Note that this produces the maximum *turbine* efficiency, which is not necessarily the same as the maximum efficiency for the OWC-WEC system. This control action is shown in Figure 5.15.

Also, note that as the pressure difference decreases to zero, the turbine speed should also decrease to zero. For the calculation of the turbine speed, such a consideration is entirely possible. However, for a physical system such a speed change may be too large.

5.2.2 Performance of the turbine efficiency controller in regular waves

Figure 5.16 shows that for the turbine efficiency controller, the displacement is very similar to that seen for the linear controller.

The pressure difference for the turbine efficiency case is reduced, with pressures of 2000-2500 Pa, rather than the 3000 Pa seen for the fixed speed case, which again, is very similar to those seen for the linear controller. See Figure 5.17. The mass flow is generally larger with the turbine efficiency controller. The mass flow for the turbine efficiency controller

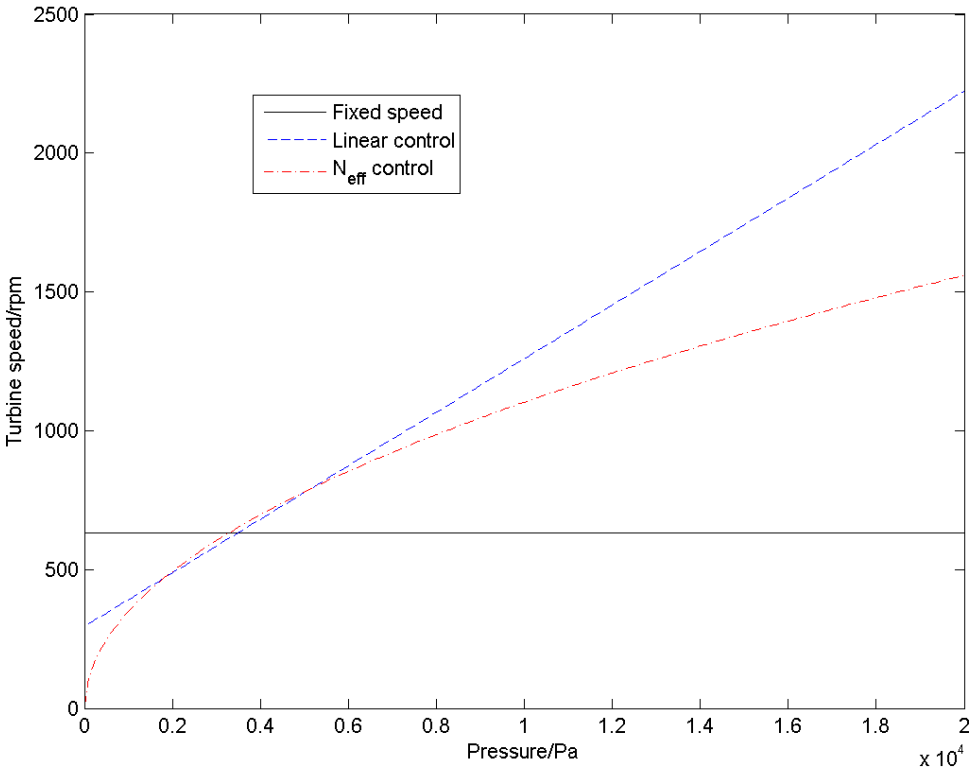

Figure 5.15: Action of the turbine efficiency controller

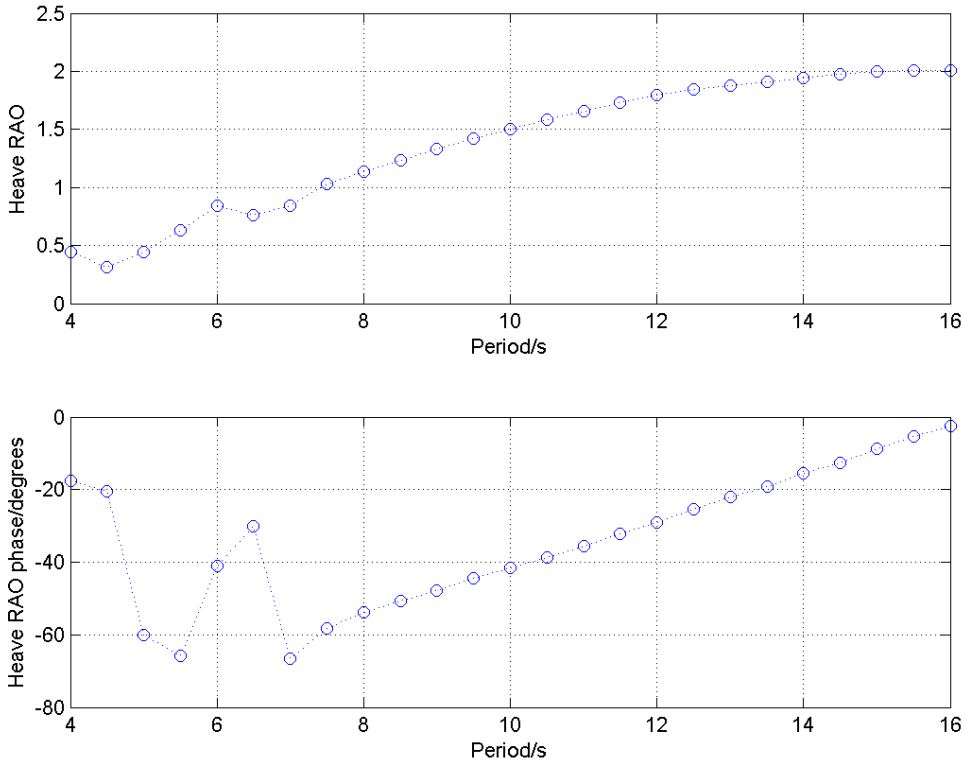

Figure 5.16: RAO of internal water surface displacement of the OWC-WEC with the turbine efficiency controller in regular waves, plotted with respect to period

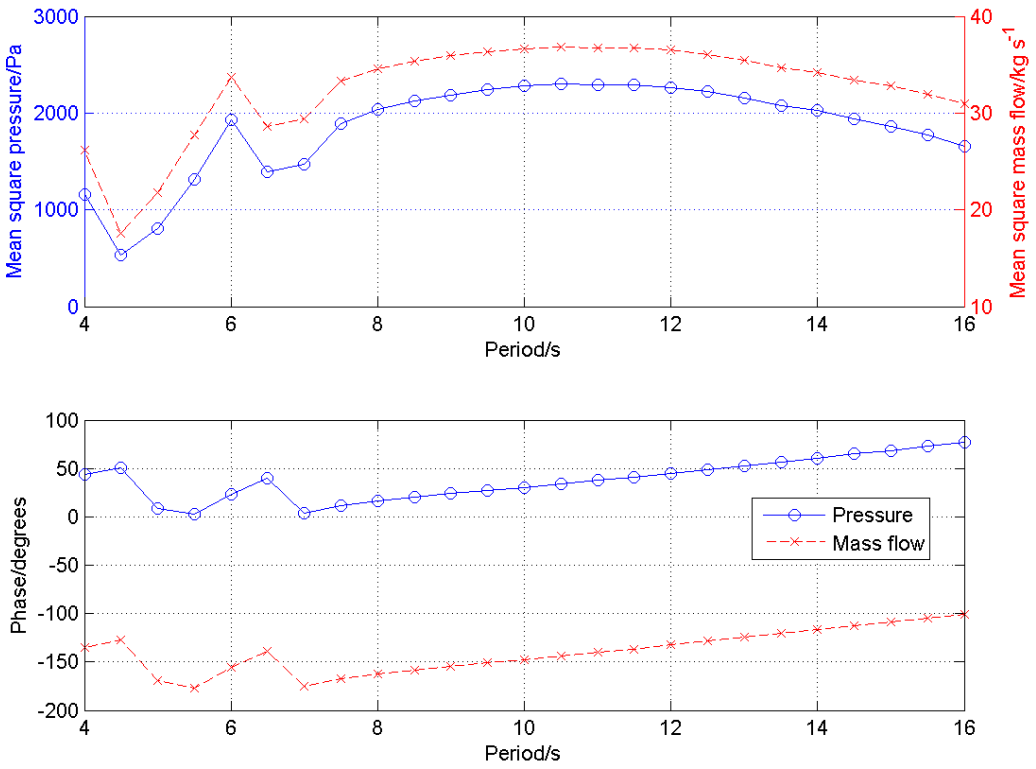

Figure 5.17: Pressure and mass flow with the turbine efficiency controller in regular waves, plotted with respect to period

is very similar to that seen for the linear controller.

The similarities in displacement, pressure and mass flow between the linear and turbine efficiency controllers is not at all surprising given the similarity in their control action, and the fact that these values are based on the average of the variables. As such, the power follows the same pattern, as shown in Figure 5.18, albeit with a slightly higher peak for the central wave periods.

5.2.3 Performance of the turbine efficiency controller in irregular waves

The same incident waves are used as in the case of the fixed speed controller and the linear controller. The displacements are very similar and are shown in Figure 5.19.

The most clear pattern from the pressure and mass flow trace of Figure 5.20 is that the pressure and mass flow are not close to being in anti-phase using the turbine efficiency controller: the mass flow shows broader peaks than for the other cases, while the pressure difference is similar.

The power output is very similar to the linear case and is shown in Figure 5.21.

The turbine speed changes, shown in Figure 5.22, are even larger than for the linear

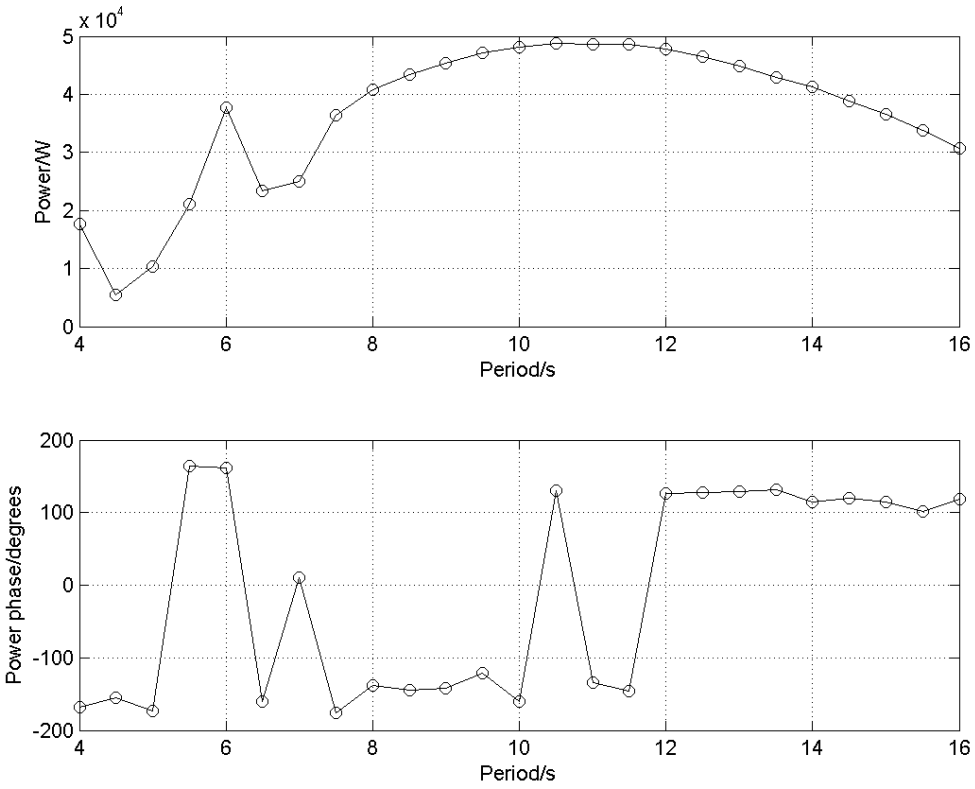

Figure 5.18: Power with the turbine efficiency controller in regular waves, plotted with respect to period

controller case. The change from 0-295 rpm has very little effect on the power output due to the low pneumatic power available during this phase of the wave cycle. However, this roughly doubles the change of speed required. This could have large implications for controller energy requirements.

5.2.4 Performance of the turbine efficiency controller in various sea states

The average power output when using this turbine efficiency controller in each sea state is shown in Figure 5.23. The peak power per sea state has risen from 177 kW for the linear controller to 312 kW for the turbine efficiency controller. These mechanical power outputs are given in Table C.3.

For the turbine efficiecny controller, the periods of the sea states for which most energy is converted increase with increasing wave height. For the linear controller, which was optimised for a specific sea state, the period at which the OWC-WEC is converting most energy remains the same with increasing wave height.

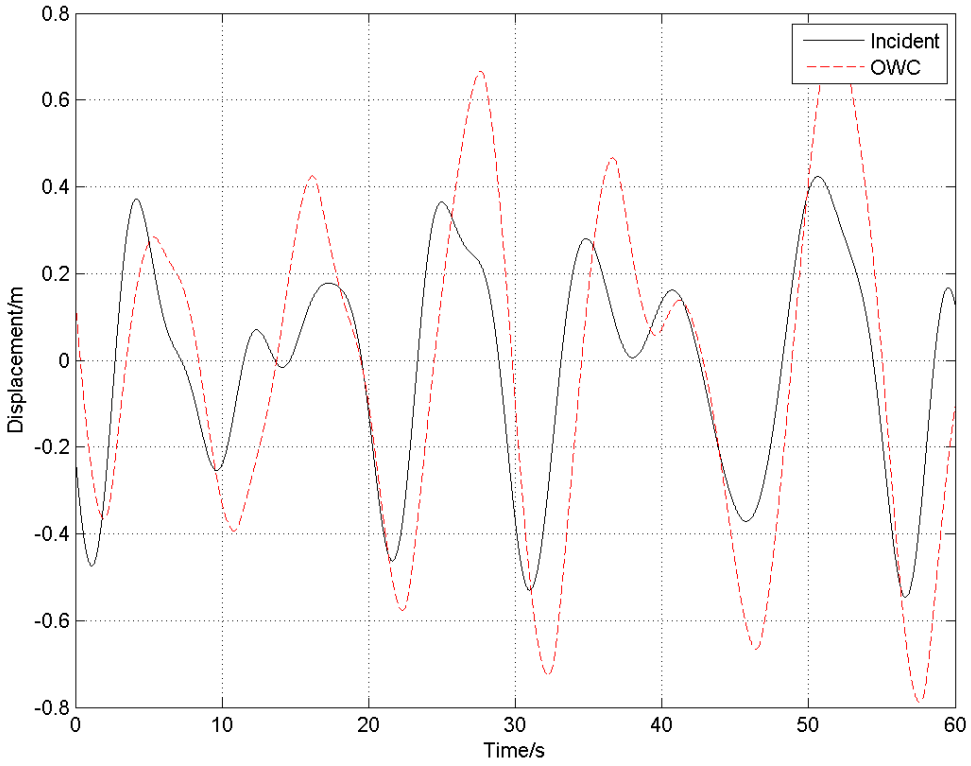

Figure 5.19: Displacement of the internal water surface with the turbine efficiency controller for irregular waves, from a Pierson-Moskowitz spectrum, with 1.25 m wave height and 8.5 s peak period

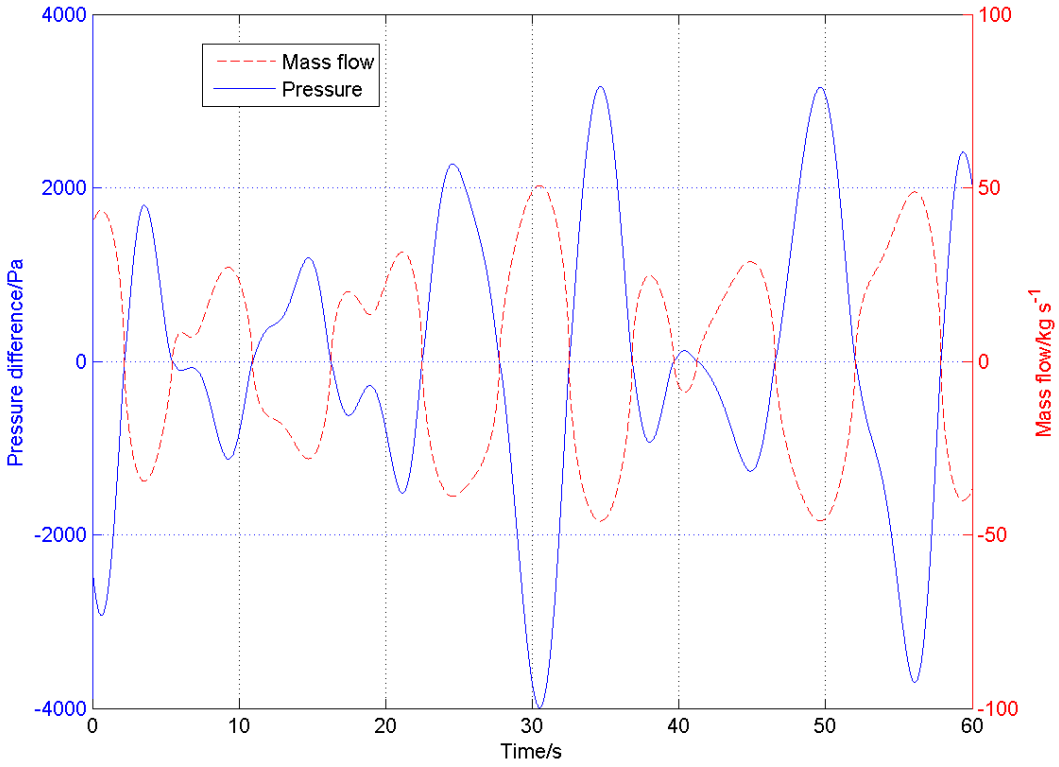

Figure 5.20: Pressure and mass flow for the OWC-WEC with linear controller for the same irregular waves as in Figure 5.19

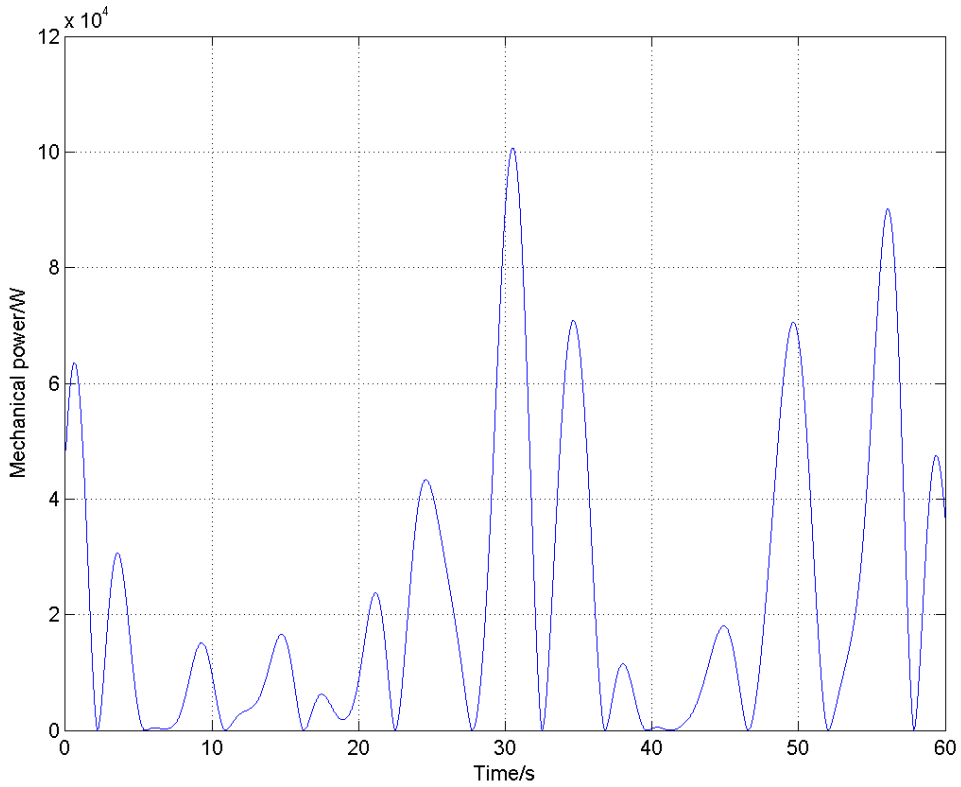

Figure 5.21: Power for the OWC-WEC with linear controller for the same irregular waves as in Figure 5.19

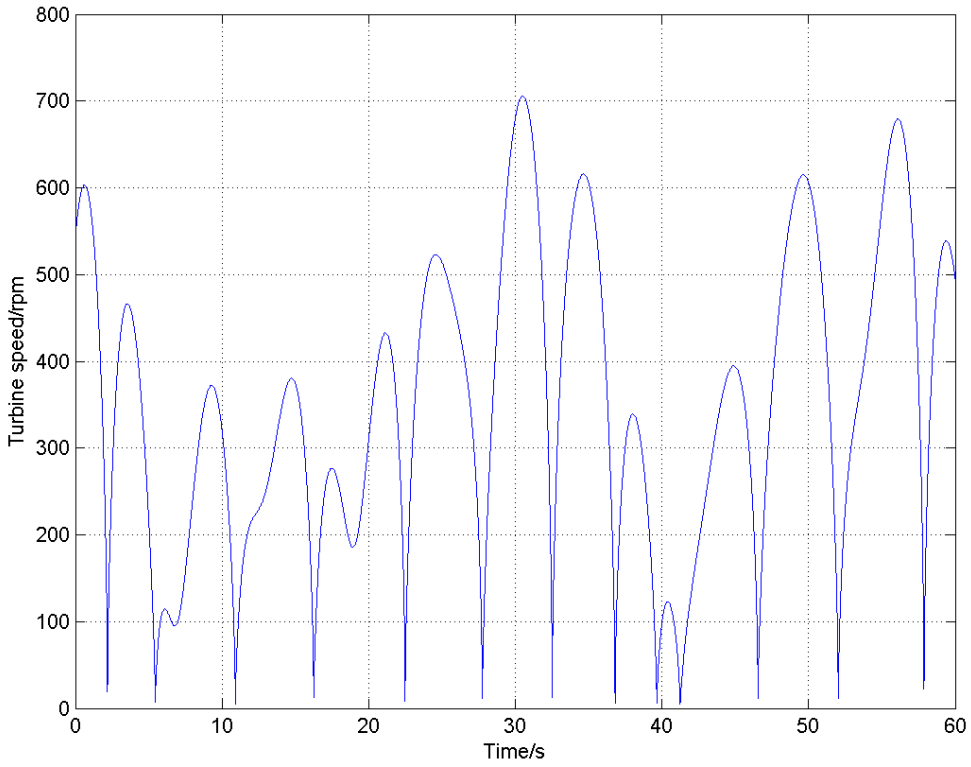

Figure 5.22: Turbine speed for the OWC-WEC with linear controller for the same irregular waves as in Figure 5.19

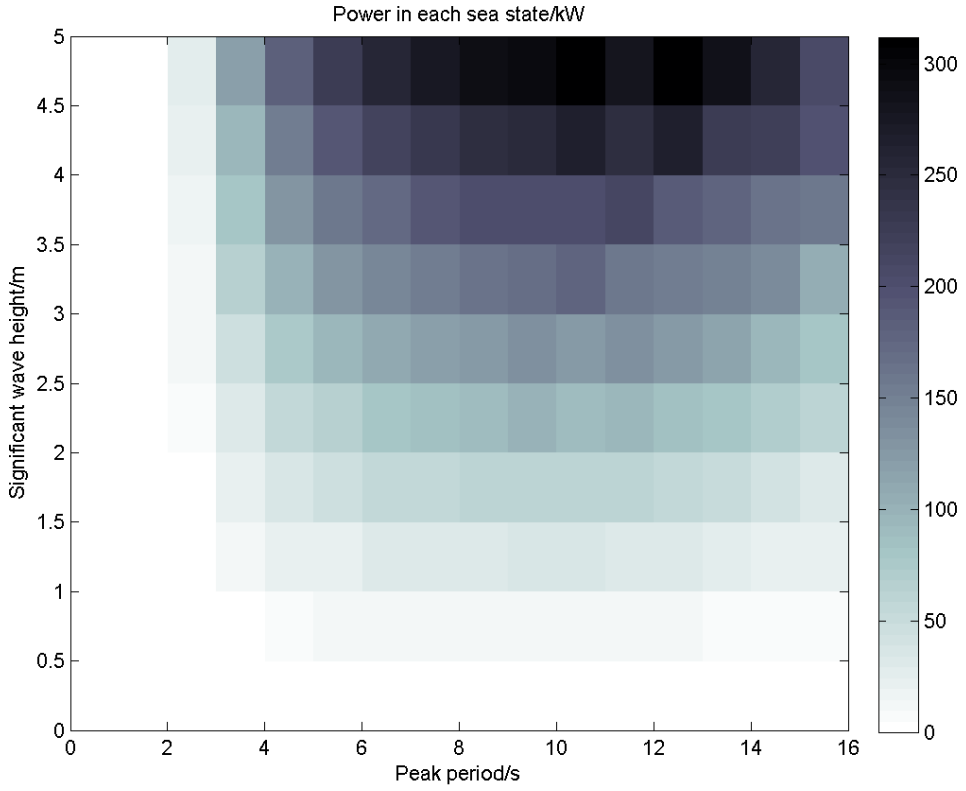

Figure 5.23: Average power in each sea state using the turbine efficiency controller

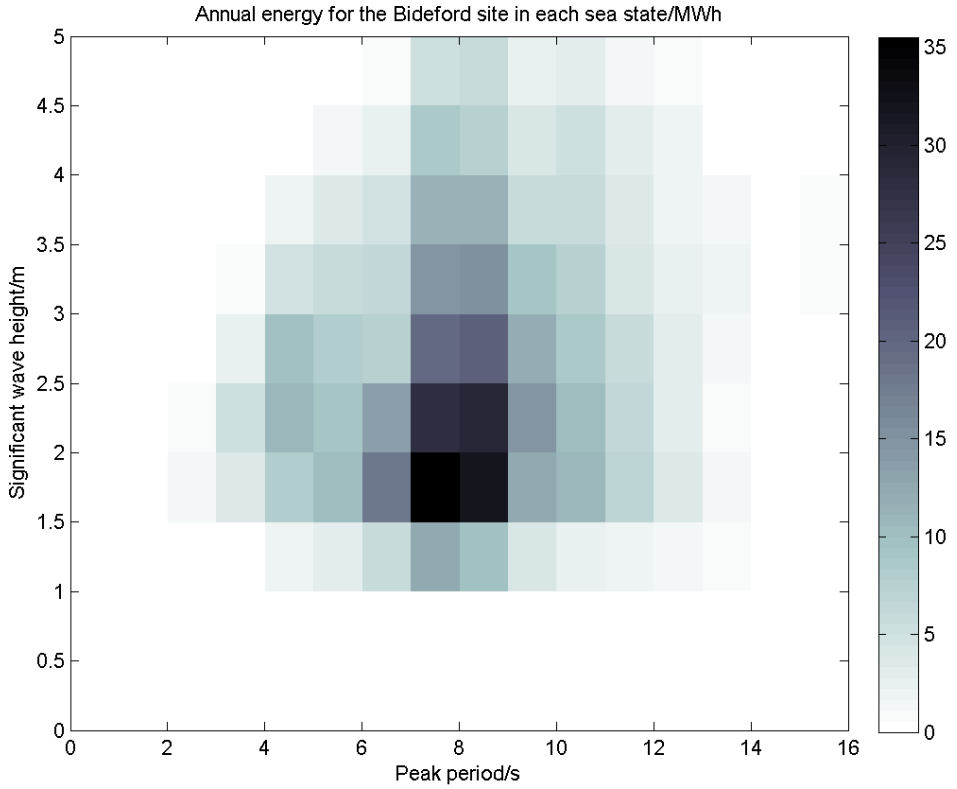

Figure 5.24: Energy converted under the Bideford wave climate using the turbine efficiency controller

5.2.5 Performance of the turbine efficiency controller in the Bideford wave climate

Figure 5.24 shows the energy converted using the turbine efficiency controller across the average year. This gives an annual energy conversion of 604 MWh, which is the equivalent of an average annual power of 69.0 kW, and increase of 90.1% over the fixed speed control option. In the sea state for which the other controllers were optimised, the turbine efficiency controller gives an average power of 33.5 kW, which is 35.6% more energy than for the fixed speed control.

5.3 Discussion of the controller findings

This chapter has shown that the energy converted by the central column OWC-WEC can be increased via the use of a turbine speed controller. Table 5.1 gives the average power calculated for the sea state with $H_s = 1.25$ m and $T_e = 8.5$ s, and the annual performance for each of the control options.

In comparison to the Pico plant, the range of average power is similar. Tables 1

Control type	H_s = **1.25 m,** T_e = **8.5 s sea state**	**Bideford wave climate**
Fixed speed	24.7 kW	36.3 kW
Linear	32.4 kW	58.4 kW
Turbine efficiency	33.5 kW	69.0 kW

Table 5.1: Comparison of controller performance under different conditions

and 2 of Brito-Melo *et al.* (2007) show that the range of pneumatic power over a certain period was 19.21-141.94 kW, while the range of electrical power was 19.12-65.82 kW. This is similar to the mechanical powers seen for the linear controller in Figure 5.13 and Table C.1. However, losses in moving from mechanical to electrical power are not included in this thesis. The range of mechanical power output for the turbine efficiency controller is larger, as shown in Figure 5.23 and Table C.3. This may more closely correspond to these Pico values. That said, Monk *et al.* (2013) shows that a value of 68 kW is now possible under a new control scheme. Thus high efficiency in moving from mechanical to electrical power would be required to match this if it is a true reflection of the annual value. The Pico chamber is of a similar scale to that described in this thesis, but the wave climate that it experiences is larger, so it would not be surprising to find larger power outputs for a converter located on an Atlantic island.

5.3.1 Discussion of the linear controller

The linear controller has a single input and a single output (SISO). It is the turbine speed which is controlled, and this is only based on the magnitude of the pressure difference. As was done for the fixed speed controller, the MATLAB function `fminsearch()`was used to optimise the coefficients of the linear controller for the sea state with $H_s = 1.25$ m and $T_e = 8.5$ s, the most frequently occurring sea state for the Bideford Bay site.

Findings for the linear controller

For the sea state for which it is optimised, the linear controller increases the amount of energy converted by the OWC-WEC in comparison to the fixed speed case. It does this by increasing the mass flow through the turbine without greatly changing the pressure difference.

The changes of speed required for the control action are quite fast. The peaks require a change of around 100% in 1-2 s. This might be achievable on a physical system, but would certainly require a lot of energy to make such a change so quickly.

Limitations to the linear controller

The linear controller is very simple, having only two parameters. It is possible to make a more detailed controller which is still linear. For example, it would be possible to include more terms in the controller, for example to have a coefficient proportional to the derivative of the pressure and so on.

Another limitation of this controller is that it was only optimised for a single sea state. Combining linear controllers optimised for three or four different sea states might prove valuable, as more energy could be converted if the optimisation of the controller parameters reflected the range of chamber pressure for the larger seas.

Energy cost of the linear control action

The major limitation is that there is no calculation of the energy required to change the turbine speed, so the cost function uses converted energy rather than net converted energy. This is suitable during an initial investigation, but would need to be remedied in order to calculate whether the controller gave a benefit good enough to implement. That the average power in this sea state increases from 24.7 kW to 32.4 kW (31.2%) does mean that there is a lot of energy available that makes a net energy conversion increase likely even if the control action were found to be energy intensive.

Including the energy cost could be done via modelling the inertia of the turbine directly. It would be wise to include within such a model an estimate of the actuation behaviour that could be used to influence such changes. This is the behaviour described by Cross *et al.* (2011) for a WEC with hydraulic PTO. If the speed changes do take some time to have their full effect, the control parameters which are found to be optimal on such a system are likely to be different to those seen here. For example, the amount of speed change would be reduced.

Inclusion of further variables by the controller

The linear controller has a single input and a single output. That is, only the pressure difference is used to change the turbine speed. This means that it cannot incorporate other variables, such as mass flow, a valve position, or the current efficiency of the turbine. Extensions such as this could prove very useful.

5.3.2 Discussion of the turbine efficiency controller

A nonlinear turbine speed controller was applied to the central column of a five column OWC-WEC. This was a controller was ensured that the turbine was always operating at its most efficient point. Because efficiency of the turbine has a major influence on the mechanical power conversion of the system, this was found to significantly increase converted energy.

In Starzmann *et al.* (2013), such a turbine efficiency method was used. Their primary concern was with reducing acoustic noise due to stall, but their Figure 11 shows an increase the shaft power as stall is avoided. Peak shaft power is around 3 kW for the Starzmann *et al.* (2013) case, for a pressure of 3000 Pa. However, the turbine used is much smaller, with a diameter of 0.4 m.

Limitations of the turbine efficiency controller

The turbine efficiency control action required very large changes in turbine speed. For the sea states with large waves, this lead to very large increases in converted energy. However, for the sea states of similar size to that for which the linear controller was optimised, there was not a very large change in average power. Thus, because as for the linear controller, no account was taken of the energy required to change the turbine speed, or the time in which this change could take place, the turbine efficiency controller may not be the best option for a physical system.

5.3.3 Combining controllers

The linear controller is optimised to work in a single sea state. It would be possible to produce more controllers of this type, but optimised for different sea states. An overall controller could switch between these linear options depending on the incident sea state. Such switched control could also use any other controllers: for example, a control action designed to work in those sea states for which the wave-structure interaction is highly nonlinear.

Such a controller would thus combine control in a manner shown schematically in Figure 5.25, where switching is between four linear controllers and a nonlinear controller on the basis of the incident sea state. The nonlinear controller may be the one under discussion in Section 5.2, but could alternatively be a controller determined for those sea states where the linear wave-structure interaction model does not hold. The linear

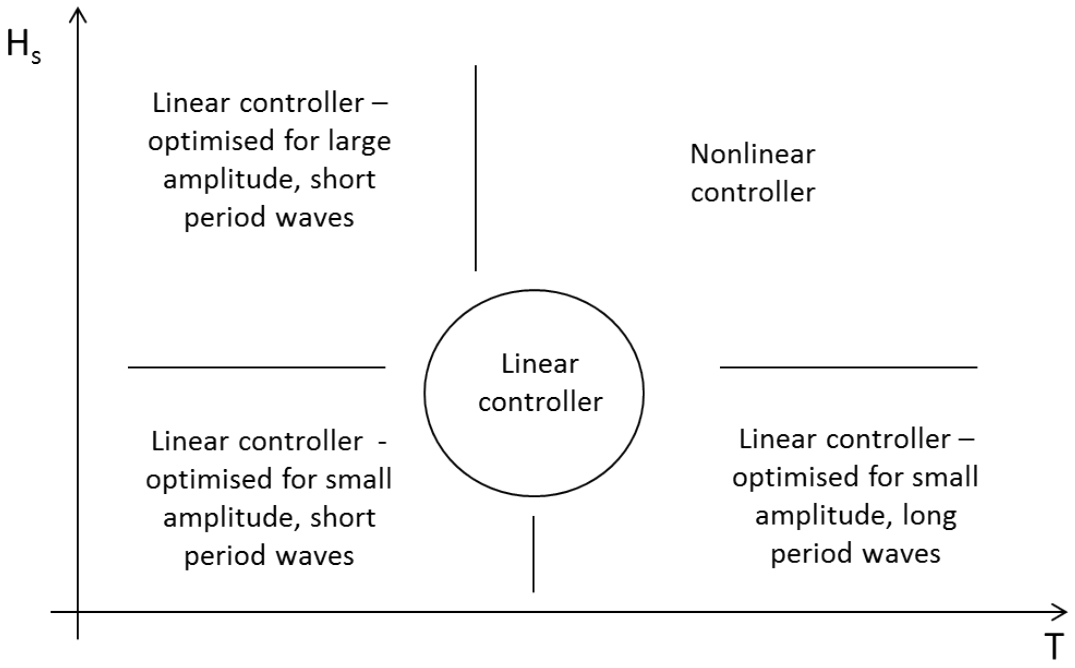

Figure 5.25: Schematic diagram of switching control

controllers are shown as the linear controller for medium period waves with moderate wave height (discussed in Section 5.1), with extra linear controllers included which are optimised for sea states where the waves are small in amplitude - with optimisation for short and for long periods, and where the waves are large in amplitude and short in period such that the wave-structure interaction is still approximately linear.

If it were deemed worthwhile given the turbine speed actuation cost, some of these control regions could use the nonlinear, turbine efficiency controller instead of variations on the linear controller. The most pressing need for further work is thus clearly for calculation of *net* energy conversion, rather than basing the optimisation and comparison on converted energy. With this information, combining controllers would then be useful to understand the likely annual (net) energy conversion.

Conclusions regarding the controllers

Using both controllers, the converted energy was found to increase. For the linear controller in the sea state of interest, an average power of 32.4 kW was found, while for the turbine efficiency controller, the average power was 33.5 kW in this sea state: a 31% and 36% increase on the fixed speed controller's conversion, respectively.

The linear controller was found to approximate the control action of the turbine efficiency controller for the sea state over which it was optimised. Although it did not convert

as much energy, the control action was less extreme than that of the turbine efficiency controller. It is very important therefore that the net converted energy, rather than only the converted energy is tested, as this will allow a more secure judgement between the control schemes.

Summary

- A linear and a nonlinear controller were tested on the most frequently occurring sea state for the Bideford Bay site.
- The controllers mapped the magnitude of pressure difference in the chamber to the speed of turbine rotation
- The linear controller was found to approximate the control action of the turbine efficiency controller for the sea state over which it was optimised.
- The nonlinear (turbine efficiency) controller was found to be the most effective at converting energy, converting 33.5 kW in the relevant sea state, to the 32.4 kW of the linear controller and the 24.7 kW of the fixed speed controller.

Chapter 6

Discussion

This thesis describes a method by which an OWC-WEC forming a breakwater may be investigated numerically. The investigation provides a method for estimating the PTO forces on the water surface that may then be used in further investigations into the effect of an OWC on its neighbours. It also provides a framework in which turbine speed (or other turbine properties) may be investigated for their effect on the amount of converted energy.

In this chapter, the discussion of the various parts of the investigation will be explored. First the hydrodynamic interaction will be discussed in Section 6.1. Then the time domain modelling of the OWC-WEC with PTO and its baseline performance will be discussed in Section 6.2. Finally, in Section 6.3, the control investigation will be discussed.

6.1 Hydrodynamics

In this thesis a study of the wave structure interaction was described for an open isolated OWC and for a breakwater OWC with five columns, as well as for stages in between. Of particular note is the difference in response between the structures. The isolated column responds smoothly across all frequencies and for different incident angles of the wave. For the breakwater structures, this is not the case, with both incident wave angle and period playing important roles in the response of the OWC due to coupled modes between the columns.

6.1.1 Major findings

For the head-on waves with long periods, the response of the five column OWC looks broadly similar to that of a single-chamber with a back-board. However, as the period

decreases, other modes can be excited which allow for the OWCs to interact with each other.

For an isolated column, the angle of incidence makes almost no difference to the response. The period of the wave does make a difference, with amplification of the motion at 5 s for this particular geometry, and a phase lag with respect to the incident wave which increases as the period gets shorter.

For an OWC system which forms part of a multi-column breakwater, it was found that the response of the internal water surface is sensitive to period and to the direction of the incident wave.

6.1.2 Importance

Knowing that there are likely to be different modes excited while in operation is important for the design of multi-column OWCs. This is true for power estimation, of course, but also for the calculation of fatigue and extreme loading.

6.1.3 Relation to other work

Previous work by Martins-rivas & Mei (2009) used a cylindrical OWC which was cliff-mounted. Hong & Hong (2012) investigated a rectangular OWC which was bottom-mounted. Both of these studies used geometry-specific analytical frameworks, which means that if the geometry is altered, the equations must be redefined. With the velocity potential solver ANSYS™ AQWA®, the extension to include different geometries and multiple columns is relatively straightforward.

Martins-rivas & Mei (2009) noted that the internal water surface displacement for a column with a cliff behind it was often not flat and piston-like. They also saw that the magnitude of the displacement was increased in comparison to that seen for an isolated column due to reflection from the cliff. Such shape change and amplification was seen in this work.

Other research has been done into multiple-column OWCs using physical testing. In physical testing, the impact of waves from many directions is simple to simulate, and scaled PTOs can be modelled. The effects of turbulence are included, although the effect of scale is not simple. Both Kelly *et al.* (2013b) and Ruol *et al.* (2011) looked at rectangular chambers arranged in lines, at an angle to the prevailing/incident wave direction. Both studies use non-return-valves and a single turbine PTO across their columns, so details of

individual OWC motion are not given.

6.1.4 Limitations

ANSYS™ AQWA® is a velocity potential solver and, as such, turbulent motion is not included. This means that where the water interacts with the structure or the ocean floor, the potential must be smooth. This is a limitation on the modelling of the lip of the OWCs and also at the foot of the the breakwater wall.

The turbulence issues are just one aspect of the limitation due to approximate linear theory. The water may never drop below the lip of the OWC, and only small motions around the equilibrium are mathematically accurate. Results for any larger motion should be taken as purely indicative and tested physically or with Navier-Stokes CFD solvers.

The ocean floor is a difficulty for ANSYS™ AQWA® in that it will only work where the ocean extends around and behind the structure. This makes using it for direct comparison between the breakwater-type and the cliff-type OWCs impossible. The software is not at all limited for floating structures, however, and would in fact have no difficulty in modelling the water interaction around a moored, floating version of a similar structure. For example, a structure like that described by Ruol *et al.* (2011) as breakwater protection in the Venice Lagoon.

6.1.5 Further work

More numerical work that examines the interactions of neighbouring OWCs in a breakwater would be interesting to see. Including the PTO as a linear damping lid in ANSYS™ AQWA®, or another velocity potential method, could show the effect of the PTO on the water around it, rather than solely the effect of the water on the PTO. The challenge is in getting the damping from the PTO included *correctly*, as the hydrodynamic damping is linear. Obviously the real situation is more complicated, especially if a controller is implemented.

A relatively simple extension which would be applicable for cases such as that described by Ruol *et al.* (2011) and Kelly *et al.* (2013b), would be to run the ANSYS™ AQWA® analysis for a floating structure. ANSYS™ AQWA® can incorporate mooring properties as standard. Floating versions may involve using the structure as an attenuating device and so a different range of directionality would be assumed important for PTO. Such a floating device would be more complex to model with an impedance-type,

force-displacement mapping time domain model. The initial hydrodynamics would not be more complex to model using this software package.

6.2 Time domain modelling

In order to describe the hydrodynamics of the central column of the five-column, breakwater-mounted OWC-WEC in the time-domain, a force-displacement mapping model is used. This allows the PTO force to be fed back such that the hydrodynamics and the PTO may interact.

6.2.1 Major findings from the time domain modelling

For WECs, and OWCs in particular, the difficulty in modelling occurs with the combination of waves, which are best described using the frequency domain, and thermodynamic and turbine properties, which are best described using the time domain.

In spar-type buoys, or OWCs where the water moves as a single unit, individual forces (buoyancy force, radiation damping, etc.) may be calculated. For the system described here, this approach is not reliable. The water does not oscillate as a solid unit and thus the sum over forces method does not represent what is really happening. Thus, the time domain model described in this thesis used a simple system identification method to give magnitude and phase motion of the internal water surface matching that which was seen in the hydrodynamic modelling (Section 3.1). This approximation was assumed to be valid across a range of frequencies. Crucially, the system identification approximation allows for appropriate behaviour in phase (moving from motion in-phase for waves with long periods, through resonant motion to motion in anti-phase for high frequency waves), which is very important for power prediction and for control.

The thermodynamic and turbine modelling were based on previously applied set ups. These appear to function well in this context, with the thermodynamic properties showing phase and shape shifts seen elsewhere. Although the turbine efficiency was modelled with a look-up-table, the power outputs behaved quite smoothly.

The performance of the OWC-WEC in the annual wave climate off North Devon was estimated to be 300 MWh, which would be 34.2 kW of power if it was distributed uniformly throughout the year. This assumed a single year in which were seen the mean wave conditions over the four year period 2009-2012, and that a fixed speed of 632 rpm was used. Zero energy was assumed to be converted for those sea states that experienced

an extreme internal water surface where the displacement was equivalent to reaching the chamber roof (and thus flooding the turbine), but this limit was never reached for any of the Bideford sea states. This assumption was due to the likelihood of the shut-down of the device during such seas. The internal water surface was allowed to drop below the 2.5 m draft front lip of the device. Clearly this means that the model is no longer within the regime covered by the velocity potential method, but such motion is possible, and such displacement was only achieved for the very largest sea states.

6.2.2 Importance of the time domain modelling

A wave to wire model was developed which used a simple force-displacement hydrodynamics model, along with a thermodynamics and turbine model which included the efficiency. The simple modelling method may well be of use to those looking to understand WECs in which the OWC is sensitive to wave period.

The methodology for forming the time domain model is quite straightforward. It could easily be applied where known forces and displacements exist, such as for physical models. The findings regarding the scale of the pressure force and the damping of the water surface motion could be very useful for those looking at the first stages of array modelling. However, for fully interacting columns with PTOs, further work would need to be done.

6.2.3 Relation to other work

Force-displacement mapping

The force-displacement mapping method described in this thesis is somewhat like the impedance method applied in standard WEC modelling. However, it is not based on finding coefficients to represent separate terms associated with radiation damping, added mass and so on, but is instead concerned with the identification of the whole hydrodynamic system.

The force-displacement mapping used here is also similar to the transfer function method used by Nunes *et al.* (2011). In that case, the transfer functions were used to simplify the processing of a calculation which already included the PTO, rather than as the first part of a calculation of converted power.

Because the system identification used a force to displacement map, the thermodynamic and PTO system can interact with the hydrodynamic one via the chamber pressure

force. Such an interaction enables the testing of changing turbine parameters.

Thermodynamics and turbine modelling method

The thermodynamic equations and turbine set-up are the same as those tested for a floating OWC-WEC by Falcão & Rodrigues (2002). Broadly the same model was used by Nunes *et al.* (2011) and Gervelas *et al.* (2011). However, neither of these studies included the efficiency of the turbine in converting energy. These studies therefore over-estimate the energy converted by the OWC-WEC by using a wave to pneumatic power setup rather than a wave to mechanical power setup.

Performance

The performance at the Bideford Bay site in the South West of England is calculated using a standard methodology, estimating the energy converted for a series of sea states and then weighting these by their frequency of occurrence over an average year.

There is no sea state seen at the Bideford site for which the OWC-WEC must be in a survival mode. This suggests that the WEC is probably suited to a larger wave climate.

6.2.4 Limitations

There are some limitations of the model which are due to moving from the velocity potential model to the time domain model (TDM). Others are due to the TDM itself and some are due to the application of the TDM.

Limitations due to moving from the velocity potential model to the time domain model

The behaviour of the multi-column OWC showed a dependence on the incident angle of the wave. The time-domain model does not include this directionality. While the Bideford Bay site would have a prevailing direction for waves, there would be some spread.

It would be possible to include the non-perpendicular incident angles in the excitation force by summing over spectra at different angles. However, because the behaviour is different at different angles, a new force-displacement mapping model would be required. While such a mapping could be based on a series of linear models for each angle, a nonlinear system identification approach may be easier to handle.

Limitations due to the time domain model itself

With the TDM itself, because of the need to remove degrees of freedom, the water surface is effectively assumed to be horizontal when this is not true in reality. For the purposes of idealised thermodynamic properties, a flat water surface is not a difficulty. On the other hand, there is no inclusion of turbulence in either the water or the air. Thus the chamber properties may differ and have greater damping than is modelled.

The thermodynamics is assumed to be adiabatic, which is approximately true. However, no possibility then exists for loss of energy in the thermodynamic system. The properties might also allow for a greater spring effect in the chamber. Thus both the damping and the spring terms that are associated with the chamber are likely to be under-predicted, which means that the real OWC-WEC behaviour would be less linear than the time domain model predicts.

A major issue with the turbine of the time domain model is that it has not been designed for this particular system of waves and structure. Thus the range specified for good efficiency had not been optimised for this application. The turbine is therefore not as efficient as it might be and so the power estimated is likely to be lower than in comparable applications.

Another issue with the application of the TDM to a real sea situation is that spectral waves are not the same as those in the real sea. For example, no tests have been made in multi-modal seas.

Limitations to application of the time domain thermodynamics to the hydrodynamic system

Finally, in moving back from the time domain model to the velocity potential model, there is not a good model of what changes about the water interaction when the PTO force is imposed as the initial velocity potential model has open columns. If the water were to behave very differently due to PTO forcing, the surface displacement, chamber pressure and power output may change significantly. It is likely that an iterative process could be effective, of which this modelling is the first step: the damping found with the time domain model is approximated and fed back into the velocity potential model, where new hydrodynamic force approximations are calculated; a new time domain model is then constructed based on the new force-displacement mapping; the damping force thus found is fed back into the velocity potential model, and so on.

6.2.5 Further work

It would be of great benefit to the performance modelling of the OWC-WEC to have a turbine design which was optimised to work well for this application. In effect, a turbine coefficient and efficiency curve which were achievable, but better suited to this OWC-WEC and wave climate should be produced. One way of finding this is to calculate performance under some options, e.g. a range of K_t, different turbine efficiency shapes, and test turbine performance for the resulting pressure difference to find out whether a turbine may be built which has these properties. Again, an iterative process would be required.

In order to see more clearly how this particular OWC-WEC set-up corresponds to others, a sensitivity study on the model parameters could be done. This would show the effect that the different sections have on energy conversion. For example, whether or not small changes in hydrodynamics, chamber size or turbine properties cause large differences in power. As has been seen in Chapter 4, where turbine speed and diameter were chosen, seemingly moderate changes in one parameter can lead to large changes in power.

Another aspect of sensitivity is how sensitive the overall system is to changes in wave climate. Given that the wave climate is not fixed year-to-year, the OWC needs to be able to work well across very different situations. It is assumed that much of this alignment can be done by the controller. Changes in wave climate cover a range of wave heights and periods, but also could involve sensitivity to multi-modal seas.

6.3 Controller

The baseline performance estimation was calculated by assuming a turbine rotating with a fixed speed of 632 rpm. This speed was chosen by estimating the converted energy for a year at the Bideford Bay site for a range of turbine sizes and speeds, and choosing the turbine size which converted the most energy annually, and the turbine speed which converted the most energy in the sea state which was the most frequently occurring.

A feedforward linear controller was tested which turned the magnitude of the pressure difference into turbine speed. This was a controller with an offset speed and a term proportional to absolute pressure difference. Both the proportional coefficient and the offset speed were coefficients were then optimised for the most frequently occurring sea state at the Bideford site. The optimisation was done using the MATLAB `fminsearch()` function, with maximisation of average power converted as its target.

The resulting control action gave a turbine speed which moved quickly from the offset with each wave. The rates of change of speed were high, but appears to be possible for a real system. The energy cost required to make such a change in speed was not included in the optimisation. It was only converted energy, and not net converted energy that was used used to determine the optimum values.

Having found that turbine efficiency was a major factor in the effectiveness of the overall system, a turbine efficiency controller was also tested. Here, the turbine speed was chosen such that the turbine was always operating at its maximum efficiency. This turbine speed controller was found to require very fast and significant changes in turbine speed, although converted energy was also significantly greater.

Having tested the linear and nonlinear controllers on the most frequently occurring sea state, their performance was next tested across all of the sea states observed in the Bideford wave climate.

6.3.1 Major findings for the controller

It was found that the controller could significantly increase the energy converted by the OWC-WEC in the sea state for which the turbine speed controllers were optimised. The linear and turbine speed controllers increased average power conversion in the most frequently occurring sea state from 24.7 kW to 32.4 kW and 33.5 kW, respectively.

The linear controller proved quite effective especially in the sea state for which it was optimised. Note that the linear controller's speed control law approximates that of the turbine efficiency controller over that range of pressure difference seen in this sea state.

The turbine efficiency controller is effective in converting energy in all of the sea states. However, large and fast changes in turbine speeds were required in order to achieve this.

6.3.2 Importance of this controller

For OWC control it is the generation of the controller reference which is key. In Amundarain *et al.* (2011), a reference for generator slip was made by trial and improvement using laboratory data. Their control studies then consider different methods to have the generator system follow this reference. The mass flow controller of Nunes *et al.* (2011) also has a previously generated reference to follow.

Monk *et al.* (2013) used an artificial neural network (ANN) to find those valve positions that work well for different combinations of wave properties.

The campaign of controller testing described in this thesis describes a method by which a controller reference may be found by numerical testing offline. It shows that even a very simple speed controller can have a large impact on the performance.

6.3.3 Relation of the controller to other work

For the generic model described here, while the chosen controller is specific to this geometry, turbine and wave conditions, the *method* for control and optimisation is certainly applicable to other projects. For example, projects that are in the planning stage. Once an OWC plant exists, a controller tuned to its specifics is then viable.

In Monk *et al.* (2013) an ANN is used to change the valve position at the Pico plant. It is difficult to extend such an ANN model to sea conditions other than those already observed, or to other plants.

In their eqn (22), Nunes *et al.* (2011) look at changing the amount of mass flow directly (as a variable pitch turbine rather than any kind of valve). The extra mass flow, α, can range from 0 to 1000 kg/s. The value of 1000 kg/s is a *lot* more than is seen in normal conditions, and corresponds to approximately a 10 m by 10 m by 10 m volume of air moving through the turbine per second. The powers that they look at are purely pneumatic (or a 100% efficiency turbine). This means that the power calculated for this thesis is more realistic.

The ideal method would be a nonlinear MPC. (See Section 1.4.1.) This would take all of the information that is available at a given time and calculate the current best settings for maximum energy conversion (or alternatively a combination of maximum energy conversion and damage limitation) given some knowledge of future inputs and an expectation of plant behaviour ahead in time. In fact, as such MPC for maximum energy conversion increases its premonition time, the controller tends to the ideal "optimal control" solutions (Hals *et al.* (2011), Falnes (2002b)) that rely on long (technically infinite) future premonition times. However, such MPC requires that the model be very close to reality, especially in extreme scenarios where the point of operation for maximum energy production must be balanced against the safe limit for the device.

6.3.4 Array control

Hierarchical control would also be very important when applying control to more than one column at any time. There has already been quite some research published into arrays of

WECs, but the most common version of these arrays is to have spaced point absorbers (Westphalen *et al.*, 2011; Child & Venugopal, 2010). Control for multiple units has also been investigated by Zhang (2011) who described a 3-body point absorber and investigated control for each arm. Lucas *et al.* (2012) shows control for a flap-type WEC array, although this only describes results when the PTO force approximates a pure damping.

Research into OWC neighbour control has scope for improvements in energy conversion: the way that such neighbours work together, especially where the linked column modes of Chapter 2 are possible is clearly a very interesting topic.

This study does not allow the PTOs of neighbouring devices to interact, but the motion of the water around non-interacting PTOs is included. Thus the control action of one device does not interact with the control action of another. In order to include this, the time domain model would have to be completely reformulated. One aspect that could be investigated using this set-up would be to find the best lid damping properties for each chamber for maximum overall power output.

6.3.5 Limitations of the controller

A particular geometry of device was used, as was a particular turbine. The modelled turbine was not optimised for this particular OWC device, so in order to increase converted energy a different turbine, and thus different controller settings are likely.

Limitations of the controller due to optimisation region

The controller has only been optimised in one sea state. Thus, although the controllers may be tested in the other sea states, the control which would be optimal in these other sea states has not been tested. In order to have an appropriate linear controller in each sea state, the optimisation procedure could be undertaken for each one. However, identification of the sea state may be incorrect, so these linear controllers should have speed offset and proportional coefficients which work well for neighbouring sea states. Optimisation which ties a controller too closely to a given sea state can also fail in the real sea, where the waves are not formed from a mathematically exact spectrum (and include different incident angles). In large seas, optimisation against this time-domain model may also be unwise as the wave interaction with the structure will be far from linear.

Energy cost

A crucial limitation is that the energy cost of actuating the turbine to give the desired speeds is not included in the optimisation. This means that the optimisation of the linear controller and the comparison between the baseline, linear and turbine efficiency controllers is based on the converted energy rather than the net converted energy. If changing the speed of the turbine requires a lot of energy, this could be a severe limitation. However, it is also possible that holding the turbine at a fixed speed requires energy. This cost is not included in the baseline time domain model. Such considerations are dependent on the specific turbine and generator combination and as such were not included in this study.

The controller is assumed to act instantaneously which (especially with the importance of phase for power output) could change the optimal controller settings. Non-instantaneous control may require a reliance on prediction of the wave. This would change the controller's inputs, but also possibly the nature of the controller, making model predictive control (MPC) more necessary.

Other aspects that were not included in the cost function were maximum and minimum power spikes, which may need to be avoided so as to limit damage to the machine or to avoid financial costs from the grid operator. Again, these considerations are highly dependent on the particular project.

This model does not look at the effect of power smoothness. The eventual price for energy will be likely to depend on the smoothness with which it is delivered to the grid. Thus, a smooth power profile is likely to be of benefit. This was not taken into account for these controllers, but could be incorporated in a more detailed model.

6.3.6 Further work on the controller

Energy cost

Including the energy cost, or an approximation to it would give a better understanding of whether inclusion of control is good for net energy conversion. Energy cost clearly depends on the specific turbine and generator combination, but testing control strategies with assumptions about the limitations of different generator combinations would allow designers to focus on the specifications which are of most importance for increasing energy conversion, for example, the range of rotational speeds or the speed at which these may be changed.

Actuator delay

A crucial aspect is that the controller is assumed to act instantaneously. If this were not the case, the optimised controller action would not remain the same. It would be very interesting to see the nature of the change to the controller action for non-instantaneous actuation.

Predictive and model-based control

In this study, no prediction of the future wave displacement, chamber pressure or flow rate has been used to influence the turbine settings. Such prediction could lead to more effective control, especially in the non-instantaneous control action case.

Although the controller clearly has feedback in the form of the system itself, direct feedback about the current turbine speed has not been used. Incorporating this within the controller or using a hierarchy of speed controller and speed actuation feedback controller would be vital for non-instantaneous control, as mentioned in Section 1.4.4.

Findings from this discussion

The multi-column OWC model and the wave-to-wire time-domain model of the OWC-WEC are a stage towards array modelling for multi-chamber OWC-WECs. The coupled modes seen in the hydrodynamic study of Chapter 2 drive the necessity for a time domain model which can deal with an OWC-WEC which is sensitive to the incident wave period. A force to displacement transfer function model is a simple way of capturing the hydrodynamic behaviour of the OWC.

Equations for the thermodynamics and turbine can be incorporated to produce a wave-to-mechanical power time-domain model of the OWC-WEC.

The linear controller tested here is optimised offline to give a reference for the turbine parameters to follow. Turbine efficiency was found to have a very large effect on mechanical power, so a turbine efficiency controller was also tested. In order to make the optimisation and comparison process more appropriate, the energy cost and actuation delay of the controller should be included.

Control for different sea states was seen to improve performance, but here no estimations were made about the improvements that could be generated if the PTOs of the various columns were to work together.

Summary

- The velocity potential and time domain models give a good base from which to investigate multi-column OWCs
- This should be extended to incorporate the effect of each PTO on its neighbours so as to enable the investigation of multi-*chamber* OWC-WECs.
- The linear and nonlinear control testing showed that simple controllers can have a large effect on the energy converted by the OWC-WEC
- The *net* energy converted should be investigated. This requires a turbine model which can calculate the energy expenditure for speed change, and give a reasonable prediction for the time over which such changes will occur.

Chapter 7

Conclusions

For a breakwater-mounted, multi-column OWC-WEC, the influence of neighbouring columns leads to coupled modes of motion. These linked displacements give an OWC within a multi-column structure a particular sensitivity to the period and direction of incident waves.

Very simple turbine speed controllers were found to have a significant influence on the conversion of energy.

7.1 Summary of research undertaken

The hydrodynamics of a five-column, breakwater-mounted OWC was modelled using the velocity potential method. A geometrically similar isolated OWC was also modelled, as were a single column with breakwater, a single column with breakwater and deep side-walls and three columns with breakwater.

A transfer function which maps incident wave force to the internal surface displacement of the water column was used to model the isolated OWC and the central column of five in the time domain. This force mapping can incorporate the force due to the pressure difference of the chamber, thus the pressure force can be fed back to the hydrodynamic system and therefore so can any changes due to turbine parameter control.

A time domain numerical model was developed of an OWC-WEC formed of five chambers arranged as a breakwater. The central column had a turbine power take off (PTO) and performance was tested in the wave climate of a shallow coastal region in South West England. A linear controller and a turbine efficiency controller were tested for this column.

7.2 Research findings

7.2.1 Hydrodynamics for multi-column structures

When extra OWCs are positioned next to an original OWC, the existence of the others affects the movement of water within the original. The internal water surface displacement for the original OWC is thus not simply the same as it was without neighbours. When wave periods which are close together are considered, the behaviour for a multi-column system is very different because coupled modes may be excited. This means that for an individual column, the motion may be very large for one wave period, but very small for a period only a little longer than this. A similar phenomenon is seen as the direction of the wave changes, with coupled modes making each OWC sensitive to changes in direction.

7.2.2 Time domain modelling

An OWC such as that with five columns in a breakwater formation may be modelled using a transfer function based on a system identification using force to displacement. The incident force and the damping force generated by the pressure difference between the chamber and the atmosphere may be combined as the input to the transfer function. This enables any changes made to/by the turbine system to be fed back such that the internal water surface displacement of the OWC is acted on by this force.

7.2.3 Control of OWCs

The average power converted in any sea state (or wave climate) can be significantly increased when using a controller, although this is tempered by the amount of energy which is required to achieve the changes in turbine parameters.

A linear control rule which was based on turbine speed with an offset and a term proportional to absolute pressure difference, led to energy conversion of 32.4 kW in the investigated sea state, in comparison to 24.7 kW for the fixed speed controller for the sea state for which they were optimised. It achieved this by increasing the mass flow through the turbine without significantly changing the chamber pressure.

A turbine efficiency controller was tested which ensured that the turbine was always operated at its maximum efficiency. Because the turbine efficiency has such a large effect on the overall mechanical power converted, this controller was found to lead to large energy conversions. In the sea state for which the fixed speed, and the linear controller

coefficients were optimised, the turbine efficiency controller converted energy such that its average power was 33.5 kW.

Extending these control choices over all sea states and using the Bideford Bay wave climate, the annual average power was estimated to be 36.3 kW for the fixed speed (632 rpm) controller, 58.4 kW for the linear controller and 69.0 kW for the turbine efficiency controller. Clearly the two controllers which were optimised for the small wave sea states were outperformed by the turbine efficiency controller based on the converted energy criterion.

7.3 Suggestions for further research

7.3.1 Further research for the time domain model

Incorporating the damping values estimated from the time domain modelling into the velocity potential model would give a better indication of the behaviour of this multi-column breakwater when acting as a WEC.

Investigating the effects of PTO, or damping values, for each chamber on its neighbours requires a model in which this influence may be tracked. This could be done by breaking down the motion by changing the damping of one chamber at a time. Use of PTOs on all of the chambers is clearly crucial here. A model which uses system identification techniques would be a good method for identifying these effects of neighbouring PTOs on each other. A neural network model for example would be able to include the nonlinear effects of the water motion.

Another area in which system identification techniques could be beneficial is in modelling the effect of directional spread of the incident wave. A model in which the directional properties were also included would be useful because the velocity potential modelling of Chapter 2 suggests that systems with a breakwater back-board, and systems with multiple chambers (and thus coupled modes) are particularly affected by the incident wave angle. Therefore, any model that could include this would give a much more accurate picture of the real-sea situation.

Using the same time-domain model, different turbines could be compared. For example, an impulse turbine could be tested on the system, using similar mass flow and turbine efficiency approaches.

7.3.2 Further research for the controller

The OWC-WEC modelled in this thesis used neither a by-pass valve nor a shut-off valve. Such a valve can have a large effect on the chamber pressure and thus on the overall response and level of energy conversion. If valves were included in the model, their positions could be changed to help to increase energy conversion. The valve positions could then be incorporated into the nonlinear controller as extra variables. As well as the valve positions leading to extra control rules, more complicated controller actions could be tested.

The inclusion of the energy cost of implementing the control action is needed to determine whether the controller is worth implementing. Calculation of this control energy cost should come with a more detailed model of the turbine so that the cost of maintaining the turbine speed is correctly accounted for. Any actuator which changes the speed or allows changes in speed will not be able to act instantaneously, so an actuator delay function may be included and a new optimisation run to find the types of controller which are effective.

If there is then the situation in which there is a model with PTOs which may interact, then control over multiple units may be tested. This could include a master controller which predicts the workings of each model, or tests different rule groups across all of the OWCs. It could also use hierarchical control in which each OWC is given an objective by a higher controller which aims to help the OWCs work together to increase total energy conversion.

Concluding remarks

This thesis presents the methods by which certain steps on the road to multiple chamber OWC control may be modelled and understood. It presents as likely the possibility of using different units to different maximum powers in different sea states and directions. It also shows that great increases in average output power may be achieved through turbine speed control.

Clearly there is much to learn about the OWCs' interaction with one another, especially the interaction of their PTOs. This leaves open exciting possibilities in multiple column control.

References

Alves, Marco, & Sarmento, António. 2005. Non-linear and viscous diffraction response of OWC wave power plants. *Pages 11–18 of: 6th European Wave and Tidal Energy Conference.*

Alves, Marco, Vicente, Miguel, Sarmento, António, & Guerinel, Mathieul. 2011. Implementation and Verification of a Time Domain Model to Simulate the Dynamics of OWCs. *In: 9th European Wave and Tidal Energy Conference.*

Amundarain, Modesto, Alberdi, Mikel, Garrido, Aitor J, & Garrido, Izaskun. 2011. Modeling and Simulation of Wave Energy Generation Plants: Output Power Control. *IEEE Transactions on Industrial Electronics*, **58**(1), 105–117.

ANSYS. 2012. *ANSYS AQWA, Release 14.0, Help System, AQWA User Manual, ANSYS Inc.*

Bacelli, Giorgio, Ringwood, John V, & Gilloteaux, Jean-christophe. 2011. A control system for a self-reacting point absorber wave energy converter subject to constraints. *Pages 11387–11392 of: IFAC world conference.*

Belmont, M.R. 2010. Increases in the average power output of wave energy converters using quiescent period predictive control. *Renewable Energy*, **35**(12), 2812–2820.

Brito-Melo, A, Neuman, F, & Sarmento, A. 2007. Full-scale data assessment in OWC Pico plant. *Pages 447–454 of: Proc. 17th Int. Offshore and Polar Engineering Conf.*

Brito-melo, Ana, Sarmento, A.J.N.A., Clement, A.H., & Delhommeau, G. 1999. A 3D boundary element code for the analysis of OWC wave power plants. In: Proceedings of the Ninth International Offshore and Polar Engineering Conference, Brest, ISOPE, I., pp. 188–195. *Pages pp. 188–195 of: Proceedings of the Ninth International Offshore and Polar Engineering Conference.*

Bull, Diana, & Johnson, Erick. 2013. Optimal Resistive Control Strategy for a Floating OWC Device. *In: 10th European Wave and Tidal Energy Conference.*

Child, B.F.M., & Venugopal, V. 2010. Optimal configurations of wave energy device arrays. *Ocean Engineering*, **37**(16), 1402–1417.

Cooper, P, & Gareev, A. 2007. Numerical Analysis of a Variable Pitch Reversible Flow Air Turbine for Oscillating Water Column Wave Energy Systems. *Pages 1–7 of: Proc. 7th European Wave and Tidal Energy Conference.*

Cretel, J, Lewis, A. W., Lightbody, G, & Thomas, G. P. 2010. An Application of Model Predictive Control to a Wave Energy Point Absorber. *In: IFAC Conference on Control Methodologies and Technology for Energy Efficiency.*

Cross, P, Taylor, C J, & Aggidis, G A. 2011. State Dependent Feed – Forward Control for Wave Energy Conversion. *In: Proc. 9th European Wave and Tidal Energy Conference.*

Delaure, Lewis. 2003. 3D hydrodynamic modelling of fixed oscillating water column wave power plant by a boundary element methods. *Ocean Engineering*, **30**, 309–330.

Deng, Z, Huang, Z, & A.W.K., Law. 2014. Wave power extraction from a bottom-mounted OWC converter with a V-shaped channel. *Proc. Royal Soc. A*, **470**.

Deng, Zhengzhi, Huang, Zhenhua, & Law, Adrian W.K. 2013. Wave power extraction by an axisymmetric oscillating-water-column converter supported by a coaxial tube-sector-shaped structure. *Applied Ocean Research*, **42**(Aug.), 114–123.

Evans, D, & Porter, R. 1995. Hydrodynamic characteristics of an oscillating water column device. *Applied Ocean Research*, **17**(3), 155–164.

Falcão, A.F.de O, & Rodrigues, R.J.A. 2002. Stochastic modelling of OWC wave power plant performance. *Applied Ocean Research*, **24**(2), 59–71.

Falcão, António F. De O. 2002. Control of an oscillating-water-column wave power plant for maximum energy production. *Applied Ocean Research*, **24**(2), 73–82.

Falcão, António F. De O., & Justino, P.A.P. 1999. OWC wave energy devices with air flow control. *Ocean Engineering*, **26**(12), 1275–1295.

Falnes, Johannes. 2002a. *Ocean Waves and Oscillating Systems.* Cambridge University Press.

Falnes, Johannes. 2002b. Optimum control of oscillation of wave-energy converters. *International Journal of Offshore and Polar Engineering*, **12**(2), 147–154.

Fleming, Alan, Penesis, Irene, Macfarlane, Gregor, Bose, Neil, & Denniss, Tom. 2012. Energy balance analysis for an oscillating water column wave energy converter. *Ocean Engineering*, **54**(Nov.), 26–33.

Folley, Matt, & Whittaker, Trevor. 2005. The effect of plenum chamber volume and air turbine hysteresis on the optimal performance of oscillating water columns. *Pages 1–6 of: OMAE2005*.

Freeman, Kate, Dai, Ming, & Sutton, Robert. 2014. Control strategies for oscillating water column wave energy converters. *Underwater Technology*, **32**(1), 3–13.

Fusco, Francesco, & Ringwood, John V. 2010. Short-Term Wave Forecasting with AR models in Real-Time Optimal Control of Wave Energy Converters. *Electronic Engineering*, 2475–2480.

Gervelas, R., Trarieux, F., & Patel, M. 2011. A time-domain simulator for an oscillating water column in irregular waves at model scale. *Ocean Engineering*, **38**(8-9), 1007–1013.

Gkikas, G.D., Xiros, N.I., Athanassoulis, G.A., & Belibassokis, K.A. 2006. A Nonlinear Model for Oscillating Water Column Analysis, Design and Control. *Pages 408–415 of: ISOPE-2006: Sixteenth(2006) International Offshore and Offshore and Polar Engineering Conference Proceedings*, vol. 4. San Francisco, California: International Society of Offshore and Polar Engineers, P. O. Box 189, Cupertino, CA, 95015-0189, USA,.

Gomes, R.P.F., Henriques, J.C.C., Gato, L.M.C., & a.F.O. Falcão. 2012. Hydrodynamic optimization of an axisymmetric floating oscillating water column for wave energy conversion. *Renewable Energy*, **44**(Aug.), 328–339.

Guanche, R., de Andrés, A.D., Simal, P.D., Vidal, C., & Losada, I.J. 2013. Uncertainty analysis of wave energy farms financial indicators. *Renewable Energy*, **68**, 570–580.

Hals, J., Falnes, J., & Moan, T. 2011. A Comparison of Selected Strategies for Adaptive Control of Wave Energy Converters. *Journal of Offshore Mechanics and Arctic Engineering*, **133**(3), 031101.

Heath, T.V. 2007. The Development of a Turbo-Generation System for Application in OWC Breakwaters. *Pages 1–6 of: Proc. 7th European Wave and Tidal Energy Conf., Porto (Portugal)*.

Hodgins, N, Mueller, M A, Tease, W K, & Staton, D. 2008. Measurement and modelling of induction generator performance in an Oscillating Water Column wave energy converter. *Pages 76–80 of:* IET (ed), *Power Electronics, Machines and Drives, 2008. PEMD 2008. 4th IET Conference on*.

Hong, Do Chun, & Hong, Key Yong. 2012. Performance Prediction of an OWC Wave Power Plant. *In: OCEANS, 2012*.

Hong, Keyyong, & Song, Museok. 2012. Wave Energy R & D Activities in Korea. *In: 4th International Conference on Ocean Energy*.

Hotta, Hitoshi, Washio, Yukihisa, Yukozawa, Hitoshi, & Miyazaki, Takeaki. 1996. R & D on Wave Power Device " Mighty Whale ". *Renewable Energy*, **9**(1-4), 1223–1226.

Imai, Yasutaka, Toyota, Kazutaka, & Nagata, Shuichi. 2011. An Experimental Study on Generating Efficiency of a Wave Energy Converter" Backward Bent Duct Buoy. *In: 9th European Wave and Tidal Energy Conference*.

Iturrioz, Arantza, Guanche, Raul, Armesto, Jose A., Vidal, Cesar, & Losada, Inigo J. 2013. Experimental and numerical development of a floating multi-chamber OWC device. *In: 10th European Wave and Tidal Energy Conference*.

Jayashankar, V, Udayakumar, K, Karthikeyan, B, Manivannan, K, Venkatraman, N, & Rangaprasad, S. 2000. Maximizing power output from a wave energy plant. *Pages 1796–1801 vol.3 of: Power Engineering Society Winter Meeting*, vol. 3.

Jayashankar, V, Anand, S, Geetha, T, Santhakumar, S, Jagadeeshkumar, V, Ravindran, M, Setoguchi, T, Takao, M, Toyota, K, & Nagata, S. 2009. A twin unidirectional impulse turbine topology for OWC based wave energy plants. *Renewable Energy*, **34**(3), 692–698.

Johnson, F. 2003. *Multi Resonant Converter Wave Energy Device: Sea trials vehicle*. Ph.D. thesis, University of Plymouth.

Josset, C, & Clement, A. 2007. A time-domain numerical simulator for oscillating water column wave power plants. *Renewable Energy*, **32**(8), 1379–1402.

Joubert, James R, & Niekerk, Johannes L Van. 2013. Design of a Novel Breakwater Wave Energy Converter for the South African Coast. *In: 10th European Wave and Tidal Energy Conference.*

Kelly, T, Dooley, T, Campbell, J, & Ringwood, J.V. 2013a. Frequency Domain Testing and Simulation of a 32-OWC Floating Wave Energy Converter. *Energies*, **6**, 4045–4077.

Kelly, Thomas, Dooley, Thomas, Campbell, John, & Ringwood, John. 2013b. Modelling and Results for an Array of 32 Oscillating Water Columns . *In: 10th European Wave and Tidal Energy Conference.*

Kiprakis, A E, Nambiar, A J, Forehand, D, & Wallace, A R. 2009. Modelling arrays of wave energy converters connected to weak rural electricity networks. *Pages 1–7 of: Sustainable Power Generation and Supply, 2009. SUPERGEN '09. International Conference on.* Nanjing, China: IEEE.

Koo, Weoncheol. 2009. Nonlinear time–domain analysis of motion-restrained pneumatic floating breakwater. *Ocean Engineering*, **36**(9-10), 723–731.

Le Crom, I, Brito-Melo, A, Neumann, F, & Sarmento, A J N A. 2007. Portuguese Grid Connected OWC Power Plant : Monitoring Report. *In: 7th European Wave and Tidal Energy Conference.*

Leigh, J.R. 2004. *Control Theory.* 2nd edn. London, UK: The Institution of Electrical Engineers.

Li, Guang, & Belmont, Mike R. 2013. Model Predictive Control of an array of Wave Energy Converters. *In: 9th European Wave and Tidal Energy Conference.*

Lopes, M F P, Ricci, Pierpaolo, Gato, L M C, & Falcão, A F De O. 2007. Experimental and numerical analysis of the oscillating water column inside a surface-piercing vertical cylinder in regular waves. *In: Proc. 7th European Wave and Tidal Energy Conf., Porto (Portugal).*

Lopes, M.F.P., Hals, J., Gomes, R.P.F., Moan, T., Gato, L.M.C., & Falcão, A.F.de O. 2009. Experimental and numerical investigation of non-predictive phase-control strategies for a point-absorbing wave energy converter. *Ocean Engineering*, **36**(5), 386–402.

Lucas, J, Livingstone, M, Vuorinen, M, & Cruz, J. 2012. Development of a wave energy converter (WEC) design tool – application to the WaveRoller WEC including validation of numerical estimates. *In: 4th International Conference on Ocean Energy.*

Magagna, Davide, Carr, David, Stagonas, Dimitris, Mcnabola, Aonghus, Gill, Laurence, & Muller, Gerald. 2011. Experimental Evaluation of the Performances of an Array of Multiple Oscillating Water Columns. *In: 9th European Wave and Tidal Energy Conference.*

Martins-rivas, Hervé, & Mei, Chiang C. 2009. Wave power extraction from an oscillating water column along a straight coast. *Ocean Engineering*, **36**(6-7), 426–433.

Mavrakos, S. A. 1985. Wave loads on a stationary floating bottomless cylindrical body with finite wall thickness. *Applied Ocean Research*, **7**(4), 213—-224.

Mendes, A C, & Monteiro, W M L. 2007. Performance analysis of a model of OWC energy converter in non-linear waves. *In: 7th European Wave and Tidal Energy Conference.*

Moisel, C, & Carolus, T H. 2013. Comparison of axial and radial blade cascades for bi-directional wave energy air-turbines. *Pages 2–8 of: 10th European Wave and Tidal Energy Conference.*

Monk, Kieran, Conley, Daniel, Lopes, Miguel, & Zou, Qingping. 2013. Pneumatic Power Regulation by Wave Forecasting and Real-Time Relief Valve Control for an OWC. *In: 10th European Wave and Tidal Energy Conference.*

Morris-Thomas, MT, Irvin, R, & Thiagarajan, K. 2005. The Hydrodynamic Efficiency of an Oscillating Water Column. *In: Offshore Mechanics and Arctic Engineering Conference.*

Mundon, Timothy R. 2006. *Optimising the Output of an Articulated WEC Through the Use of a Biologically-Inspired and Artificially Evolved Neural Network.* Ph.D. thesis, University of Edinburgh.

Nader, Jean-Roch, Zhu, Song-Ping, Cooper, Paul, & Stappenbelt, Brad. 2012. A finite-element study of the efficiency of arrays of oscillating water column wave energy converters. *Ocean Engineering*, **43**(Apr.), 72–81.

Natanzi, Shahab, Teixeira, Joao Amaral, & Laird, George. 2011. A Novel High-Efficiency Impulse Turbine for Use in Oscillating Water Column Devices. *In: 9th European Wave and Tidal Energy Conference.*

Neill, Simon P., & Hashemi, M. Reza. 2013. Wave power variability over the northwest European shelf seas. *Applied Energy*, **106**(June), 31–46.

Nunes, Guilherme, Valério, Duarte, Beirão, Pedro, & Sá da Costa, José. 2011. Modelling and control of a wave energy converter. *Renewable Energy*, **36**(7), 1913–1921.

Patel, Sandeep K, Ram, Krishnil, Ahmed, M Rafiuddin, & Lee, Young-ho. 2011. Performance Studies on an Oscillating Water Column Employing a Savonius Rotor. *Sci. China Tech. Sci.*, **54**(1), 1674–1679.

Pereiras, B, Montoya, D, & de la Villa, A. 2011a. Design of a Turbine-Generator joint for an oscillating water column. *In: 7th European Wave and Tidal Energy Conference.*

Pereiras, Bruno, Castro, Francisco, Marjani, Abdelatif El, & Rodríguez, Miguel a. 2011b. An improved radial impulse turbine for OWC. *Renewable Energy*, **36**(5), 1477–1484.

Pontes, MT, Cândido, J., Henriques, JCC, & Justino, P. 2005. Optimizing OWC sitting in the nearshore. *Pages 389–394 of: Proc. 6th European Wave and Tidal Energy Conference.*

Price, A.A.E., Dent, C.J., & Wallace, A.R. 2009. On the capture width of wave energy converters. *Applied Ocean Research*, **31**(4), 251–259.

Rossiter, J.A. 2003. *Model- based predictive control: a practical approach.* Taylor & f edn. CRC Press.

Ruol, Piero, Martinelli, Luca, & Pezzutto, Paolo. 2011. Multi-chamber OWC Devices to Reduce and Convert Wave Energy in Harbour Entrance and Inner Channels. *Pages 622–629 of: Proc. Twenty-first Int. Offshore and Polar Engineering Conf.*, vol. 8.

Saulnier, Jean-baptiste M G, Maisondieu, Christophe, Ashton, Ian G C, & Smith, George H. 2011. Wave Hub Test Facility : Sea State Directional Analysis from an Array of 4 Measurement Buoys. *In: Proc. 9th European Wave and Tidal Energy Conference.*

Setoguchi, Toshiaki, & Takao, Manabu. 2006. Current status of self rectifying air turbines for wave energy conversion. *Energy Conversion and Management*, **47**(15-16), 2382–2396.

Sphaier, S, Torres, F, Masetti, I, Costa, A, & Levi, C. 2007. Monocolumn behavior in waves: Experimental analysis. *Ocean Engineering*, **34**(11-12), 1724–1733.

Stappenbelt, Brad, Cooper, Paul, & Fiorentini, Massimo. 2013. Prediction of the Heave Response of a Floating Oscillating Water Column Wave Energy Converter. *In: 10th European Wave and Tidal Energy Conference.*

Starzmann, R, Moisel, C, & Carolus, TH. 2013. Assessment method of sound radiated by cyclically operating Wells turbines. *Journal of Marine Energy*, 1–10.

Strong, B, Bouferrouk, A, & Smith, G H. 2012. Measurement and Evaluation of the Wave Climate near the Wave Hub using a 5-Beam ADCP. *In: International Conference on Ocean Energy.*

Sykes, R K, Lewis, A W, & Thomas, G P. 2007. A Physical and Numerical Study of a Fixed Cylindrical OWC of Finite Wall Thickness. *In: Proc. 7th European Wave and Tidal Energy Conf., Porto (Portugal).*

Sykes, R K, Lewis, A W, & Thomas, G P. 2009. A hydrodynamic study of a floating circular OWC. *Pages 618–627 of: Proceedings of the 8th European Wave and Tidal Energy Conference.*

Taha, Zahari, & Sawada, Tatsuo. 2010. A comparison of computational and experimental results of Wells turbine performance for wave energy conversion. *Applied Ocean Research*, **32**(1), 83–90.

Takao, Manabu, & Setoguchi, Toshiaki. 2012. Air Turbines for Wave Energy Conversion. *International Journal of Rotating Machinery*, **2012**, 1–10.

Taylor, C J, Stables, M A, Cross, P, Gunn, K, & Aggidis, G A. 2009. Linear and nonlinear modeling and control of a power take-off simulation for wave energy conversion. *Pages 1–8 of: Proceedings of the 8th EuropeanWave and Tidal Energy Conference, Uppsala, Sweden, 2009.*

Thakker, a. 2004. Effects of turbine damping on performance of an impulse turbine for wave energy conversion under different sea conditions using numerical simulation techniques. *Renewable Energy*, **29**(14), 2133–2151.

Thakker, Abdulhadi. 2008. The performance of a Wells turbine under bi-directional airflow. *Renewable Energy*, **33**, 2467–2474.

Tietje, E David III, Folley, Matt, Beatty, Scott, Raftery, Michael, & Ricci, Pierpaolo. 2011. Standardized Performance Assessment of Wave Energy Converters. *In: 9th European Wave and Tidal Energy Conference.*

Vögler, Arne, & Morrison, James. 2013. Assessment of the Grid Capacity Sharing Potential for Wave and Wind Energy Conversion Systems in the Outer Hebrides of Scotland. *In: 10th European Wave and Tidal Energy Conference.*

Voith. 2012. Siadar Wave Energy Project: Siadar Scoping Report. *Voith Hydro Wavegen (Xodus Group Ltd., Stromness)*, 1–57.

Weber, J. 2007. Representation of non-linear aero-thermodynamic effects during small scale physical modelling of OWC WECs. *In: Proc. 7th European Wave and Tidal Energy Conf., Porto (Portugal)*, vol. c.

Westphalen, J, Bacelli, G, Balitsky, P, & Ringwood, J. 2011. Control strategies for arrays of wave energy devices. *In: Proceedings of the 9th European Wave and Tidal Energy Conference.*

Zhang, Yali, Zou, Qing-Ping, & Greaves, Deborah. 2012. Air–water two-phase flow modelling of hydrodynamic performance of an oscillating water column device. *Renewable Energy*, **41**(May), 159–170.

Zhang, Zhe. 2011. *Development of Adaptive Damping Power Take-Off Control for a Three-Body Wave Energy Converter with Numerical Modeling and Validation.* Master of Science, Oregon State University.

Appendix A

Background data for wave-structure interaction

This appendix has background data for the wave structure interaction including the extra plots for the single column, deep-walled structure with breakwater and the three column moon pool structure.

A.1 RAO and phase for the single moon pool, with breakwater and deep walls

Figures A.1 and A.2 show the magnitude and phase response of the deep-walled moon pool structure with breakwater.

A.2 RAO and phase for the three moon pool system

Shown in Figures A.3 to A.6 are the free water surface responses on which Figures 2.10 to 2.12 are based.

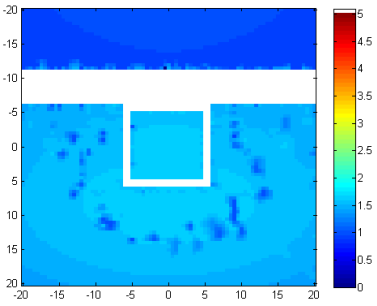

(a) 17.49 second waves

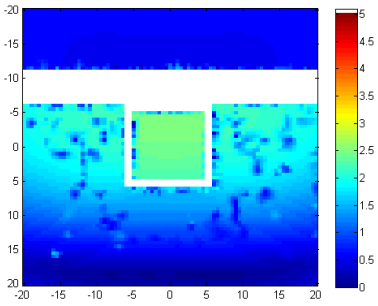

(b) 9.54 second waves

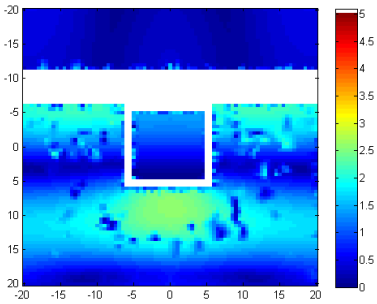

(c) 5.0 second waves

Figure A.1: The RAOs for a single, deep-walled moon pool in front of a breakwater with waves incident head-on.

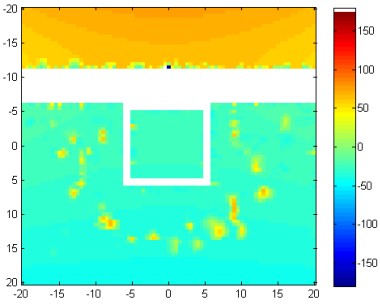

(a) 17.49 second waves

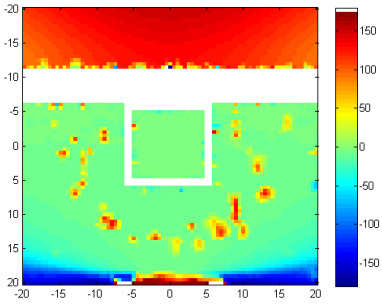

(b) 9.54 second waves

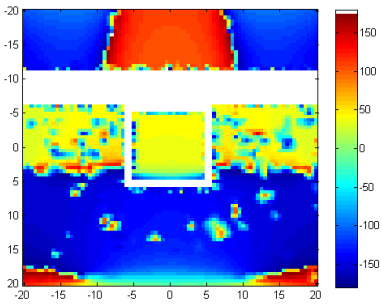

(c) 5.0 second waves

Figure A.2: The phase responses for a single, deep-walled moon pool in front of a breakwater with waves incident head-on.

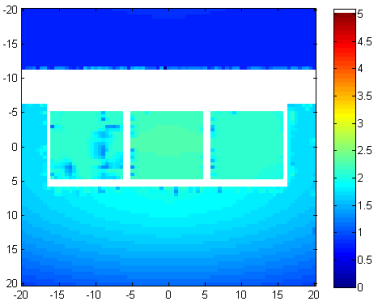

(a) 12.34 second waves

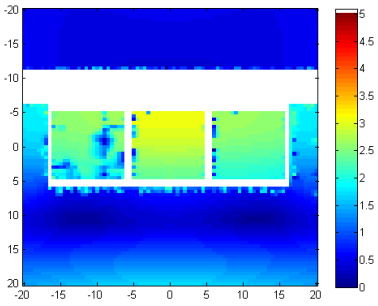

(b) 7.7 second waves

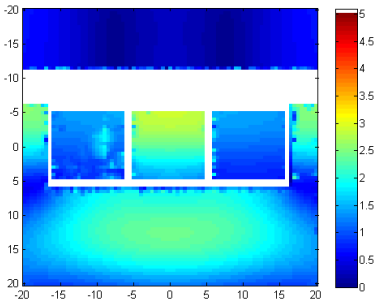

(c) 5.67 second waves

Figure A.3: RAOs for the free surface around three moon pools with a breakwater with waves incident head-on.

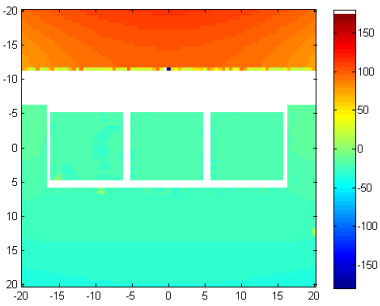

(a) 12.34 second waves

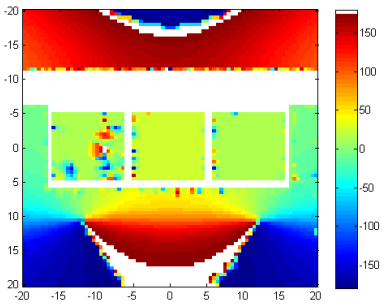

(b) 7.7 second waves

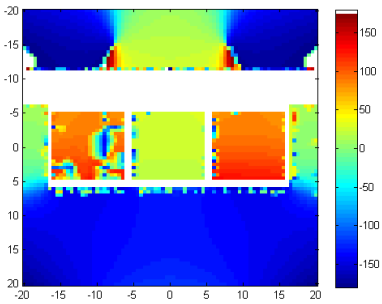

(c) 5.67 second waves

Figure A.4: Phase response for the free surface around three moon pools with a breakwater with waves incident head-on.

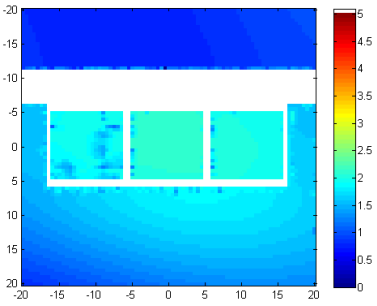

(a) 12.34 second waves

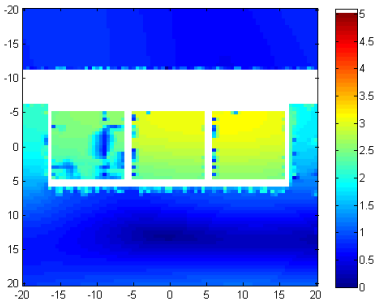

(b) 7.7 second waves

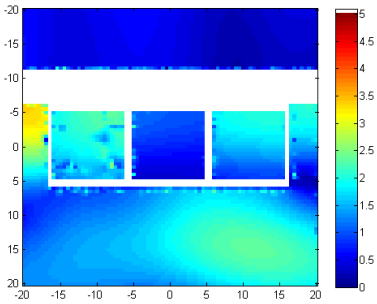

(c) 5.67 second waves

Figure A.5: The RAOs for the free surface around three moon pools with a breakwater with 30 ° angle incident waves

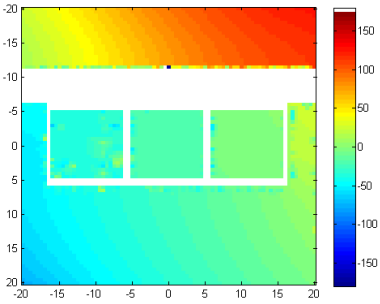

(a) 12.34 second waves

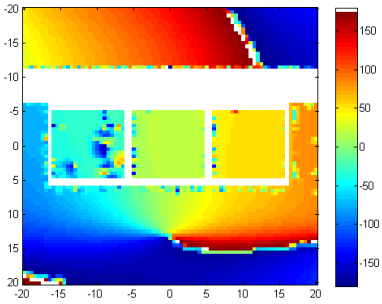

(b) 7.7 second waves

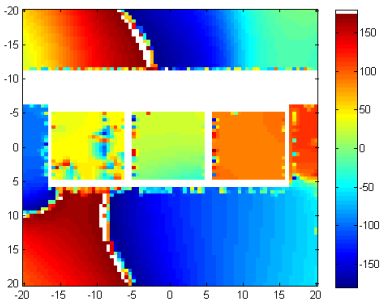

(c) 5.67 second waves

Figure A.6: The phases for the free surface around three moon pools with a breakwater with 30 ° angle incident waves

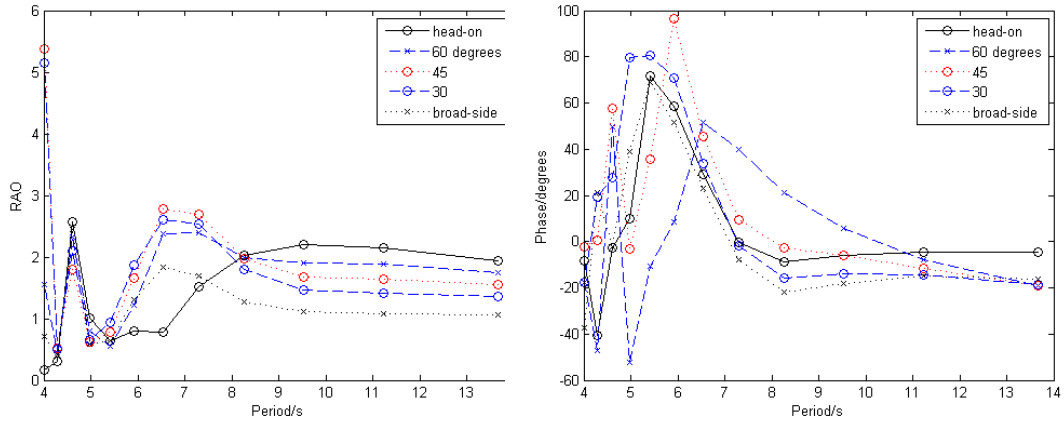

(a) Magnitude (b) Phase

Figure A.7: Magnitude and phase for the RAO of the single moon pool with breakwater, for waves of various incident angle

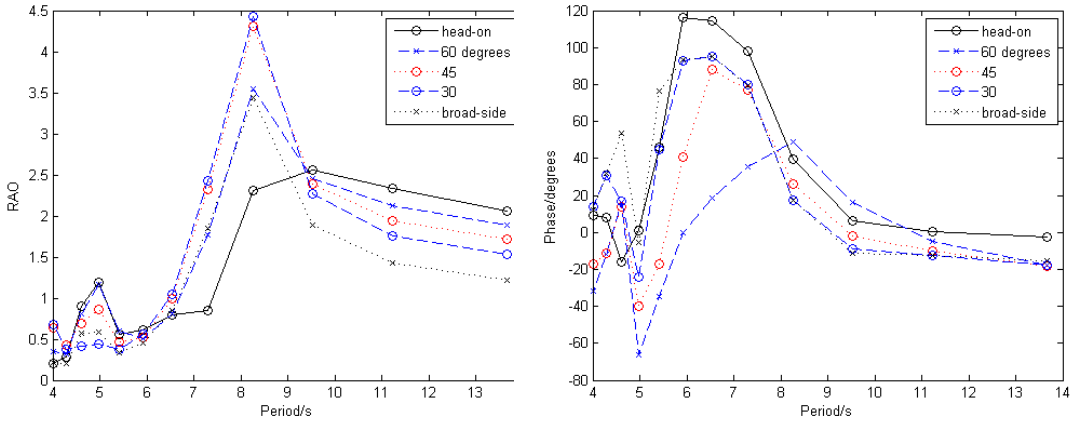

(a) Magnitude (b) Phase

Figure A.8: Magnitude and phase for the RAO of the single moon pool with deep walls and breakwater, for waves of various incident angle

A.3 Aggregate motion results for additional structures

A.3.1 The single moon pool with breakwater

Figures A.7 and A.8 show the aggregated surface displacement for the single moon pool with breakwater for shallow walls and deep wall respectively.

A.3.2 The three column moon pool with breakwater

Figures A.9 and A.10 show the aggregated surface displacement for the single moon pool with breakwater for shallow walls and deep wall respectively.

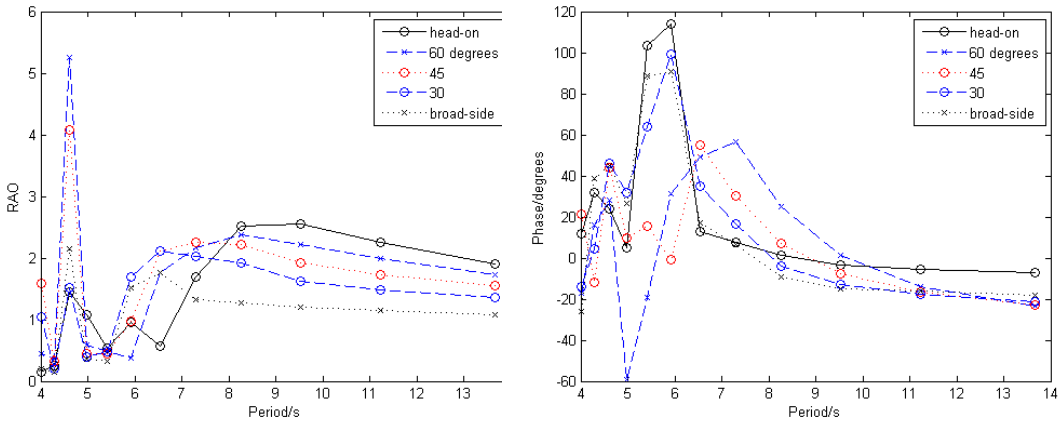

(a) Magnitude (b) Phase

Figure A.9: Magnitude and phase for the RAO of the three column moon pool with shallow walls and breakwater, for waves of various incident angle

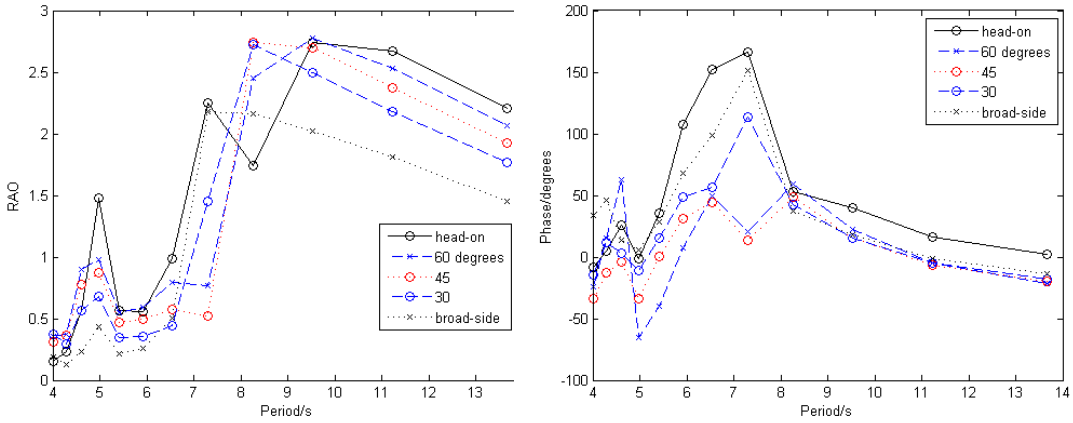

(a) Magnitude (b) Phase

Figure A.10: Magnitude and phase for the RAO of the three column moon pool with deep walls and breakwater, for waves of various incident angle

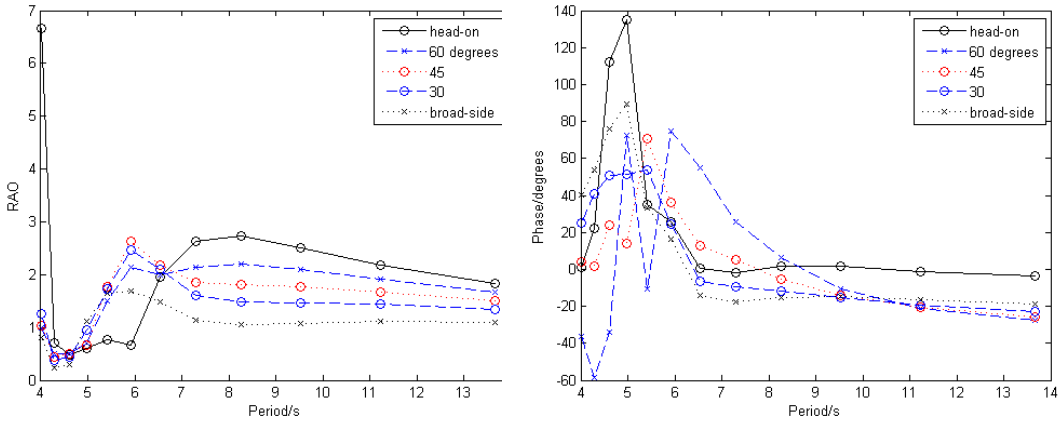

(a) Magnitude (b) Phase

Figure A.11: Magnitude and phase for the RAO of the five column moon pool with shallow walls and breakwater, for waves of various incident angle

A.3.3 The five column moon pool with shallow walls and breakwater

Figure A.11 shows the aggregated surface displacement for the five column moon pool with shallow walls and breakwater.

Appendix B

Wave climate information

Table B.1 shows the joint occurrence data for the spectra at the Bideford Bay site using the mean of the years 2009-2012.

	0-1s	1-2s	2-3s	3-4s	4-5s	5-6s	6-7s	7-8s	8-9s	9-10s	10-11s	11-12s	12-13s	13-14s	14-15s	15-16s
0-0.5m	0.002	0.000	0.000	0.000	0.000	0.000	0.000	0.000	0.000	0.000	0.000	0.000	0.000	0.000	0.000	0.000
0.5-1.0m	0.790	0.433	0.364	0.458	0.359	1.201	1.508	2.166	4.334	3.252	1.348	0.888	0.655	0.504	0.362	0.000
1.0-1.5m	0.190	0.676	2.048	2.889	1.747	2.498	2.659	3.819	7.193	5.997	2.402	1.956	1.219	0.700	0.332	0.000
1.5-2.0m	0.000	0.032	0.369	1.668	1.839	2.263	1.555	1.952	3.778	3.731	1.732	1.314	0.797	0.426	0.152	0.000
2.0-2.5m	0.000	0.000	0.010	0.220	0.581	1.503	1.000	0.802	1.840	1.932	1.042	0.820	0.483	0.281	0.140	0.000
2.5-3.0m	0.000	0.000	0.000	0.042	0.169	0.536	0.536	0.501	1.099	1.076	0.601	0.489	0.311	0.200	0.169	0.000
3.0-3.5m	0.000	0.000	0.000	0.000	0.018	0.149	0.254	0.306	0.665	0.653	0.326	0.324	0.207	0.112	0.089	0.000
3.5-4.0m	0.000	0.000	0.000	0.000	0.002	0.013	0.072	0.125	0.413	0.347	0.194	0.239	0.140	0.090	0.020	0.000
4.0-4.5m	0.000	0.000	0.000	0.000	0.000	0.005	0.002	0.042	0.220	0.227	0.100	0.110	0.065	0.028	0.007	0.000
4.5-5.0m	0.000	0.000	0.000	0.000	0.000	0.000	0.002	0.002	0.110	0.104	0.032	0.035	0.020	0.007	0.003	0.000

Table B.1: Joint occurrence of spectral seas determined by wave height and period at the Bideford Bay site

Appendix C

The power performance of the OWC-WEC

In this appendix, the performance matrix is given for the OWC-WEC using different controllers.

C.1 Fixed speed control

Figure C.1 shows the average power output in kW for the OWC-WEC in various sea states using the fixed speed controller with a speed of 632 rpm.

C.2 Linear control

Figure C.2 shows the average power output in kW for the OWC-WEC in various sea states using the linear controller.

C.3 Nonlinear control

Figure C.3 shows the average power output in kW for the OWC-WEC in various sea states using the turbine efficiency controller.

	0-1s	1-2s	2-3s	3-4s	4-5s	5-6s	6-7s	7-8s	8-9s	9-10s	10-11s	11-12s	12-13s	13-14s	14-15s	15-16s
0-0.5m	0.0	0.0	0.0	0.0	0.0	0.1	0.1	0.1	0.2	0.1	0.2	0.2	0.1	0.1	0.1	0.0
0.5-1.0m	0.0	0.0	0.0	1.1	3.0	4.6	6.1	7.2	7.9	7.6	7.4	6.8	6.8	5.3	4.2	3.1
1.0-1.5m	0.0	0.0	0.2	5.6	13.1	17.8	19.2	23.7	24.7	24.8	24.3	23.3	21.7	19.8	18.2	14.0
1.5-2.0m	0.0	0.0	0.8	14.6	26.6	30.3	34.4	38.6	37.9	39.5	36.6	38.5	37.6	32.7	30.4	28.7
2.0-2.5m	0.0	0.0	2.2	24.3	36.5	41.2	44.1	48.8	48.5	49.7	49.1	46.2	46.4	41.0	41.0	38.7
2.5-3.0m	0.0	0.0	4.1	33.7	43.9	48.6	54.0	55.2	57.3	55.2	56.8	54.1	54.3	53.0	50.6	40.9
3.0-3.5m	0.0	0.0	7.2	39.2	51.2	54.9	62.6	65.0	67.2	65.2	67.2	65.4	59.6	56.2	55.4	53.4
3.5-4.0m	0.0	0.0	10.9	46.1	58.1	65.0	71.6	74.1	76.9	78.6	75.9	73.2	72.9	65.5	61.7	58.4
4.0-4.5m	0.0	0.0	14.9	48.7	64.1	73.9	82.5	84.9	90.8	88.4	94.6	86.8	76.9	75.3	75.3	68.4
4.5-5.0m	0.0	0.0	20.3	53.5	71.4	83.9	94.5	102.0	NaN	106.8	105.8	101.5	99.9	91.6	81.6	73.8

Table C.1: Average mechanical power (in kW) in various sea states using fixed speed control

	0-1s	1-2s	2-3s	3-4s	4-5s	5-6s	6-7s	7-8s	8-9s	9-10s	10-11s	11-12s	12-13s	13-14s	14-15s	15-16s
0-0.5m	0	0.0	0.0	0.1	0.4	0.6	0.7	0.8	0.8	0.7	0.7	0.6	0.5	0.4	0.3	0.2
0.5-1.0m	0	0.0	0.3	3.4	6.5	8.9	10.3	11.7	11.3	12.7	11.1	10.3	9.5	7.9	6.4	5.7
1.0-1.5m	0	0.0	1.4	10.8	18.7	24.7	28.7	31.3	32.4	32.1	32.7	30.2	27.6	24.4	21.2	19.0
1.5-2.0m	0	0.0	3.3	20.7	35.0	43.3	48.8	51.4	57.1	54.7	57.5	55.2	54.8	45.8	40.5	32.5
2.0-2.5m	0	0.0	6.1	33.7	51.4	64.7	67.0	78.9	85.3	83.4	79.2	72.9	73.1	70.9	67.4	62.6
2.5-3.0m	0	0.0	9.5	46.2	72.8	83.2	96.0	94.8	107.5	104.8	102.4	101.2	101.6	89.9	89.7	79.2
3.0-3.5m	0	0.0	13.1	58.2	87.5	103.9	113.7	123.5	123.0	128.2	124.4	117.0	115.5	112.0	97.9	94.3
3.5-4.0m	0	0.0	17.8	75.9	103.1	119.4	137.3	133.4	139.7	136.6	142.0	143.4	139.2	122.6	128.1	108.8
4.0-4.5m	0	0.0	22.1	87.4	121.8	143.3	145.8	157.8	156.9	160.8	160.1	159.9	153.4	149.7	144.8	134.7
4.5-5.0m	0	0.0	26.1	101.0	139.7	153.4	165.6	173.5	172.3	177.0	171.0	176.2	176.3	158.5	160.1	153.7

Table C.2: Average mechanical power (in kW) in various sea states using the linear controller

	0-1s	1-2s	2-3s	3-4s	4-5s	5-6s	6-7s	7-8s	8-9s	9-10s	10-11s	11-12s	12-13s	13-14s	14-15s	15-16s
0-0.5m	0.0	0.0	0.0	0.4	0.8	1.2	1.3	1.3	1.3	1.3	1.1	0.8	0.7	0.6	0.4	0.3
0.5-1.0m	0.0	0.0	0.6	4.5	8.1	10.3	11.6	12.8	13.2	13.4	12.2	11.3	9.8	8.3	6.8	5.6
1.0-1.5m	0.0	0.0	2.2	11.8	20.3	24.0	29.8	32.2	33.5	35.6	34.3	30.8	29.6	26.1	21.0	19.9
1.5-2.0m	0.0	0.0	4.5	22.1	36.1	44.0	53.8	56.4	60.2	59.6	62.1	62.5	56.2	50.1	43.7	33.2
2.0-2.5m	0.0	0.0	7.6	33.8	55.4	68.0	78.8	85.5	89.8	97.8	88.7	93.8	83.7	81.3	71.8	62.6
2.5-3.0m	0.0	0.0	11.1	47.3	75.6	92.8	108.3	121.3	123.1	131.8	122.9	132.9	122.1	112.9	93.0	80.8
3.0-3.5m	0.0	0.0	14.5	63.4	100.3	127.4	144.8	154.4	160.9	170.5	175.7	159.9	155.7	147.3	137.8	105.8
3.5-4.0m	0.0	0.0	18.4	81.4	129.1	158.6	173.7	194.3	203.3	203.5	202.0	212.8	187.6	176.7	164.9	160.1
4.0-4.5m	0.0	0.0	23.5	97.4	154.6	193.2	216.4	233.8	246.3	251.4	265.3	246.4	267.8	224.5	219.5	195.4
4.5-5.0m	0.0	0.0	27.9	118.1	184.5	224.4	254.2	276.1	291.5	297.0	311.9	280.6	307.5	282.9	257.0	208.9

Table C.3: Average mechanical power (in kW) in various sea states using the turbine efficiency controller controller